UNIVERSITY OF CALIFORNIA

Los Angeles

Optimizing Morphology of Bulk Heterojunction Polymer Solar Cells

A dissertation submitted in partial satisfaction of the

requirements for the degree Doctor of Philosophy

in Materials Science and Engineering

by

Jing Gao

2014

ABSTRACT OF THE DISSERTATION

Optimizing Morphology of Bulk Heterojunction Polymer Solar Cells

by

Jing Gao

Doctor of Philosophy in Materials Science and Engineering

University of California, Los Angeles, 2014

Professor Yang Yang, Chair

The performance of bulk heterojunction polymer solar cells is profoundly influenced by the spatial arrangements of microstructure at various length scales in its photo-active layer, referred to as morphology. Due to their complex chemical structures, polymers usually exhibits low crystallinity and carrier mobility, leading to a limited thickness ~100 nm of the active layer for a typical polymer solar cell. Such thin films are incompatible with the prevailing large-area coating techniques, thus increasing the difficulty to realize the high-throughput production of polymer-based photovoltaics in industry. On the other hand, for most high-performance low-band-gap polymers, during their film-casting process, processing solvent additives are usually

essential for morphology optimization, which help boost device efficiency. However, most commonly-used solvent additives such as 1, 8-Diiodooctane (DIO), are disturbingly reactive to oxygen or water in air, leading to deteriorated performance of devices made under the ambient environment. Therefore, fabrication processes involving DIO have to be limited to an air-free environment, which is quite unfavorable for large-area fabrication techniques, as majority of them are carried on under the ambient environment. Therefore, an efficient air-stable solvent additive would be greatly appreciated in terms of OPV industrialization. As a result, in order to achieve thick active layers as well as to find an air-stable alternative additive for industrial applications, a thorough and systematic study on morphology is necessitated.

First, via rational modification of polymer chemical structure(fine-tuning on side chains), new polymers with enhanced structure order (e.g., crystallite size increases from 35 Å to 53 Å) and higher hole mobility (from ~10^{-5} to ~10^{-4} $cm^2/(V\ s)$) are obtained, enabling thicker optimum active layers ~200 nm with a larger thickness tolerance up to ~350 nm for the corresponding bulk heterojunction devices. This result is of great potential for relaxing the required level of precision in active layer thickness, which has important industrial implications for large-area film deposition.

Second, through examining those solvents with a great potential to satisfy the criteria for efficient additives, a new efficient air-stable solvent additive –1,2-dichlorobenzene (DCB) was successfully found for the Diketopyrrolopyrrole-based narrow bandgap polymer under investigation in this work, with a much larger working operation window (up to 80%) and higher device efficiency than DIO. The reason for improved performance lies in higher hole mobility due to polymer crystallinity enhancement in films cast from solution processed by both additives,

as demonstrated by Transmission Electron Microscopy (TEM), photoluminescence (PL) and Grazing Incident Wide Angle X-ray Scattering (GIWAXS) results. Small Angle Neutron Scattering (SANS) and UV-visible absorption spectroscopy were also conducted on polymer structures in solution, and their results revealed a novel working mechanism of DCB for morphology control, which involves the modified solution-stage polymer conformations due to the polymer-additive interaction. Upon incorporating DCB into blend solution, the resultant polymer configurations in solution would have a high tendency to preserve into crystalline regions in the as-cast films and this unique way of tuning thin-film morphology via altering polymer conformations in solution has established a new guide for future additive selection in other polymer systems.

Results of this manuscript will resolve the current obstacle for high-throughput process in industry and should be of great potential to contribute to practical OPV applications in the near future.

The dissertation of Jing Gao is approved.

Benjamin J. Schwartz

Yu Huang

Yang Yang, Committee Chair

Univerisity of California, Los Angeles

2014

This dissertation is dedicated to my dearest parents, whose selfless devotion and consistent support encourage me to achieve what I have at this stage and go further in the future

Table of Contents

List of Figures

List of Tables

Acknowledgements

In retrospect to the last five years' Ph.D. study at MSE & UCLA, I feel especially grateful for all the people who have helped me to achieve what I have accomplished now. First and foremost, I would like to express my sincere gratitude to my advisor Professor Yang Yang. His great perspective and guidance always encourage me to follow my own heart and pursue beyond my expectation and limitations.

I would also like to thank the members of my dissertation committee, Professor Benjamin J. Schwartz, Professor Yu Huang, and Professor Dwight C. Streit for their valuable inputs. Special thanks to Professor Schwartz for his detailed instructions, helpful suggestions and noticeable amount of time and efforts on shaping this work.

I am also expressing my most sincere gratitude for several YY lab members who contribute significantly to my academic achievement: Dr. Gang Li for his constructive guidance, Dr. Letian Dou, Mr. Johnny Chen and Mr. Wei-Hsuan Chang for their significant technical support and assistance.

Also here I wish to acknowledge the great experimental assistance and useful advices from Dr. Wei Chen in Argonne National Laboratory.

Finally, I would like to thank my family and friends: My dearest father and mother, relatives, classmates, colleagues and all the people accompanying me through the graduate life for their friendships and support.

VITA

2009	Bachelor of Science in Materials Chemistry
	Fudan University
	Shanghai, P.R. China
2011	Master of Science in Material Science and Engineering
	University of California, Los Angeles
	Los Angeles, CA

Publications

Journal papers

1. **Jing Gao**, Wei Chen, Letian Dou, Chun-Chao Chen, Wei-Hsuan Chang, Yongsheng Liu, Gang Li, Yang Yang, "Elucidating Double Aggregation Mechanisms in the Morphology Optimization of Diketopyrrolopyrrole-Based Narrow Bandgap Polymer Solar Cells'', *Advanced Materials* , **2014**, 26, 3142
2. **Jing Gao**, Letian Dou, Wei Chen, Chun-Chao Chen, Xuanrong Guo, Jingbi You, Brion Bob, Wei-Hsuan Chang, Joseph Strzalka, Cheng Wang, Gang Li, Yang Yang, "Improving Structural Order for a High-Performance Diketopyrrolopyrrole-Based Polymer Solar Cell with a Thick Active Layer'', *Advanced Energy Materials* ***2014***, 4, 1300739
3. Wei-Hsuan Chang, **Jing Gao**, Letian Dou, Chun-Chao Chen, Yongsheng Liu, Yang Yang,

"Side-Chain Tunability via Triple Component Random Copolymerization for Better Photovoltaic Polymers", *Advanced Energy Materials* ***2014***, 4, 1300864

4. Jingbi You, Letian Dou, Ken Yoshimura, Takehito Kato, Kenichiro Ohya, Tom Moriarty, Keith Emery, Chun-Chao Chen, **Jing Gao**, Gang Li, Yang Yang, "A polymer tandem solar cell with 10.6% power conversion efficiency'', *Nature Communications, 4, 1446*
5. Letian Dou, **Jing Gao**, Eric Richard, Jingbi You, Chun-Chao Chen, Kitty C Cha, Youjun He, Gang Li, Yang Yang, "Systematic investigation of benzodithiophene-and diketopyrrolopyrrole-based low-bandgap polymers designed for single junction and tandem polymer solar cells", *Journal of the American Chemical Society ,134 (24), 10071-10079*
6. Letian Dou, Wei-Hsuan Chang, **Jing Gao**, Chun-Chao Chen, Jingbi You, Yang Yang, ''A Selenium-Substituted Low-Bandgap Polymer with Versatile Photovoltaic Applications'', *Advanced Materials, 25 (6), 825-831*
7. Jingbi You, Chun-Chao Chen, Ziruo Hong, Ken Yoshimura, Kenichiro Ohya, Run Xu, Shenglin Ye, **Jing Gao**, Gang Li, Yang Yang, ''10.2% Power Conversion Efficiency Polymer Tandem Solar Cells Consisting of Two Identical Sub-Cells', *Advanced Materials ,25 (29), 3973-3978*
8. Chun-Chao Chen, Letian Dou, **Jing Gao**, Wei-Hsuan Chang, Gang Li, Yang Yang, ''High-performance semi-transparent polymer solar cells possessing tandem structures'', *Energy & Environmental Science ,6 (9), 2714-2720*
9. Yongsheng Liu, Chun-Chao Chen, Ziruo Hong, **Jing Gao**, Yang Michael Yang, Huanping Zhou, Letian Dou, Gang Li, Yang Yang, ''Solution-processed small-molecule solar cells: breaking the 10% power conversion efficiency'', *Scientific reports, 3, 3356*
10. Letian Dou, Chun-Chao Chen, Ken Yoshimura, Kenichiro Ohya, Wei-Hsuan Chang, **Jing**

Gao, Yongsheng Liu, Eric Richard, Yang Yang, ‘‘Synthesis of 5 H-Dithieno [3, 2-b: 2′, 3′-d] pyran as an Electron-Rich Building Block for Donor–Acceptor Type Low-Bandgap Polymers’’, *Macromolecules 46 (9), 3384-3390*

Conference Presentations

1. Jing Gao, Wei Chen, Gang Li, Yang Yang, “Finely-tuning morphology of low band-gap polymer organic solar cells via mixed solvent”, Oral presentation, SPIE 2013, San Diego, CA

Chapter 1 Introduction

1.1 Polymer solar cells

Statics by the US Energy Information Administration show that the total world power consumption is ~ 10^{13} Watts in 2013 and is expected to reach ~ 10^{14} Watts in the next few years, due to the rapid population growth and industrial development at current stage.[1] However, such a high demand in energy has been exerting a tremendous pressure on those convention energy sources, such as coal and gas, the limited storage of which has caused world energy crisis since the last decade. On the other hand, in average a year, the total power received by the earth from the sun is ~ 10^{17} Watts.[1] Such a promising amount of solar energy, if utilized efficiently, would greatly relieve the global energy crisis , which is a major issue humans are confronting.

Solar cell devices, which convert electricity directly from sunlight, have been extensively studied since their invention in 1953.[2] Currently, a variety of different types of solar cells are under investigations for future applications, among them are various inorganic material-based PV devices, such as single crystal and amorphous semiconductor devices, III-V multi-junctions, polycrystalline alloy thin-films, and quantum dot nanotechnology.[3] However, due to their extremely high demand in material purity and crystallinity, the acquisition of these inorganic semiconductors usually requires a complex and multiple-step purification process, which increases production costs and causes environmental issues.[4]

Due to the issues mentioned above, there is a growing attention to developing organic-based PV technology, which is of relatively low-cost and environmental friendly.[5] In particular,

polymer solar cells have been developing at a fantastic rate over the past few years, with the highest reported power conversion efficiency (PCE) reaching over 10% (Figure.1.1).[6]

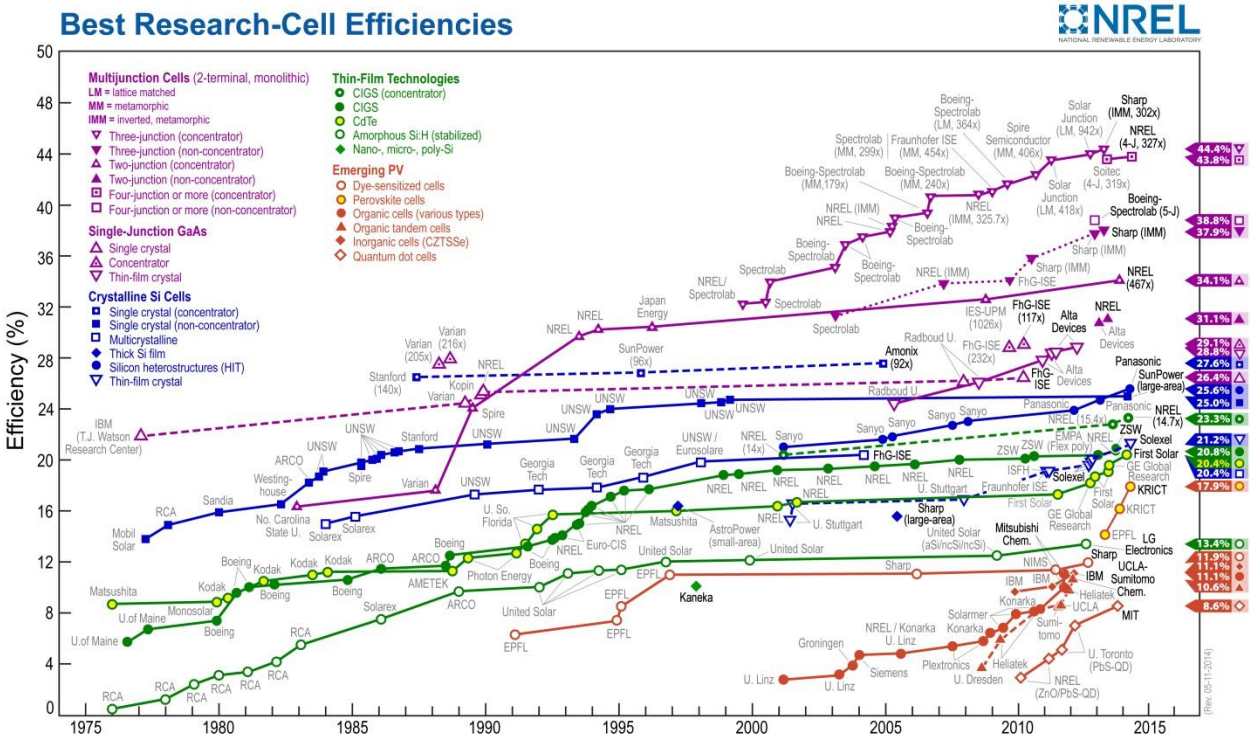

Figure 1.1 Research Cell Efficiency Records by National Renewable Energy Laboratory（NREL） [6]

In addition, polymer solar cells exhibit unique advantages. First, solution processability of polymers enables high-throughput printing techniques, which greatly enhances fabrication rate and lowers production cost. Second, polymer-based cells are light-weighted, suitable for portable devices. Third, their compatibility with flexible substrates exhibits a broad range of applications. Last but not least, the photo-electronic properties of polymer cells are tunable through rational molecular design. [7]

Organic Photovoltaic (OPV) dates back to 1979, when donor–acceptor heterojunctions were invented by Tang et al, who achieved power-conversion efficiencies (PCEs) ~ 1%.[5] Since then, polymer solar cells have become a popular research topic and their efficiency has risen at a swift pace: In 2005, Yang's group at UCLA proposed a novel solvent annealing method, which achieved a then-world record power conversion efficiency (PCE) of over 4% on devices made from the poly-thiophene derivative P3HT, certified by National Renewable Energy Laboratory (NREL).[8] In 2012, the same group successfully built a tandem polymer solar cell with certified efficiency over 10% and this milestone has kept its leading role in OPV field since then.[6]

Despite the prominent accomplishments achieved, at this stage, polymer solar cells still suffer from relatively low device efficiencies and stabilities.[9] Tremendous efforts are needed to address these issues before they can be considered equally competitive to their inorganic counterparts.

1.2 Working mechanism for polymer solar cells

One major difference between organic and inorganic semiconductor materials is the properties of their excitons, as shown in Figure 1.2.

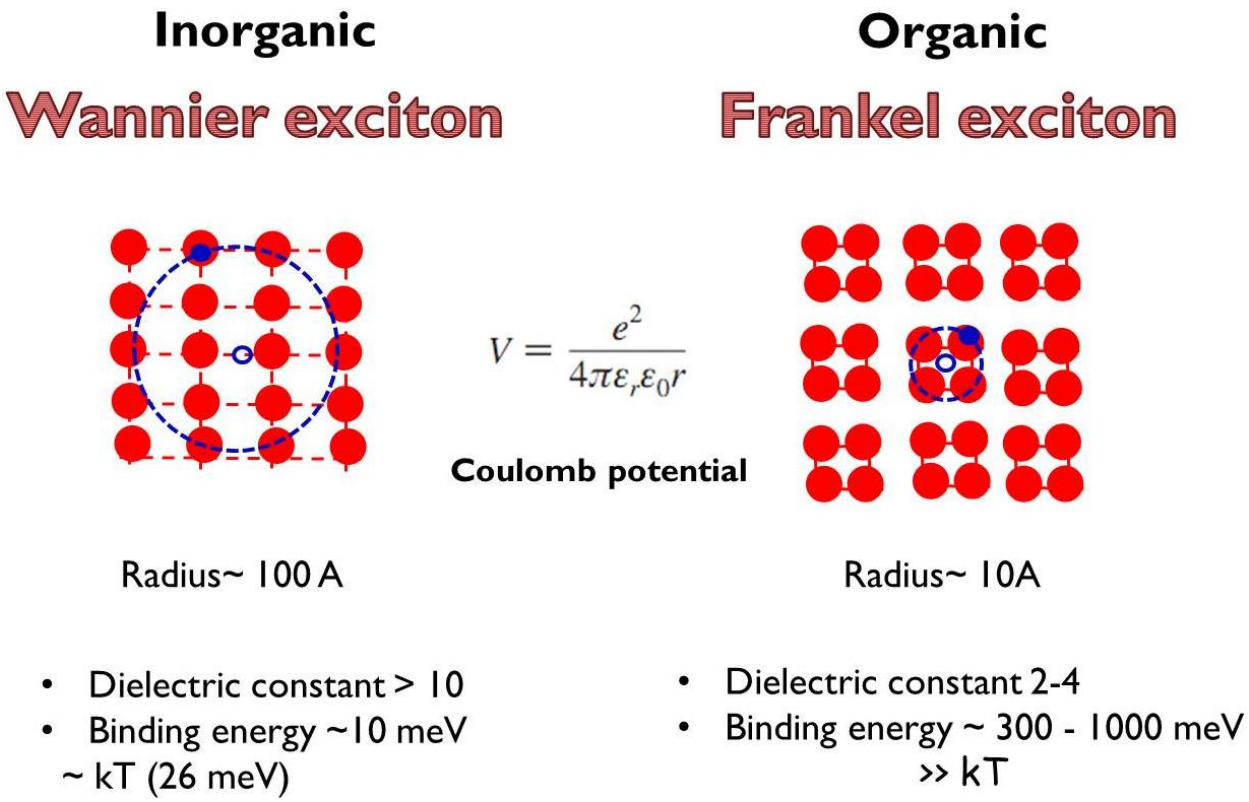

Figure 1.2 Comparison of exciton properties between inorganic/organic semiconductors

When photons are absorbed, their energy promotes an electron from the ground to an excited state, leaving a hole in the ground states. Generated electron and hole are bounded together by the Coulomb force. One such correlated electron-hole pair is referred to as an exciton. For inorganic semiconductors with a dielectric constant over 10, the radius of electron-hole pairs is of ~100 Å. This kind of excitons is called Wannier excitons, and their binding energy usually lies in the range of tens of meV. Such an amount of energy is easily overcome by lattice oscillations driven by thermal energy, which is usually ~26 meV in ambient environment. Therefore, inorganic excitons can be easily dissociated into free electrons and holes for current generation. For organic materials whose dielectric constant is between 2-4, the electrons and

holes are bound tightly within the radius ~ 10 Å and the corresponding electron-hole pairs are referred to as Frankel excitions. Their exciton binding energy can be as much as ~0.3 eV or even higher, which necessitates an extra driving force to efficiently split these excitons into mobile carriers. [10]

This problem can be addressed by blending two materials with different energy levels. One is called the donor, such as MEH-PPV and poly-thiophene derivatives, P3HT, whose structures are shown in Figure1.3. [11]

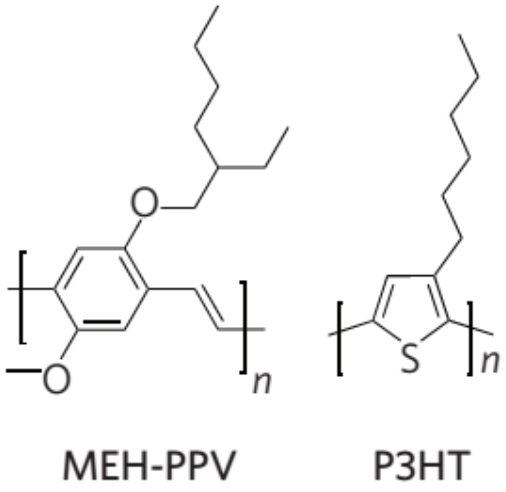

Figure 1.3 Chemical structures of firstly discovered donors [11]

The other component is called the acceptor, which are mostly fullerene derivatives, such as PCBM, bis-PCBM, ICBA etc, shown in Figure 1.4.[12]

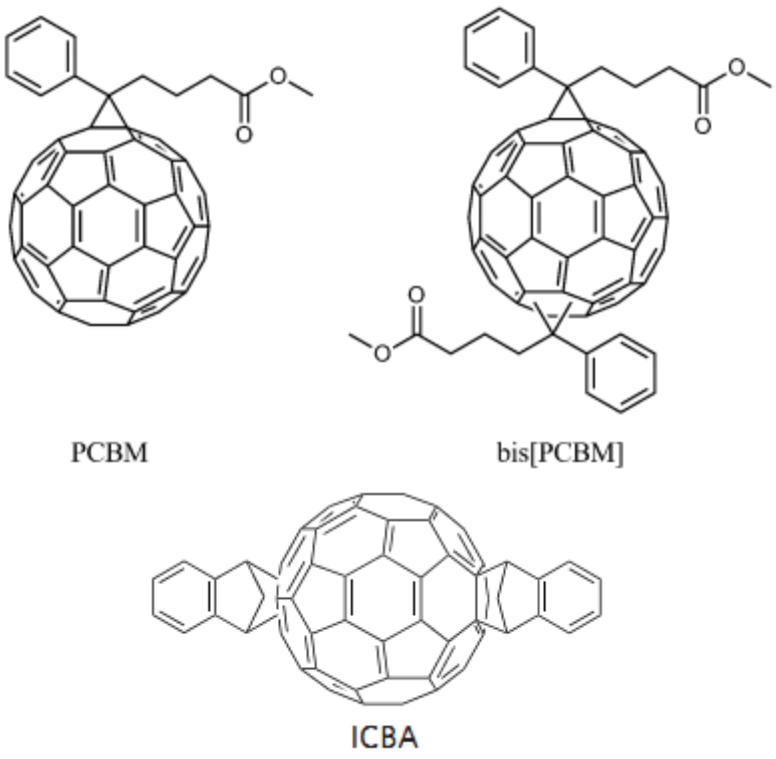

Figure 1.4 Chemical structures of typical acceptors [12]

Their difference in electron affinity provides a sufficient driving force for exciton dissociation. First, excitons are created within donor phases, and then they diffuse through the donor matrix towards the boundary. Once reaching the donor / acceptor interface, excitons dissociate into mobile electrons and holes. Separately, holes travel through the donor phase and electrons go through the acceptor phase to be collected at their respective electrodes. This photocurrent generation process is schematically illustrated in Figure 1.5[5]:

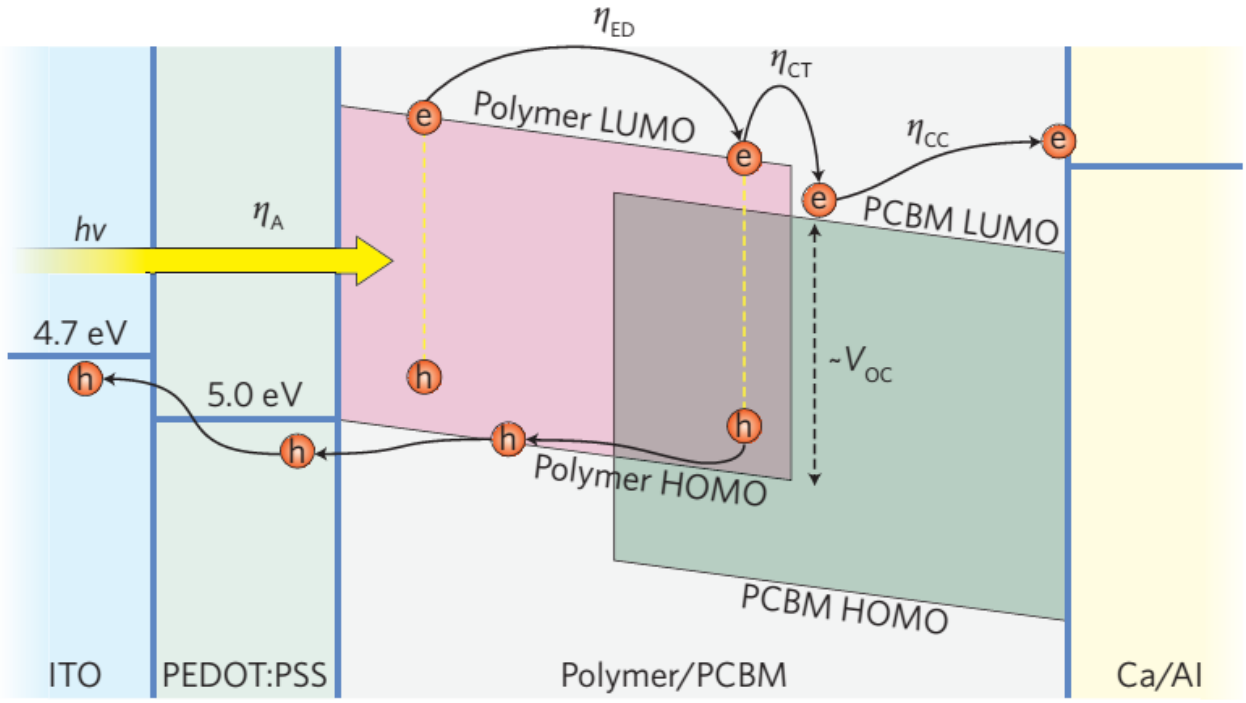

Figure1.5 Photocurrent generation process [5]

A complete photocurrent generation process is composed of four intermediate steps, and the product of each step's efficiency determines the total current value, as illustrated in Figure 1.6.[13] *J*sc is determined by the product of the efficiency of each step, including: light absorption efficiency, exciton diffusion efficiency, charge separation efficiency and charge collection efficiency. In order to achieve as high a photocurrent as possible, all four parameters need to be optimized simultaneously, and this will be discussed in detail in Section 1.4.1.

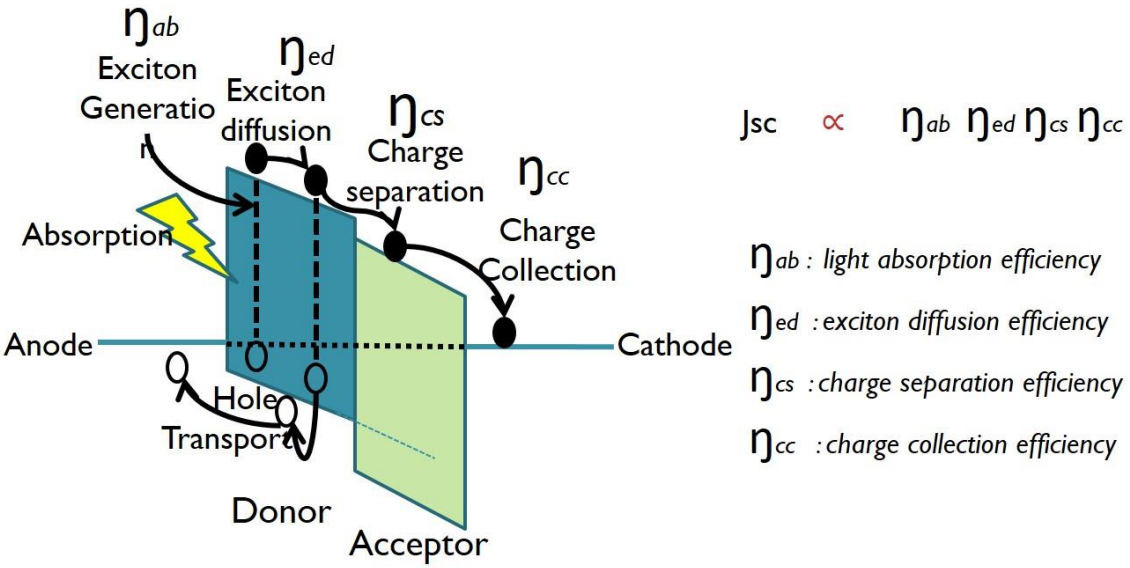

Figure1.6 Split of Jsc into the product of efficiency of four intermediate steps

However, after generation of mobile electrons and holes, during their migration towards respective electrodes, recombination between them would prevent efficient charge collection at the electrode, and this is one critical obstacle for reaching high solar cell efficiency. The degree of recombination is closely correlated with the recombination mechanisms. For a typical polymer solar cell, there are four major recombination mechanisms, which are presented in Figure 1.7. [7]

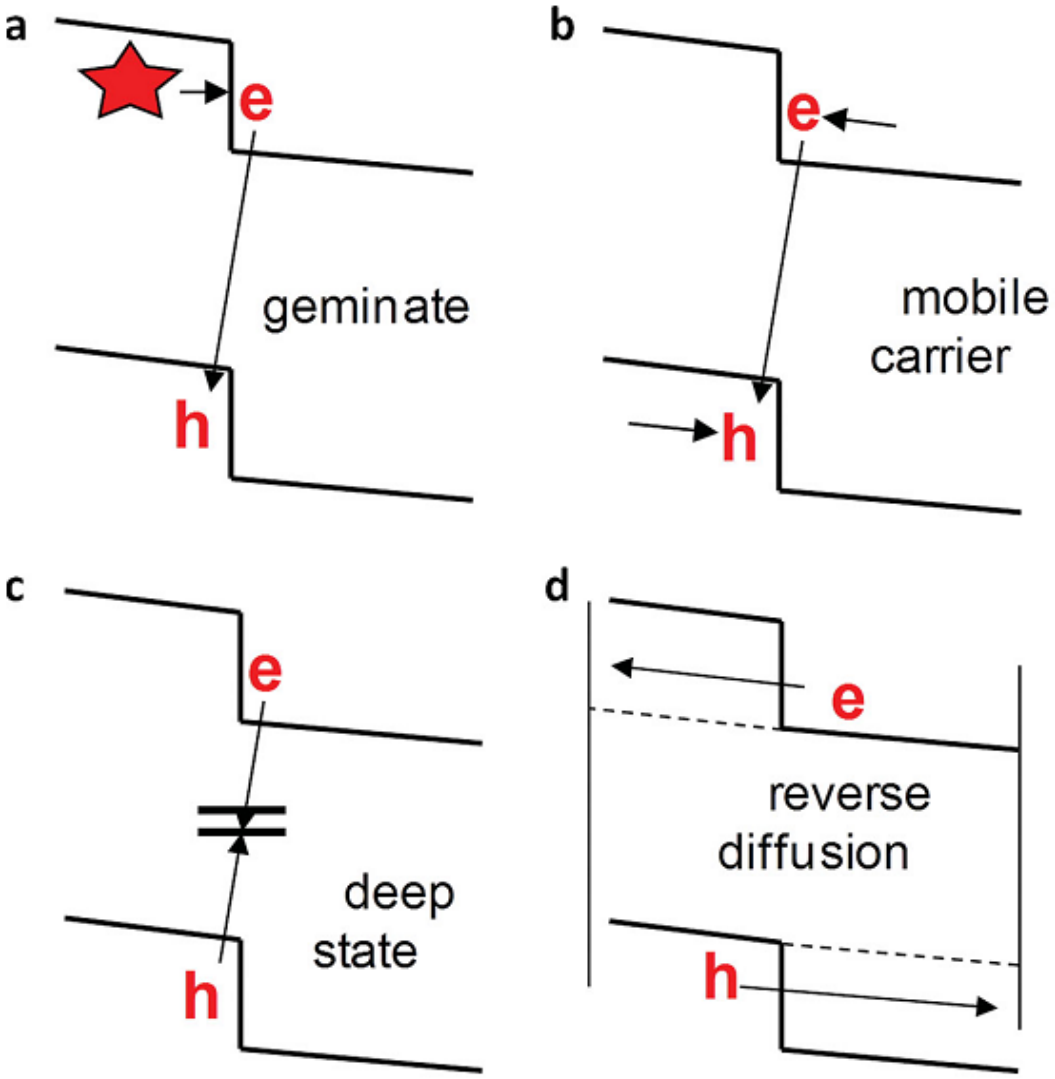

Figure 1.7 Different types of recombination mechanisms in polymer solar cells [7]

Generally speaking, recombination mechanisms are distinguished by their recombination order. First-order mechanisms are proportional to the free carrier concentration, while second-order recombination is determined by the square of the free carrier concentration.[7] Geminate recombination (Figure 1.7a) happens when the Charge-Transfer (CT) state recombines before being dissociated into free electrons and holes and it is a first order mechanism.[14] Mobile free

carrier (Langevin) recombination (Figure 1.7b) involves the annihilation of mobile electrons and holes, [15] and thus is a second-order process. Recombination involving the localized states (Figure 1.7c), which occurs between a mobile hole and a trapped electron, [16] is an important mechanism strongly dependent on the deep state density. Reverse diffusion to the contact (Figure 1.7d) is the recombination that takes place when an exciton dissociates in vicinity of the electrodes, and a "wrong" carrier diffuses in the opposite direction to the internal field and recombines at the electrode. [17] This situation is usually rare, but can become dominant in the absence of other mechanisms.

During the process when the film is cast from solution, donors and acceptors can phase-separate into a binary interpenetrating network, which is referred to as bulk heterojunction (BHJ), shown in Figure 1.8.[5] Efficient exciton dissociation occurs in bulk heterojunctin , where a large donor/acceptor interface is created throughout the film.

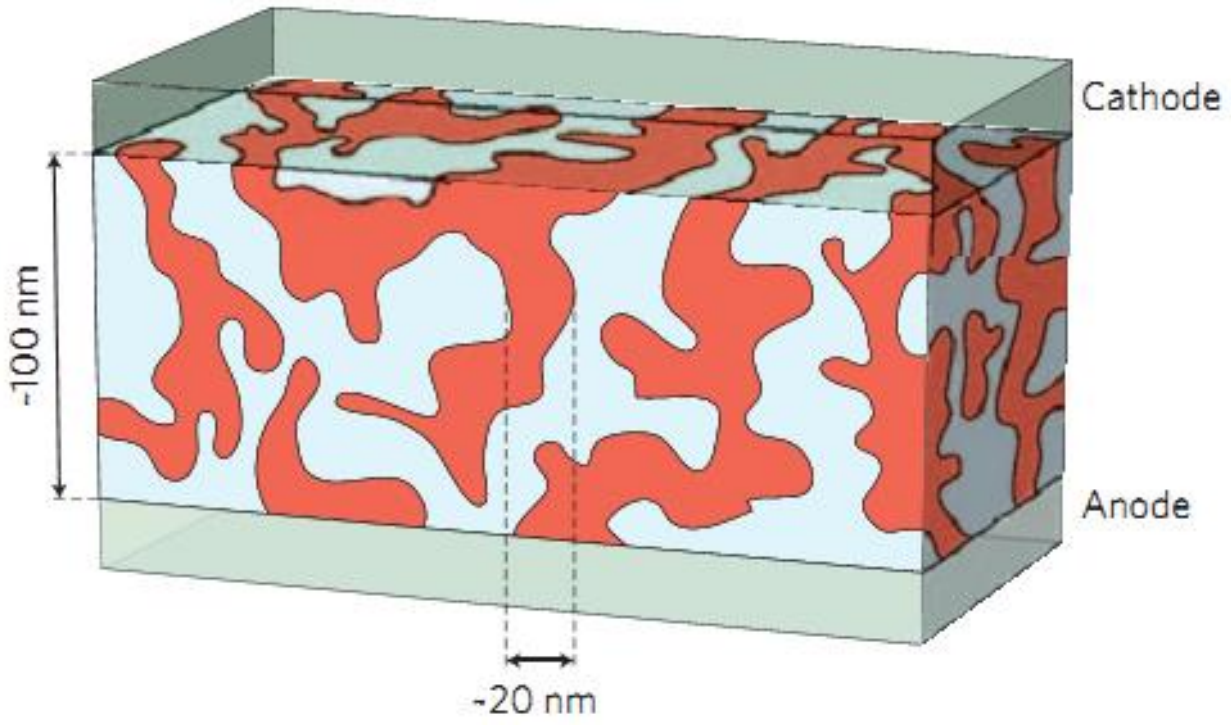

Figure 1.8 Donor & Acceptor Bulk heterojunction structures [5]

1.3 Device performance measurement

1.3.1 J-V measurement

Ideally, photovoltaic devices behave like diodes, with dark current/voltage (*J/V*) curves following the Shockley equation; in the dark in the reverse bias direction, little current flows. While in the forward bias direction, the current increases exponentially with applied voltage. [18] When the OPV (diode) is illuminated, the *J/V* curve is ideally shifted down at all potentials by the magnitude of J_{sc}, the short-circuit photocurrent. It is in the third quadrant of the *J/V* curve (see Figure 1.9) where power can be generated in an external load. This is demonstrated in Figure 1.9.

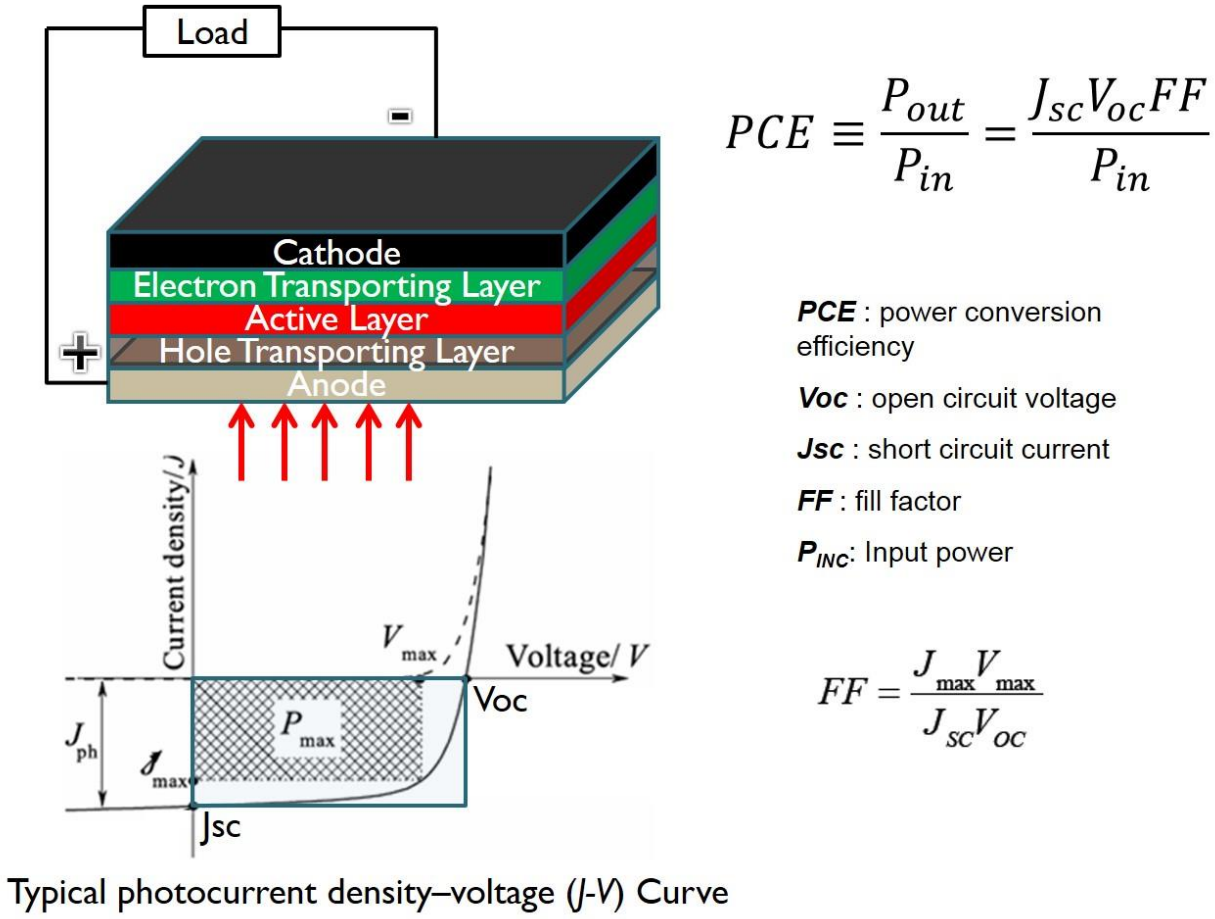

Figure 1.9 Photo I-V curves and related parameters for a typical polymer solar cell

The maximum power obtainable from an ideal OPV is the product of J_{sc} and the "open-circuit" photovoltage V_{oc} (the voltage obtained for this device at zero current) ($P_{theory} = J_{sc}*V_{oc}$). Real OPVs, however, generate substantially less power, which occurs where real current/voltage products reach their maximum value: $P_{max} = J_{max}*V_{max}$. The power conversion efficiency is then defined: $(P_{max}/P_{solar})*FF$, where P_{solar} is the power from the illumination source (sun) and FF is the "fill factor" defined as P_{max}/P_{theory}. [19]

1.3.2 External Quantum Efficiency (EQE)

The External Quantum Efficiency (EQE) is defined as the ratio of the number of charge carriers collected by a solar cell, to the number of incident photons of a given energy, as shown in Figure 1.10.

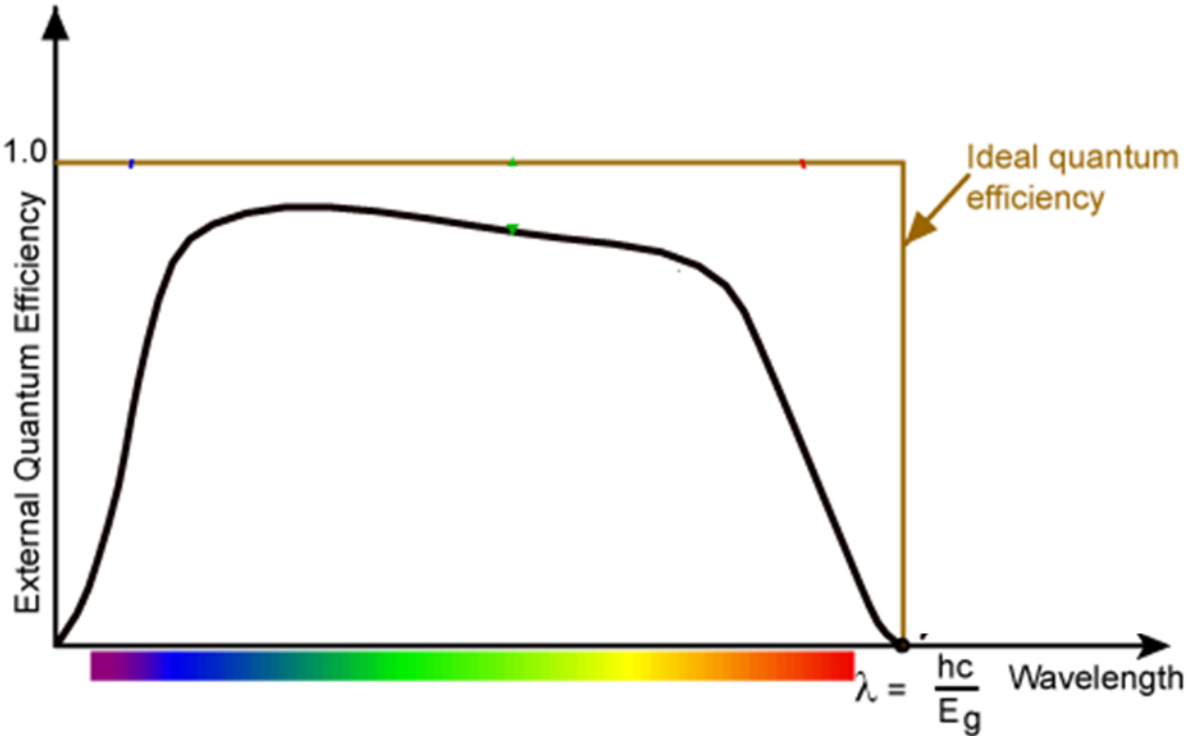

Figure 1.10 External Quantum Efficiency [16]

EQE measurements provide information on the amount of current that the cell will produce when irradiated by photons of a particular wavelength. The J_{sc} is equal to the integral of the EQE over the range of wavelengths with photoresponse, and is thus a product of the cell's responsivity and the incident solar spectral irradiance. [20]

As a result, the EQE is correlated with both the material's absorption spectrum and the device internal quantum efficiency. The first of these depends on intrinsic properties of polymers, such as the band gap and energy level. Polymers whose absorption spectrums match well with the solar spectrum will exhibit high absorption coefficients and produce large numbers of excited states, exhibiting high light absorption efficiency. Figure 1.11 shows a comparison between solar spectrum and the photoresponse of a P3HT: PCBM solar cell. As observed, P3HT-based devices can only absorb photons up to 650 nm and this limits its current to only ~10 mA/cm^2. As a result, low-band-gap (generally smaller than 2 V) polymers whose absorption range extends into the infrared region compose the majority of high performance materials. [21]

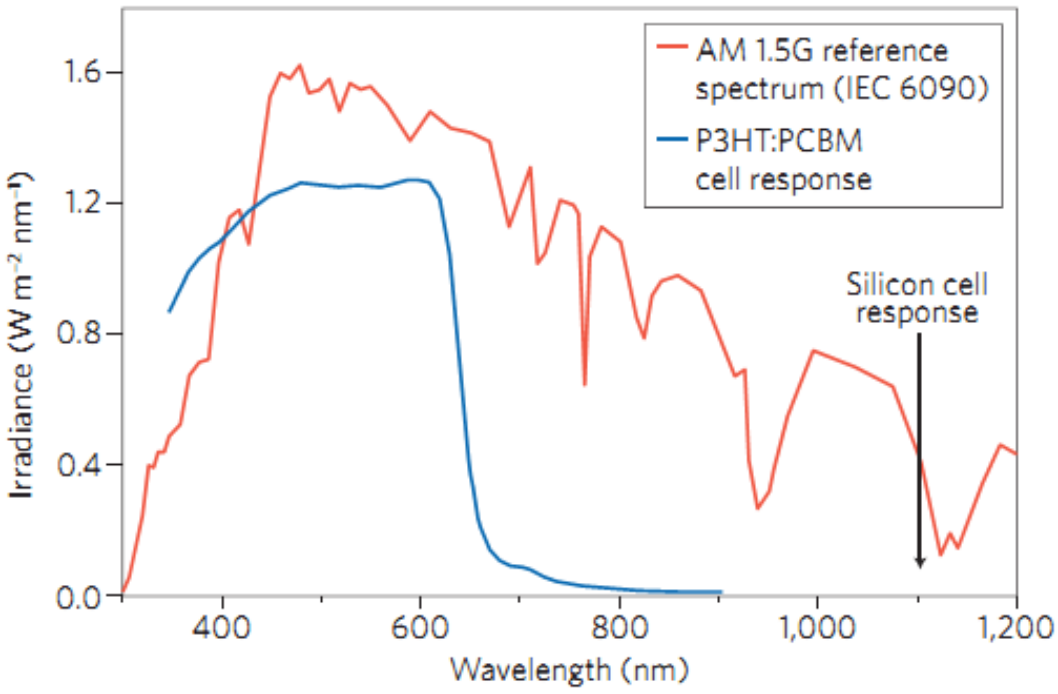

Figure 1.11 Solar spectrums vs. photo response of a P3HT: PCBM solar cell [5]

EQE is also influenced by internal quantum efficiency (IQE), defined as the ratio of the number of charge carriers collected by the solar cell to the number of photons of a given energy that shine on the solar cell from outside and are absorbed by the cell. IQE is mostly dependent on how well mobile carriers are collected at the electrode and its value is strongly morphology-related, which will be discussed later in Section 1.4.

Another thing worthy of noting is that the external quantum efficiency of a solar cell includes the effect of optical losses such as transmission and reflection, which makes the device performance interpretation more complicated. [22]

Recent studies have been focused on multiple exciton generation (MEG), through which EQE greater than 100% may be achieved when the incident photons have more than twice the band gap energy, creating two or more electron-hole pairs per incident photon.[23] The details of MEG are beyond the discussion in this work.

1.4 Morphology in bulk heterojunction polymer solar cells

1.4.1 Criteria for optimum morphology

The spatial arrangements of donor & acceptor phases at various length scales are referred to as morphology, which has a profound influence on device performance, as illustrated in Figure 1.12:

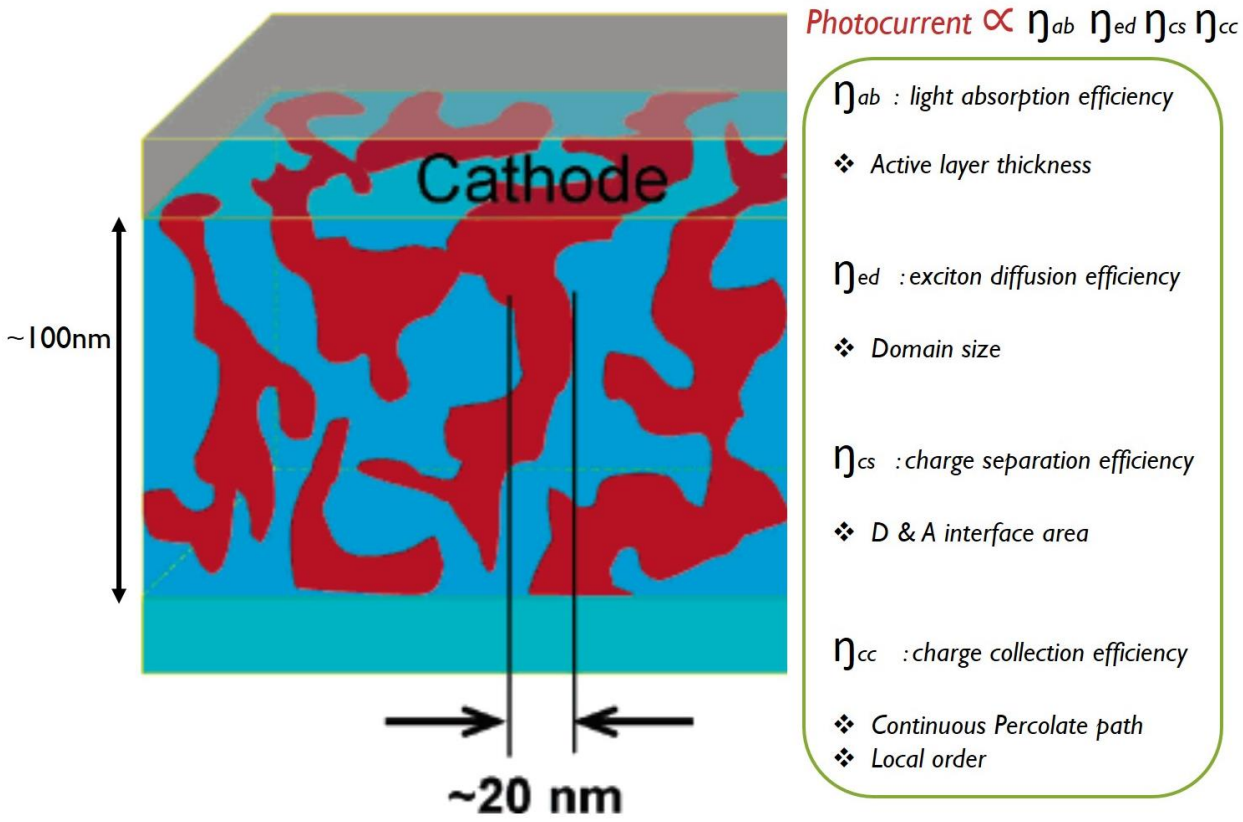

Figure 1.12 Requirements for desired morphology in PSCs

First, the thickness of the active-layer determines how many chromophores are there for light absorption. As polymers usually possess high absorption coefficients in the range of 10^4 to 10^5 /cm,[24] for a typical device with a weight ratio of 1:2 between polymer and fullerenes, ~100 nm's thickness will be good for efficient absorption. Even though thicker film is strongly desired in terms of absorption, active-layers of typical polymer solar cells could only achieve the thickness of ~100 nm, and the reason will be discussed in the following paragraphs.

Second, excitons have a diffusion length ~ 10 nm; this requires the polymer phase to be less than 20 nm in any dimension. Beyond that, excitons will recombine and give rise to

photoluminescence (PL) instead of separating into conductive electron and holes. As a result, donor domains should be kept at a proper size to assure efficient exciton dissociation. [5]

Third, a vast quantity of interface area is desired for efficient exciton dissociation, necessitating a large degree of phase-separation between the donor and acceptor phases. This is relatively easy to achieve in BHJs, as they naturally possess large quantity of interface areas. However, too many heterojunctions will disturb the completeness of one-component-rich domains, affecting carriers' transport inside the single-phase matrix. Therefore, a proper degree of phase-separation with a balance between exciton dissociation and carrier transport will be greatly appreciated.

Last but most importantly, in order to obtain high charge collection efficiency, a percolated continuous pathway is needed for both materials, as well as a large degree of structured-order to ensure high carrier mobility. However, due to their complex molecular structure, polymers usually forms domains with low crystallinity and a large density of defects, which increases the probability of carrier scattering or recombination, giving rise to a low carrier mobility. As a result, the active layer usually lies within a thickness of ~100 nm for a balance between carrier transport and absorption. [24]

In addition, vertical segregations of donor and acceptor phases also have an effect on carrier transport, and this leads to the devices' preference on certain electrode materials over others, justifying the advantages of inverted device structures over regular ones. [25]

1.4.2 Morphology characterization techniques for PSCs

1.4.2.1 Phase & domain separation

The degree of phase-separation can be characterized through techniques with resolutions of a few tens of nanometers, such as atomic force microscopy (AFM), scanning electron microscopy (SEM), and transmission electron microscopy (TEM). Figure 1.10[7] shows images obtained by these techniques conducted on a typical PSC active layer. Images acquired via these techniques usually exhibit two-dimensional features composed of binary phase-separations, the contrast of whom would be severely affected by the film thickness and surface purity. This leads to the uncertainty in data interpretation and the difficulty in linking morphology to device performances. As a result, techniques listed above could be used as complementary tools to support those more direct and convincing characterization techniques, such as X-rays and Neutrons analysis, which will be discussed in next section.

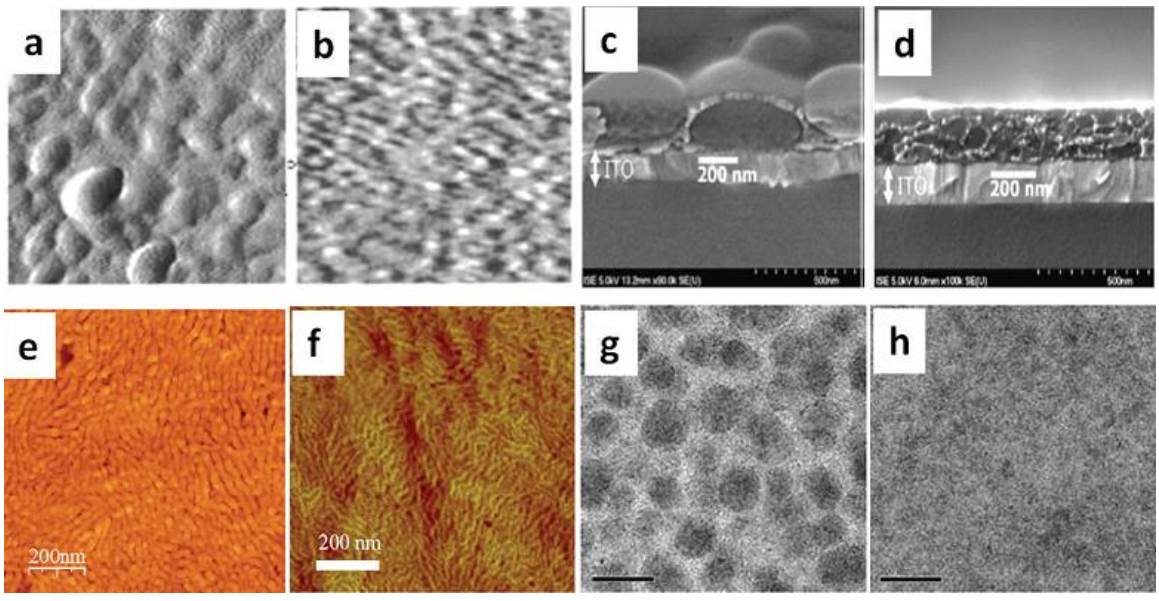

Figure 1.13[7] (a) AFM images of the MDMO-PPV: PCBM films cast from toluene and (b) CB. (c) SEM cross-section views of the MDMO-PPV: $PC_{61}BM$ films casted from toluene and (d) from CB. (e) AFM phase image of high crystalline P3HT:$PC_{61}BM$ films achieved using solvent annealing and (f) additive approaches. (g) BF-TEM images of PTB-7:$PC_{61}BM$ film casted using CB as major solvent with and (h) without DIO as additive. Polymer molecular orientation and domain crystallinity characterization

1.4.2.2 Molecular orientation & Packing manner

Currently, Grazing-incident Wide Angle X-ray Scattering (GIWAXS) is among the well-received techniques for investigating the details of polymer orientation and crystalline structure in thin films. Low crystallinity of most polymers applied in OPV requires a synchrotron beam line with a high energy and well collimated X-rays.[26] The incident X-rays are set at the grazing angle to enhance surface scattering intensity and maximize signal to noise ratio to accurately access structures at molecular level.

There are two types of polymer packing manner, referred to as face-on and edge-on, as shown in Figure 1.14. A plane formed by the backbones of polymer (main chain) is called a π-plane, who can be stacked over one another. When π-planes are placed vertically to the substrate, it is called an edge-on stacking orientation. In comparison, when π-planes are parallel to the substrate, they are stacked in a face-on orientation. For most low-band-gap polymers with relatively complex chemical structures, face-on is the dominating packing manner and the extent of packing determines carrier mobility.[27-30] In a 2-D GIWAXS profile, spacing between lamellar edges leads to (n00) reflections and spacing between π-planes gives rise to (0n0) reflections, as shown in Figure 1.14. Orientations of polymer crystallites with respect to the

substrate can be identified from the distributions of peak position and intensity between (n00) and (0n0) reflections. [27]

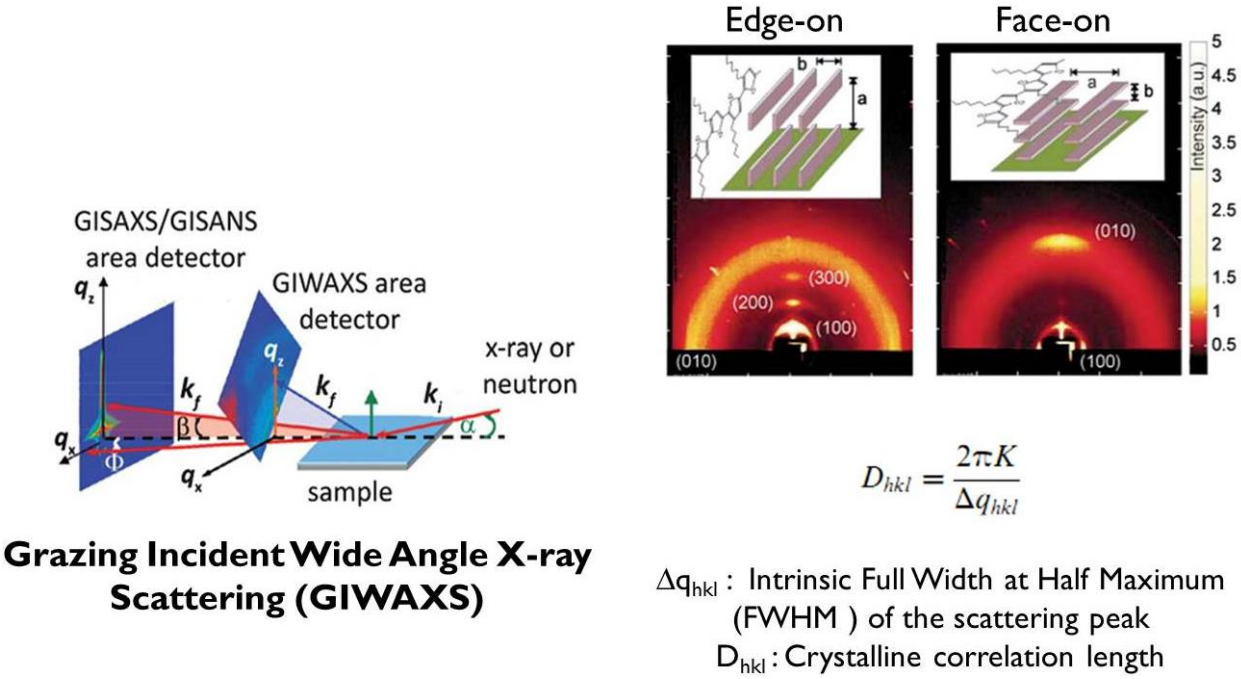

Grazing Incident Wide Angle X-ray Scattering (GIWAXS)

Figure 1.14 Characterizations of Polymer packing orientation and domain crystallinity by GIWAXS

When blending with fullerene molecules, usually polymer packing order would be disrupted to a certain degree, which introduces twists and bends to polymer domains. This leads to difficulties and uncertainties in precisely assessing polymer packing and crystallinity within a BHJ, and solutions to this issue will be elaborated in section 2.3.4.

1.5 Methodology for morphology control

The achievements of device performance optimization have been realized through chemical structure modification on donors and acceptors[28][29][30], improvement in active-layer processing methods[31][32][33][34], interfacial morphology control[35][36][37] and device structure engineering.[38][39][40] In the following paragraphs, a detailed discussion on rational engineering of chemical structure modification and processing additive selection is given.

1.5.1 Materials design

Innovations in materials science have provided efficient a variety of efficient ways to achieve the desired morphology. As films are cast through solution processing, the solute-solvent interactions based on their respective functional groups would have a substantial impact on the morphology in the resultant films, such as the degree of phase-separation and domain purities. As a result, morphology is tunable through modifications on the molecular structures of both donors and acceptors, [38] which will be discussed in section 1.5.1.1 and 1.5.1.2.

1.5.1.1 Donor materials

Over the past ten years, a couple of synthetic rules have been applied to donors and have successfully achieved morphology favorable for device performance.[7] These strategies include : adopt alternating electron-rich (donor) and electron-deficient (acceptor) units to form D-A co-polymers on the main chain for lowering band-gap purposes; search for conjugated units who possess stabled quinoid resonance structure; modify the backbone chemical structures with strong electron withdrawing functional groups such as carbonyl or fluorine atoms; finely-tune the

aliphatic alkyl side chains to change the solubility.[39][40] The way how modifications of structure promote the formation of desired morphology is illustrated in the literature.[41][42][43] Figure 1.15 shows some donor compounds synthesized following the rules mentioned above, who have been demonstrated to achieve the preferred morphology in terms of efficiency. [7]

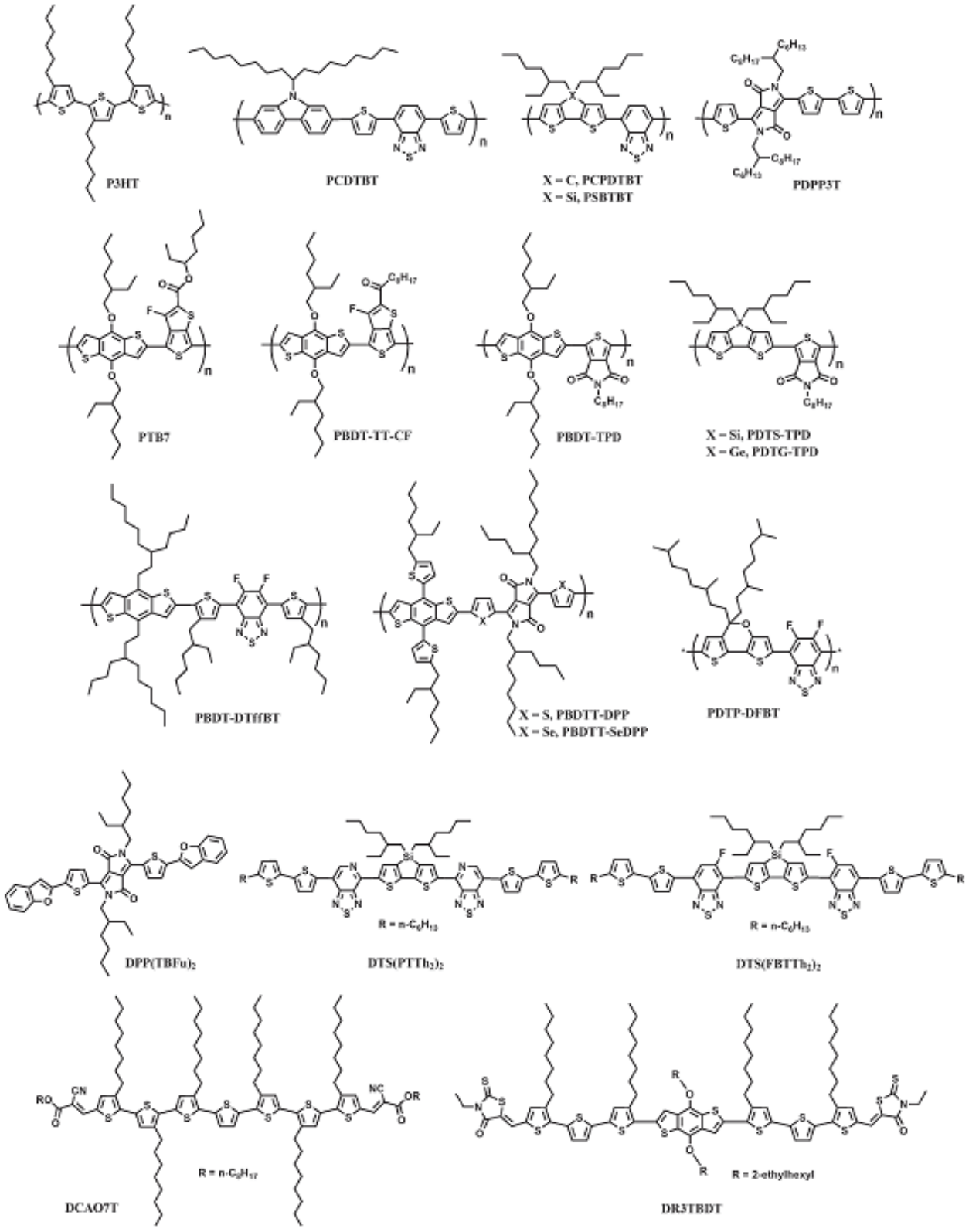

Figure 1.15 Chemical structures of some high performance donor materials [7]

1.5.1.2 Acceptor materials

Investigations on acceptor chemical structure have also been conducted at a large scale over the past years. In 1995, a soluble C_{60} derivative $PC_{61}BM$ (synthesized by Wudl et al.) was used as an acceptor and blended with a conjugated polymer donor by Heeger et al.[43] Since then, $PC_{61}BM$ and its corresponding C_{70} derivative $PC_{71}BM$ (first reported by Janssen et al.) have been widely utilized in BHJ OPV devices and achieved excellent performance. Although chemists have been trying hard in search of alternative acceptors, including chemical modifications on structures of both fullerene derivatives and non-fullerenes, at this stage $PC_{61}BM$/$PC_{71}BM$ is still the best acceptors for most low-band-gap polymers.

Length, shape and size of side chains on bulky balls would have effects on spatial arrangements of PCBM molecules within acceptor phases and at donor-acceptor interfaces.[24] During the film casting process, PCBM's side chains would affect both PCBM-polymer and PCBM-solvent interactions strongly in the solution, leading to differences in size and purities of fullerene domains in the as-deposited thin film. As a result, majority of the chemical modifications on PCBM molecules are focused on side-chain tuning.[44] Figure 1.16[7] shows some acceptors materials with excellent processing properties, who are of a great potential to achieve the desired morphology for high-performance devices.

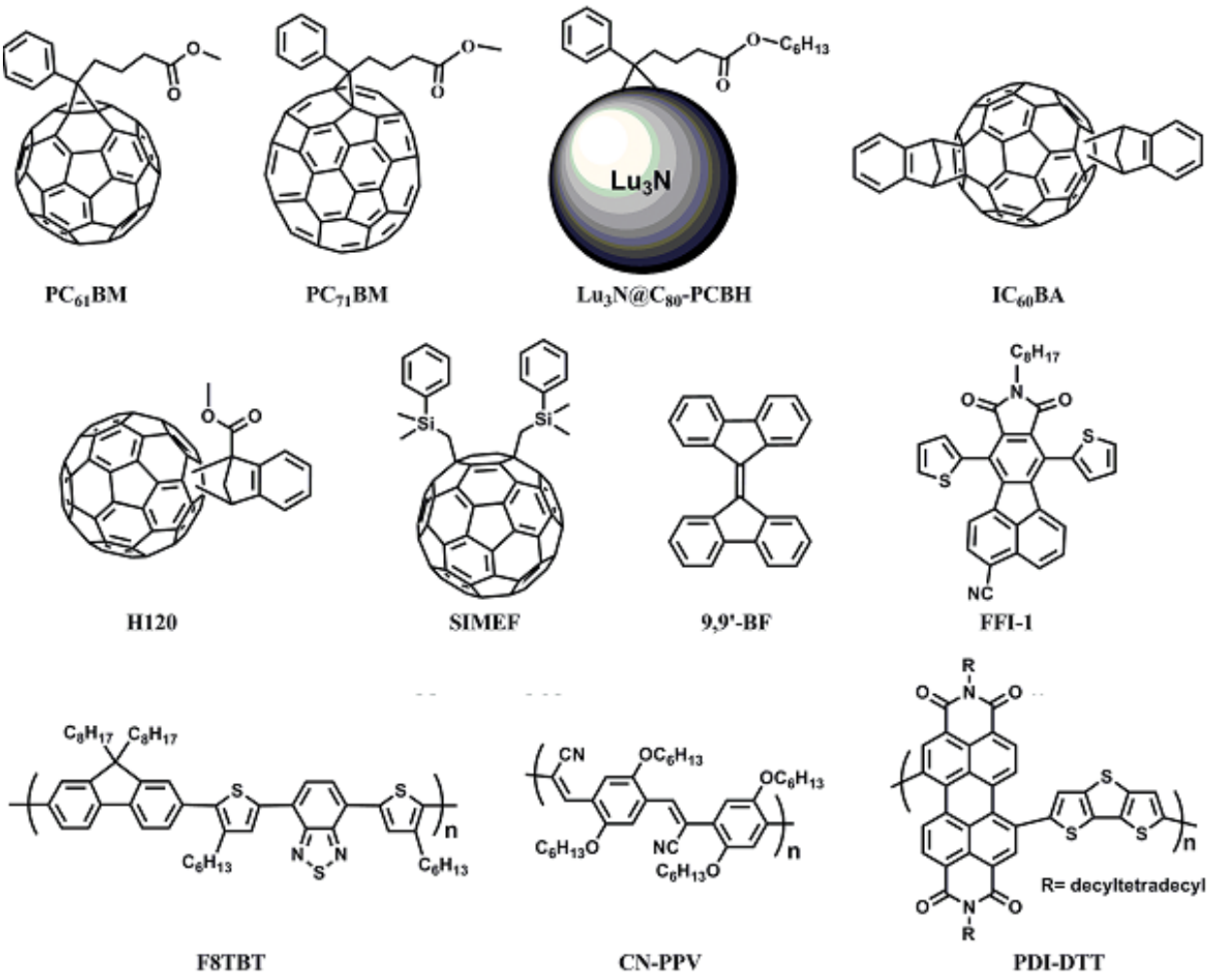

Figure 1.16 Chemical structures of some high performance n-type materials including fullerene and non-fullerenes derivatives [7]

1.5.2 Processing engineering

Thermal annealing [32] and solvent annealing [45] are among the most commonly used processing methods for morphology optimization. Other approaches, such as co-solvent [45] [46] and processing additives [31] have also been well-received by different low-band-gap polymer systems and gradually become routines for processing novel materials .

1.5.2.1 Thermal annealing

Post annealing of the as-cast film at elevated temperatures was demonstrated to improve PSC morphology to a pronounced degree by Heeger et al in 2005.[32] They found that the fast evaporation of solvents does not allow enough time for the polymer chains to stack into highly ordered regions. Thermal energy promotes polymer chains to reorganize into more stable and ordered structures. The resultant polymer domains have a significantly enhanced crystallinity, as shown in Figure.1.17 [5], indicated by fibril structures of polymer chains distributing throughout the film in both lateral and vertical directions.

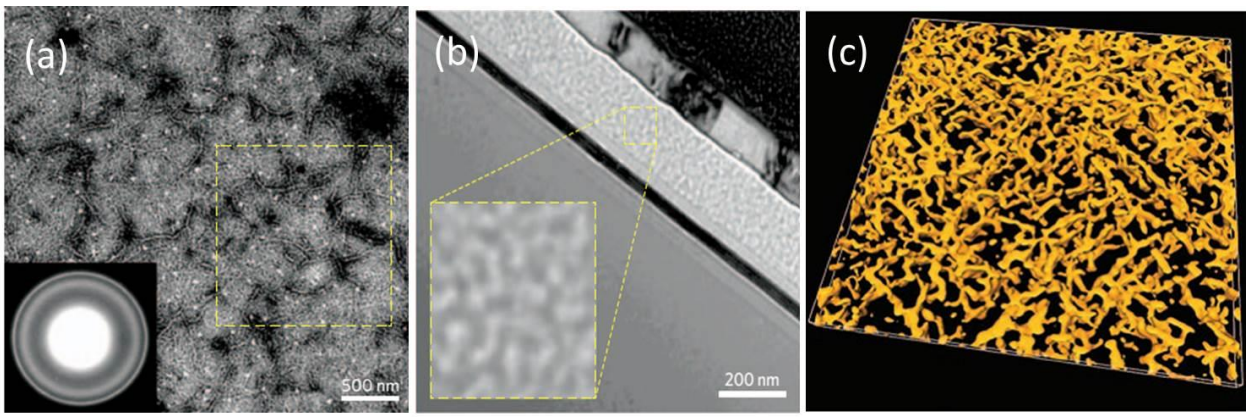

Figure 1.17 Morphology in PSCs (a), TEM image of a thermally annealed P3HT: PCBM film73. (b), Defocused cross-sectional TEM image of a P3HT: PCBM film c, Three-dimensional electron tomography image of thermally annealed P3HT–PCBM film [5]

1.5.2.2 Solvent annealing

It was not until 2005 that solvent annealing was shown to enhance PSC efficiency appreciably in Professor Yang Yang's group at UCLA.[45] By decreasing solvent evaporation

rate during the solvent removal process, sufficient time is allowed for P3HT chains to slowly stack in an ordered manner, giving rise to relatively high crystalline polymer domains. This is demonstrated in Figure 1.18 by GIWAXS. [7] In Figure 1.18, Sharp peaks of (n00) in the out-of-plane (OOP) direction provide clear evidence that the edge-on packing manner is dominating in P3HT domains in films processed by solvent annealing method. Therefore, due to their effects on thin-film morphology during the process of solution-to-film transition, evaporation rate of the processing solvents are of vital importance to achieve the desired morphology.

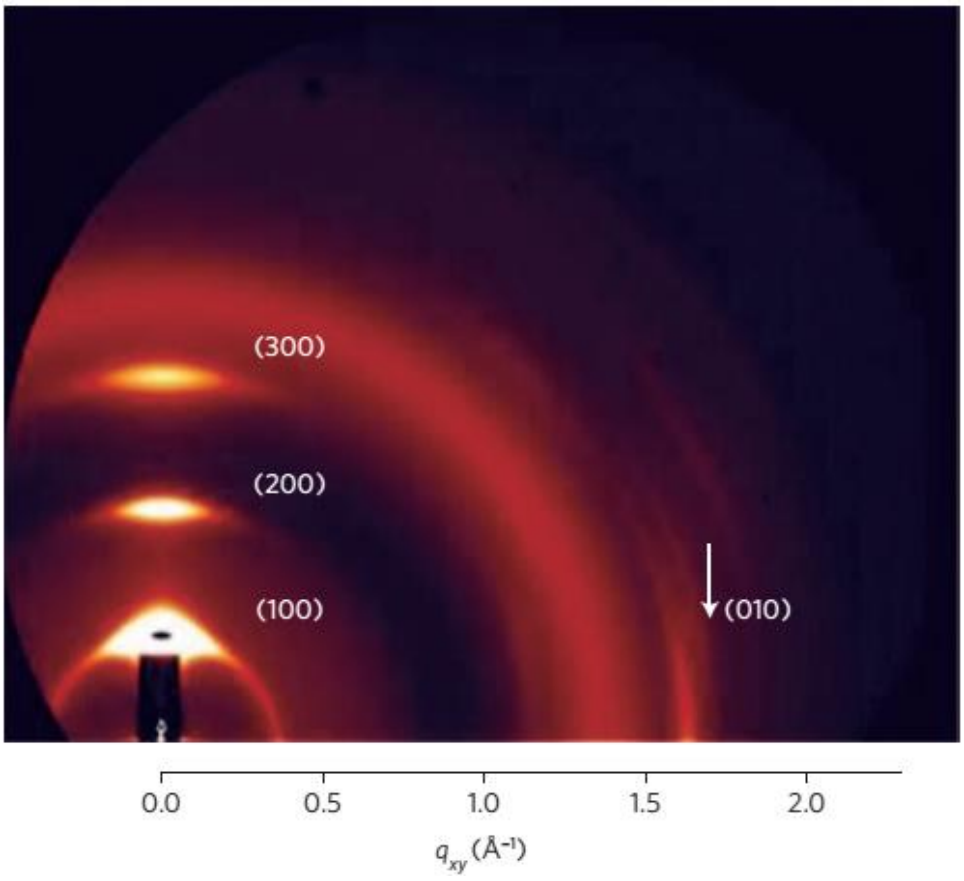

Figure 1.18 Grazing-incidence X-ray diffraction images of polymer–acceptor films of a highly crystalline P3HT: PCBM blend film by solvent annealing [7]

1.5.2.3 Additive & Solvent mixture

Additive & solvent mixture processing methods have been extensively used since the accidental discovery that devices whose active-layer was cast from solutions containing DIO residue exhibited surprisingly excellent photoelectric properties.[47-49] Zhang et al. found that the photocurrent density is significantly enhanced in polyfluorene copolymer/fullerene blends when chlorobenzene was added into chloroform.[46] Results of time-resolved spectroscopy demonstrated that charge mobility was influenced by additives and this lead to the increased current in device.[5]

An amorphous low band-gap polymer PCPDTBT was thoroughly studied by Bazan et al, and they found that through incorporating a few volume percent of alkanedithiols into the PCPDTBT/$PC_{71}BM$ blend solution, the device performance of the as-cast films is significantly improved from 2.8 % to 5.5 %.[31] According to the absorption data, they proposed that distributions between the polymer chains and/or between the polymer and fullerene phases are modified by alkanedithiols additive and this accounts for the efficiency enhancement. [31]

The additive approach is also useful for P3HT system. Figure 1.19[50] schematically illustrates the additive-assistant morphology formation process, a transition from solution-stage conformations to thin-film morphology during casting. The interactions between donor & acceptor & solvents are of vital importance for rational morphology control.[51] Generally speaking, differences in solvents' boiling point and solubility of solutes modify the degree of phase separation as well as molecular packing manners in both domains in films cast from solution.

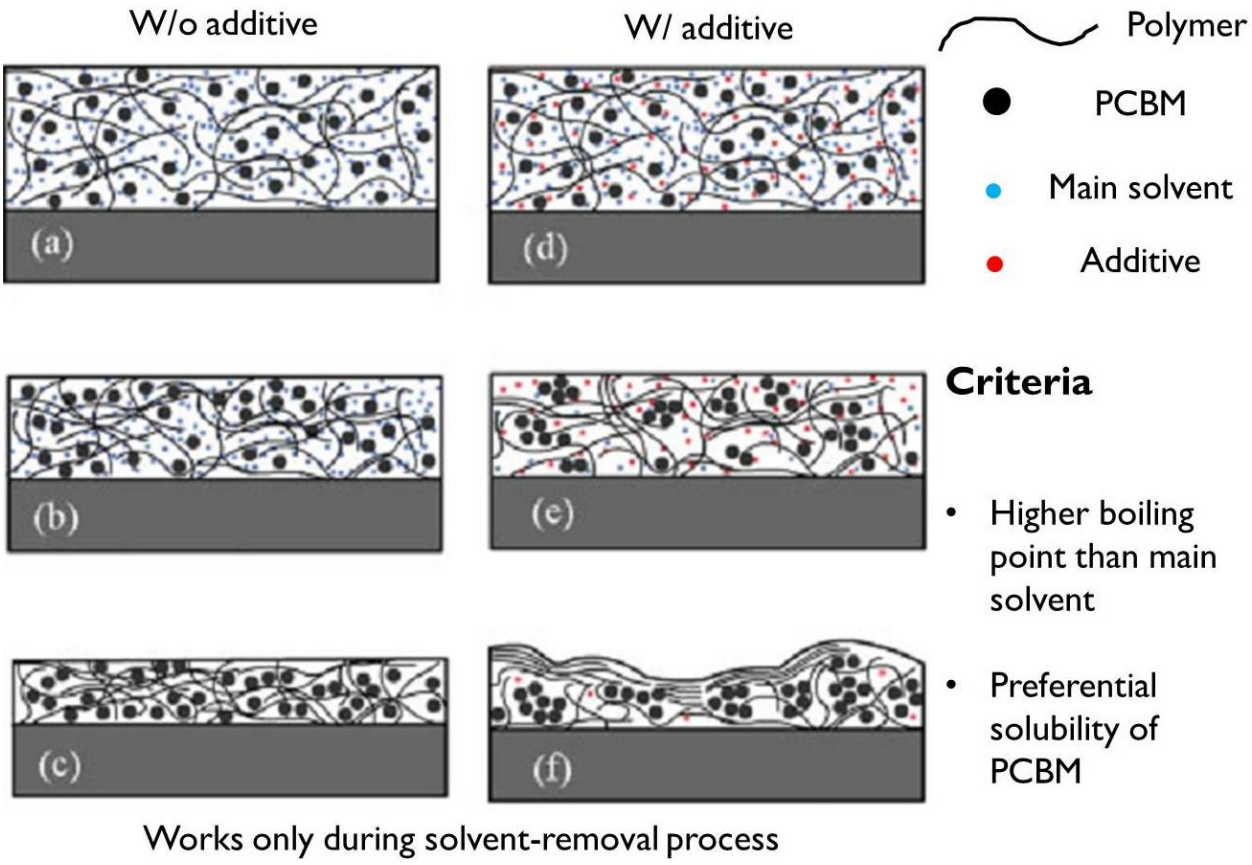

Figure 1.19 Working mechanisms for additive in morphology control [50]

The effects and working mechanisms of processing additives on morphology control will be elaborated in detail in chapter 3.

1.6 References

[1] http://www.nrel.gov/analysis/key_activities_jobs_pv_mfg_cost.html (accessed Mar 2013).

[2]S.-S. Sun, N.S.Sariciftci, *Organic Photovoltaics*, Boca Raton: CRC Press, Taylor & Francis Group, 2005. Print.

[3] M. A. Green, K. Emery, Y. Hishikawa, W. Warta, E. D. Dunlop, *Prog. Photovolt. Res. Appl.* **2012**, 20, 12.

[4] S. Gunes, H. Neugebauer, N. S. Sariciftci, *Chem. Rev.* **2007**, 107, 1324.

[5] G. Li, R. Zhu, Y. Yang, *Nat. Photon.* **2012**, *6*, 153.

[6] J. B. You, L. T. Dou, K. Yoshimura, T. Kato, K. Ohya, T. Moriarty, K. Emery, C.-C. Chen, J. Gao, G. Li, Y. Yang, *Nat. Commun*. **2013**, 4, 1446.

[7] L.Dou, J. You, Z.Hong, Z.Xu, G. Li, R. A. Street, Y.Yang, *Adv. Mater.* **2013**, 25, 6642–6671.

[8] G. Li, V. Shrotriya, J. S. Huang, Y. Yao, T. Moriarty, K. Emery, Y. Yang, *Nat. Mater.* **2005**, *4*, 864.

[9] F. C. Krebs, *Sol. Energy Mater. Sol. Cells* **2009**, 93, 394.

[10] B. C. Thompson, J. M. J. Frechet, *Angew. Chem. Int. Ed.* **2008**, 47, 58.

[11] A. C. Grimsdale, K. L. Chan, R. E. Martin, P. G. Jokisz, A. B. Holmes, Chem. Rev. 2009, 109, 897.

[12] J. H. Burroughes, D. D. C. Bradley, A. R. Brown, R. N. Marks, K. Mackay, R. H. Friend, P. L. Burns, A. B. Holmes, Nature 1990, 347, 539.

[13]I. McCulloch, M. Heeney, C. Bailey, K. Genevicius, I. Macdonald, M. Shkunov, D. Sparrowe, S.Tierney, R. Wagner, W.M. Zhnag, M. L. Chabinyc, R. J. Kline, M. D. McGehee, M. F. Toney, *Nat. Mater.* **2006**, 5, 328.

[14] M. Wojcik, M. Tachiya, *J. Chem. Phys*. **2009**, 130, 104107.

[15] K. Maturova, S. S. van Bavel, M. M. Wienk, R. A. J. Janssen, M. Kemerink, *Nano Lett.* **2009**, 9, 3032.

[16] L.Tsabari, N. Tessler, *J. Appl. Phys.* **2011**, 109, 064501.

[17] R. Sokel, R. C. Hughes, *J. Appl. Phys.* **1982**, 53, 7414.

[18] R.A. Street, M. Schoendorf, A. Roy, J. H. Lee, *Phys. Rev. B* **2010**, 81, 205307.

[19] K. Vandewal, A. Gadisa, W. D. Oosterbaan, S. Bertho, F. Banishoeib, I. Van Severen, L. Lutsen, T. J. Cleij , D. Vanderzande, J. V. Manca, *Adv. Funct. Mater.* **2008**, 18. 2064.

[20] P. W. M. Blom, V. D. Mihailetchi, L. J. A. Koster, D. E. Markov, *Adv. Mater.* **2007**, 19, 1551.

[21] R. A. Street, K. W. Song J. E. Northrup, S. Cowan, Phys. *Rev. B* **2011**, 83, 165207

[22] R. A. Street, D. Davies, P. P. Khlyabich, B. Burkhartb, B. C. Thompson, *J. Am. Chem. Soc.* **2013**, 135, 986.

[23] L. Tsabari, N. Tessler, *J. Appl. Phys.* **2011**, 109, 064501.

[24] J. Gao, L. Dou, W. Chen, C.-C. Chen, X. Guo, J. You, B. Bob, W.-H. Chang, J.Strzalka, C.Wang, G.Li, Y. Yang, *Adv. Energy Mater.* **2014**, 4, 1300739

[25] G. Li, C.-W. Chu, V. Shrotriya, J. Huang, Y. Yang, *Appl. Phys. Lett.* **2006**, 88, 253503.

[26] D. M. DeLongchamp, R. J. Kline, D. A. Fischer, L. J. Richter, M. F. Toney, *Adv. Mater.* **2011**, 23, 319.

[27] W. Chen, T. Xu, F .He, W. Wang, C. Wang, J. Strzalka ,Y. Liu, J. Wen, D. J. Miller, J. Chen, K. Hong, L. Yu, S. B. Darling, *Nano Lett*. **2011**, 11, 3707.

[28] W.-H. Chang, J. Gao, L. Dou, C.-C. Chen, Y. Liu, Y. Yang, *Adv. Energy Mater.* **2013**, 4, 1300864.

[29] H-Y. C., J.Hou, S. Zhang, Y. Liang, G. Yang, Y. Yang, L. Yu, Y. Wu, G. Li, *Nat. Photonics.* **2009**, 3, 649.

[30] Y. Li, *Acc.Chem.Res.* 2012, 45,723.

[31] J. Peet, J. Y. Kim, N. E. Coates, W. L. Ma, D. Moses, A.J. Heeger, G. C. Bazan, *Nat. Mater.* **2007**, 6, 497.

[32] W. Ma, C. Yang, X. Gong, K. Lee, A. J. Heeger, *Adv. Funct. Mater.* **2005**, 15, 1617.

[33] G. Li, V. Shrotriya, Y. Yao, Y. Yang, *J. Appl. Phys.* **2005** ,98, 043704 .

[34] F. Padinger, R.S. Rittberger, N.S. Sariciftci, *Adv. Funct. Mater. **2003***, 13, 85.

[35] V. Shrotriya, G. Li, Y. Yao, C.-W. Chu, Y. Yang, *Appl. Phys. Lett.* **2006**, 88, 073508.

[36] G. Li, C.-W. Chu, V. Shrotriya, J. Huang, and Y. Yang, *Appl. Phys. Lett*. **2006**, 88, 253503.

[37] M. S. White, D. C. Olson, S. E. Shaheen, N. Kopidakis, D. S. Ginley, *Appl. Phys. Lett.* **2006**, 89, 143517.

[38] L. Dou, J. Gao, E. Richard, J. You, C.-C. Chen, K. C. Cha, Y. He, G. Li, Y. Yang, *J. Am. Chem. Soc***. 2012,** 134, 10071.

[39] Y. J. Cheng, S. H. Yang, C. S. Hsu, *Chem. Rev.* **2009**, 109, 5868.

[40] Y. Y. Liang, L. P. Yu, *Acc. Chem. Res*. **2010**, 43, 1227.

[41] P. L. T. Boudreault, A. Najari, M. Leclerc, *Chem. Mater*. **2011**, 23, 456.

[42] Y. F. Li, *Acc. Chem. Res*. **2012**, 45, 723.

[43] a) A. J. Heeger, N. S. Sariciftci, Patent US 1992/5331183 A; b) G. Yu, J. Gao, J. C. Hummelen, F. Wudl, A. J. Heeger, Science1995, 270, 1789; c) J. J. M. Halls, C. A. Walsh, N. C. Greenham, E. A. Marseglia, R. H. Friend, S. C. Moratti, A. B. Holmes, Nature 1995, 376, 498.

[44] Y. He, H.-Y. Chen, J. Hou, Y. Li, *J.Am.Chem.Soc.* **2010**, 132, 1377.

[45] G. Li, V. Shrotriya, J. Huang, Y. Yao, T. Moriarty, K. Emery, Y. Yang, *Nat. Mater.* **2005**, 4, 864.

[46] F. Zhang, K. G. Jespersen, C. Björström, M. Svensson, M. R. Andersson,V. Sundström, K. Magnusson, E. Moons, A. Yartsev, and O. Inganäs, *Adv.Funct.Mater*. **2006**, 16, 5, 667.

[47] M. M. Wienk, M. Turbiez, J. Gilot, R. A. J. Janssen, *Adv. Mater*. **2008**, 20, 2556.

[48] J.K. Lee, W.L. Ma, C. J. Brabec, J. Yuen, J. S. Moon, Jin Y. Kim, K. Lee, G. C. Bazan, A. J. Heeger , *J. Am. Chem. Soc*. **2008** , 130 , 3619.

[49] Y. Liang, Z. Xu, J. Xia, S-T. Tsai, Y. Wu, G. Li, C. Ray, L. Yu, *Adv. Mater.* **2010**, 22, E135

[50] Y. Yao, J. Hou, Z. Xu, G. Li, Y. Yang, *Adv. Funct. Mater*. **2008**, 18, 1783

[51] J. Gao, W. Chen, L. Dou, C.-C. Chen, W.-H. Chang, Y. Liu, G.Li, Y. Yang, *Adv. Mater.* **2014**, 26, 3142

Chapter 2 High Performance Diketo-pyrrolopyrrole-based Thick Polymer Solar Cells through Improved Structural Order and Carrier Mobility

2.1 Introduction

One of the main reasons for the limited device efficiency of polymer solar cells is the relatively low charge carrier mobility of carbon-based polymeric materials.[1-5] The need for conjugated polymers with high carrier mobility, appropriate highest occupied molecular orbital (HOMO) and lowest unoccupied molecular orbital (LUMO) levels, and controllable morphology when blended with electron acceptor materials, is urgent.

To enhance the carrier mobility of conjugated polymers, several strategies have been investigated. For example, the dramatic enhancement of structural ordering in regioregular poly(3-hexylthiophene) (P3HT), as compared to regiorandom P3HT, has contributed directly to higher hole mobility and photovoltaic performance.[6] Similarly, the introduction of Si, Ge or Se heteroatoms into the backbone of conjugated polymers has brought significant enhancements in packing order and carrier mobility.[3d, 4e, 7a-c] Furthermore, by using large π-conjugated co-planar units such as benzodithiophene (BDT), thienothiophene (TT), thienopyrroledione (TPD), etc [10a-g] to construct the backbone, it is possible to facilitate intimate inter-chain packing and further increase carrier mobility.[3a,3b] Recently, the influences of molecular weight and the choice of non-conjugated side chains attached to conjugated polymers on polymer morphology and mobility also have been investigated.[8,9] Generally speaking, longer and bulkier side chains provide good solubility and ensure higher molecular weight for the polymers, while shorter and

less bulky side chains lead to better π-π stacking of the polymer chains and enhance charge carrier mobility. Despite these successes, up to now, there is a still a dearth of techniques in predicting the effects of a given side chain structure on different conjugated polymer systems. Polymer chemists can only shorten the side chains on the conjugated polymer back bones step by step until the solubility limit is reached, and this process often comes with unpredictable effects on morphology. [10f]

To achieve high performance polymer solar cells, low band gap polymers (LBG) with strong absorption are often desirable. The diketopyrrolopyrrole (DPP) unit, which was developed over the last 3 to 4 decades for high-performance pigments, has been shown to be a promising building block for LBG polymers.[11a-b] One of the DPP derivatives, furan-based DPP (FDPP), which was first reported as a donor material for solar cell applications in 2010 by Frechet et al, offered the advantages of lower material costs, higher synthetic yield, and improved solubility over its thiophene-based counterparts.[9a] Thiophene-based DPP polymers show excellent solubility with ethylhexyl (EH) side chains (Janssen et al; 2009); [8a] when the EH groups were replaced by long linear side chains such as dodecyl, tetradecyl, or hexadecyl groups to control the structural ordering, the PCE of the resulting polymer solar cells increased from 5% to 6%. [9b] However, the PCE was still limited by relatively low V_{OC} and external quantum efficiency (EQE) values. In order to overcome this problem, a series of low band gap polymers based on modified BDT and DPP units were developed, and they exhibited excellent photoelectrical properties in both single junction and tandem solar cells.[4c-4e] The argument for incorporating the BDT unit into DPP-based polymers lies in the fact that: 1) the large π-conjugated fused aromatic rings of BDT can enhance the packing of the polymer backbone and thus increase the carrier mobility and 2) BDT is a weak electron donating unit, so it results in a deep HOMO level for the

polymer, which is responsible for enhancing its V_{OC}. Given the reasons mentioned above, one of these polymers, PBDTT-FDPP, which contains alternating thienylbenzodithiophene (BDTT) and furan-substituted diketopyrrolopyrrole (FDPP) units, showed increased J_{SC} and V_{OC} over thiophene-based DPP polymers with other electron donating units.[9a][4d] With EH groups on both BDTT and FDPP units, PBDTTFDPP-EH provided a V_{OC} of 0.76 V, a J_{SC} of 13 mA/cm2, a FF of 55%, and a PCE around 5.4% in a single junction device. [4d]

In this work, we report two new polymers incorporating linear side chains on the FDPP acceptor group and BDTT donor group (PBDTTFDPP-C_{10} and PBDTTFDPP-C_{12}) to compare to PBDTTFDPP-EH. We show that by changing the branched EH groups on the FDPP unit to linear side chains, enhanced structural order and more favorable morphology are obtained for PBDTTFDPP-C_{10} and PBDTTFDPP-C_{12}, in both pristine polymer and polymer: $PC_{71}BM$ blend films.

2.2 Experimental

Materials: The polymerization route of each polymer is shown in Figure 2.1.

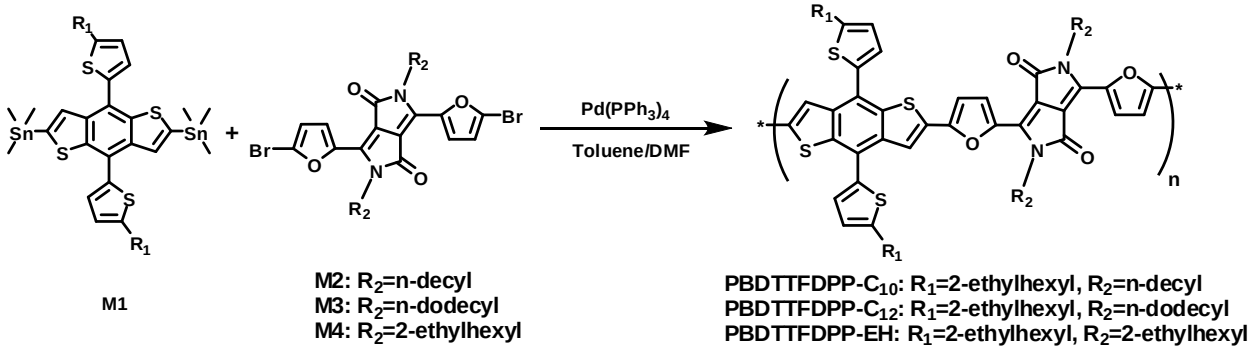

Figure 2.1 Synthetic routes for PBDTTFDPP-C_{10}, PBDTTFDPP-C_{12} and PBDTTFDPP-EH

All monomers (M1-M4) were synthesized according to reported methods. [4d] PBDTTFDPP-C_{10} was synthesized as follows: M1 (0.2222g, 0.2456 mmol) and compound M2 (0.1742g, 0.2451 mmol) were dissolved into 10 mL toluene and 1 mL DMF in a flask protected by argon. The solution was flushed by argon for 10 minutes, then 10 mg of $Pd(PPh_3)_4$ was added to the flask. The solution was flushed by argon again for 20 minutes. The oil bath was heated to 110 ℃ gradually, and the reactants were stirred for 8 hours at 110 ℃ under an argon atmosphere. Then, the mixture was cooled down to room temperature and the polymer was precipitated by the addition of 100 ml methanol. The precipitated solid was then dissolved in ~10 mL $CHCl_3$ and then passed through a short column with silica gel. The solution was then concentrated to 5~10 mL and precipitated in hexane. The polymer was thermally stable up to 270 ℃ (3% weight loss by Thermogravimetric analysis). ^{1}H NMR (400 MHz, $CDCl_3$): d=6.7-8.6 (br, 10H), 1.8-4.9 (br, 14H), 0.5-1.5 (br, 62H). Mn=42.4 k; polydispersity=2.2. PBDTTFDPP-C_{12} was synthesized and purified using the same procedure as above. The title polymer was obtained as a dark green-purple solid, yield ~60%. The polymer was thermally stable up to 270 ℃ (3% weight loss by Thermogravimetric analysis). ^{1}H NMR (400 MHz, $CDCl_3$): d=6.7-8.6 (br, 10H), 1.8-4.9 (br, 14H), 0.5-1.5 (br, 70H). Mn=40.2 k; polydispersity=2.2.

Fabrication of photovoltaic cells: PBDTTFDPP-C_{10}, PBDTTFDPP-C_{12} or PBDTTFDPP-EH was co-dissolved with $PC_{71}BM$ in 1, 2-dichlorobenzene (DCB) with a weight ratio of 1:2.5 and a polymer concentration of 9 mg/mL. 3% (volume ratio) chloronaphthalene (CN) was added into the solutions to improve the performance. A thin layer (~30 nm) of PEDOT:PSS (Baytron P VP A1 4083) was spin-coated onto the ITO surface. After being baked at 120 ℃ for ~ 20 min, the substrates were transferred into a nitrogen-filled glove box (< 0.1 ppm O_2 and H_2O). A

polymer/$PC_{71}BM$ composite layer was then spin-cast from the blend solutions at various (between 700 and 3000) rpm on to the ITO/PEDOT:PSS substrate, then the film was transferred into a thermal evaporator that is located in the same glove box. A LiF layer (~1 nm) and an Al layer (100 nm) were deposited in sequence under a vacuum of 2×10^{-6} torr. The effective area of the device was measured to be 0.10 cm^2.

Transmission Electron Microscopy (TEM) measurements: TEM images were taken using a Model JEM 1200-EX with Cs=1.9 at the accelerating voltage of 80 kV on thin films of polymer: fullerene blends processed w/ or w/o CN. The bright field images were taken at a magnification of 150,000.

Grazing Incidence Wide-Angle X-ray Scattering (GIWAXS): GIWAXS measurements were performed at the 8ID-E beamline at the Advanced Photon Source (APS), Argonne National Laboratory (ANL) using x-rays with a wavelength of λ = 1.6868 Å and a beam size of 200 μm (h) and 20 μm (v). A 2-D PILATUS 1M-F detector was used to capture the scattering patterns and was situated at 204 mm from the samples.

Space Charge Limited Current (SCLC) measurements: Hole mobility was measured using the space charge limited current model, using a diode configuration of ITO/ PEDOT:PSS/polymer-only or polymer:$PC_{71}BM$/Au in the range of 0-10 V, and fitting the results to a space charge limited form, described by

$$J = (8/9)\, \varepsilon_r\, \varepsilon_0\, \mu_e\, (V^2/L^3) \quad [14a]$$

where ε_0 is the permittivity of free space, ε_r is the dielectric constant of the polymer, μ is the hole mobility, V is the voltage drop across the device ($V = V_{appl} - V_r - V_{bi}$, where V_{appl} is the applied voltage to the device, V_r is the voltage drop due to contact resistance and series resistance across the electrodes, and V_{bi} is the built-in voltage due to the difference in work function of the two electrodes), L is the polymer or polymer: $PC_{71}BM$ thickness. The dielectric constant ε_r is assumed to be 3, which is a typical value for conjugated polymers. The thickness of the polymer and blend films was measured using a Dektak profilometer.

2.3 Results and Discussion

2.3.1 Materials synthesis and characterization

The chemical structures of PBDTTFDPP-C_{10}, PBDTTFDPP-C_{12}, and PBDTTFDPP-EH are shown in Figure 2.2.

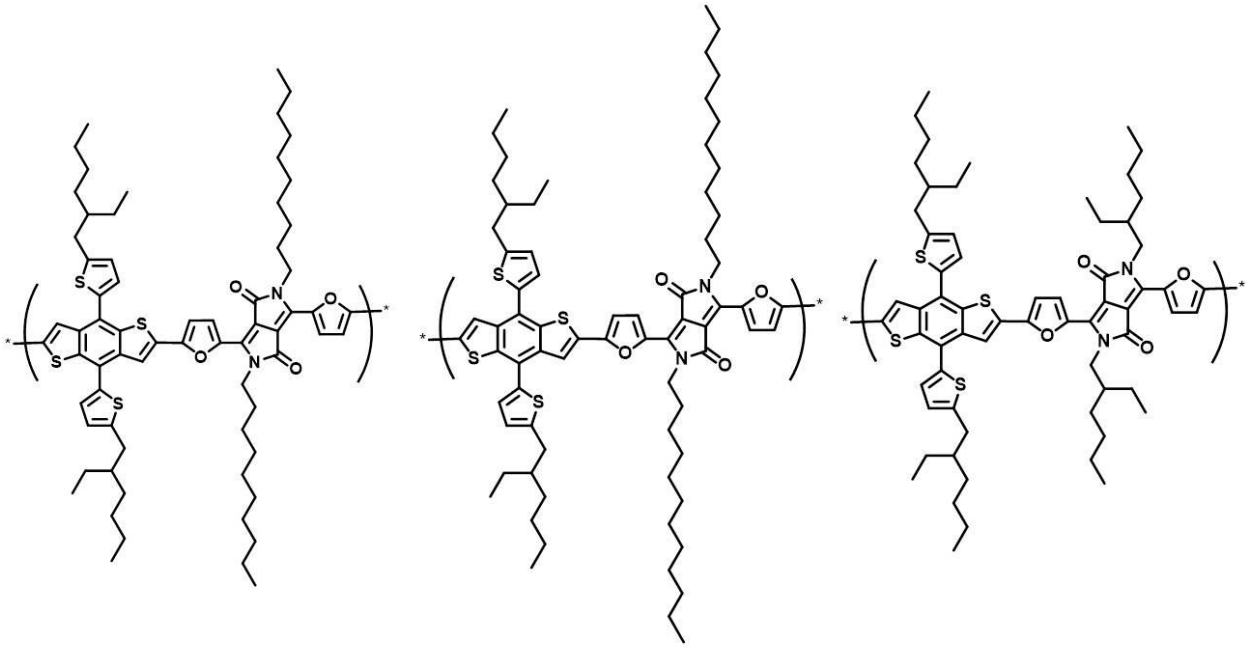

Figure 2.2 Chemical structures of PBDTTFDPP-C_{10}, PBDTTFDPP-C_{12}, and PBDTTFDPP-EH.

All these polymers were synthesized via Stille coupling polymerization using $Pd(PPh_3)_4$ as the catalyst, and toluene/N,N-dimethylformamide (DMF) as the solvent at 110 ℃. The molecular weights (M_n) range from 30k to 40k, and their polydispersity indices (PDI) are around 2.2, as determined by gel permeation chromatography (GPC). The duration of the polymerization reaction was controlled to tune the molecular weight and solubility of the resulting polymers. PBDTTFDPP-EH showed good solubility in o-dichlorobenzene (DCB) and chloroform (beyond 30 mg/mL) even at prolonged polymerization times, indicating weak inter-molecular packing due to the branched side chains. However, for PBDTTFDPP-C_{10} and PBDTTFDPP-C_{12}, after 6-8 hours of reaction the toluene/DMF solution became a gel and the resulting polymers showed

limited solubility in DCB and chloroform (up to ~15 mg/mL at room temperature). The lower solubility of PBDTTFDPP-C_{10} and PBDTTFDPP-C_{12} compared to PBDTTFDPP-EH potentially indicates better π-π stacking of the polymer backbones. [8c]

The absolute absorption coefficient spectra of PBDTTFDPP-C_{10}, PBDTTFDPP-C_{12} and PBDTTFDPP-EH thin films were determined by ultraviolet-visible (UV-Vis) measurements and can be found in Figure 2.3.

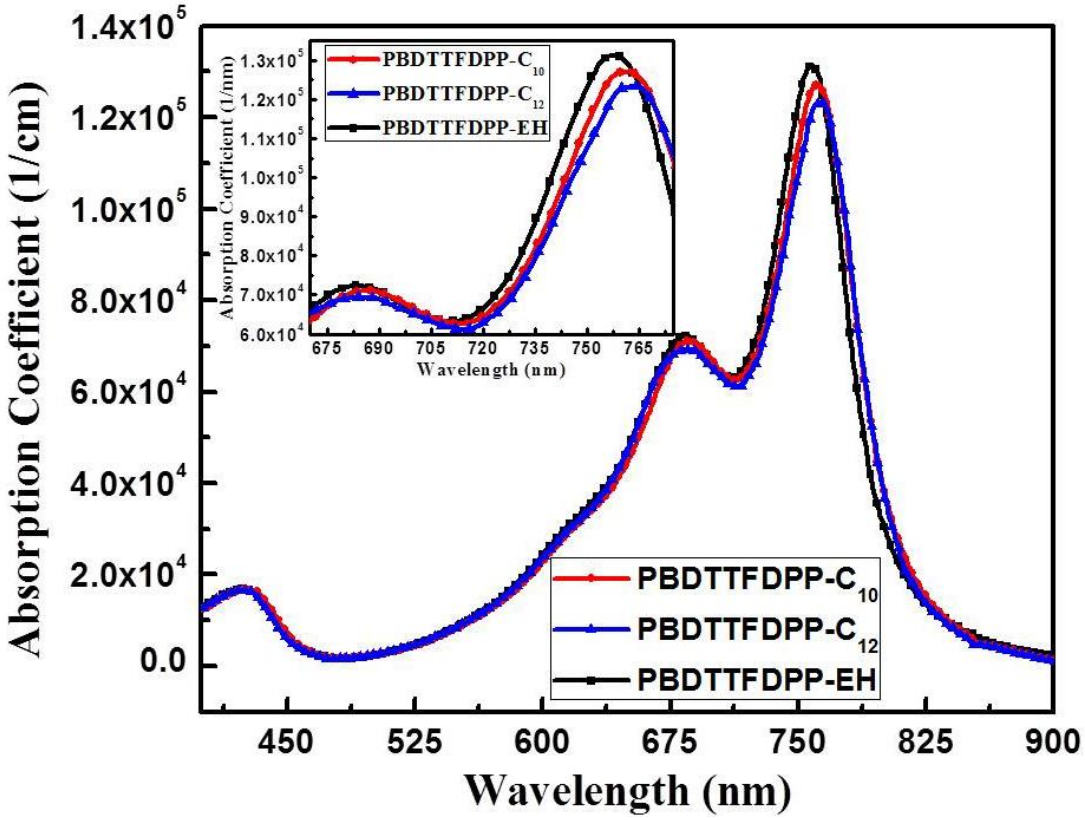

Figure 2.3 UV-Vis absorption coefficient spectra of PBDTTFDPP-C_{10}, PBDTTFDPP-C_{12}, and PBDTTFDPP-EH thin films.

PBDTTFDPP-C_{10} and -C_{12} share similar spectra with PBDTTFDPP-EH. They all display two absorption bands, one at 350-450 nm and the other at 650-800 nm. Despite these similarities, the spectra of the two linear side-chain substituted polymers are red-shifted by ~10 nm compared to their branched side-chain substituted counterparts. The PBDTTFDPP-EH film shows an absorption onset at 825 nm with a λ_{max} of 754 nm, while PBDTTFDPP-C_{10} and PBDTTFDPP-C_{12} films have nearly identical optical characteristics with absorption onsets at 825 nm and λ_{max} values around 762 nm. Almost identical absorption coefficients of all three polymers thin films indicate this structure modification of polymers does not significantly affect their absorption capabilities. The HOMO and LUMO energy levels of the polymers were determined by cyclic voltammetry (CV), and the results are shown in Figure 2.4.

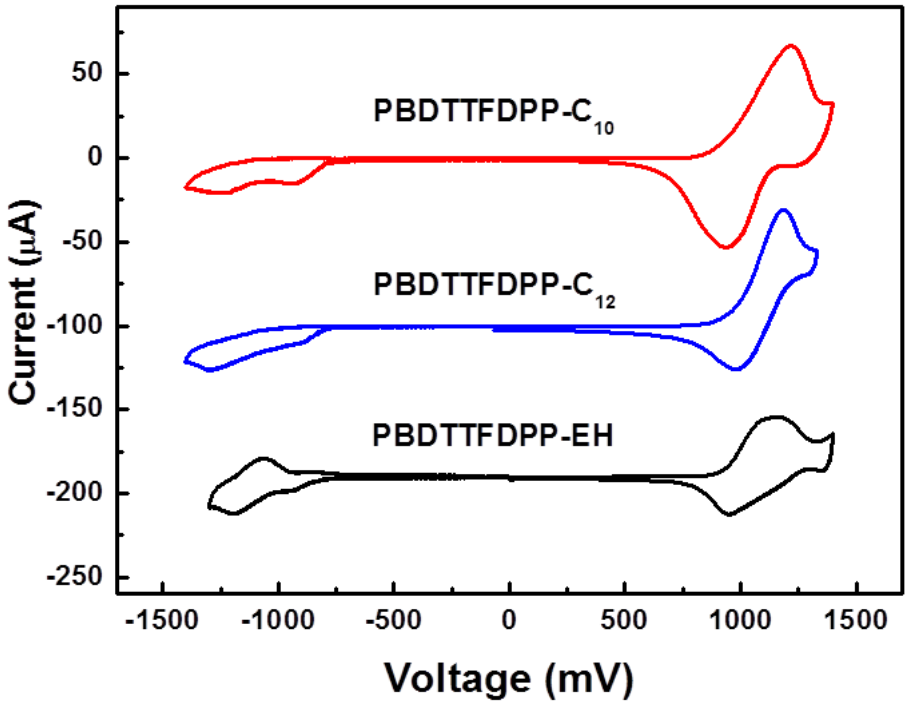

Figure 2.4 Cyclic voltammograms (CV) of PBDTTFDPP-C_{10}, PBDTTFDPP-C_{12}, and PBDTTFDPP-EH thin films.

HOMO/LUMO levels are extracted from the onset position of the oxidation and reduction peaks. The HOMO/LUMO levels for PBDTTFDPP-C_{10}, PBDTTFDPP-C_{12}, and PBDTTFDPP-EH are -5.25/-3.61, -5.26/-3.61, and -5.28/-3.59 eV, respectively. Slightly higher HOMO levels and lower electrochemical bandgaps are observed for polymers with linear alkyl side chains compared to those with EH chains.

2.3.2 Photovoltaic device performance

In order to characterize the photovoltaic performance of each of the polymers, bulk heterojunction thin-film solar cells were fabricated with a conventional structure of ITO/PEDOT:PSS/polymer:$PC_{71}BM$/LiF/Al, using PBDTTFDPP-C_{10}, PBDTTFDPP-C_{12}, and PBDTTFDPP-EH as electron donors and $PC_{71}BM$ as the electron acceptor at a 1:2.5 ratio by weight. A small amount of the high boiling-point additive 1-chloronaphthalene (CN) was used to improve film morphology.[12a-12d] Figures 2.4 (a) and (b) show the current density-voltage (J-V) curves and EQE curves of PBDTTFDPP-C_{10},-C_{12},and-EH based devices.

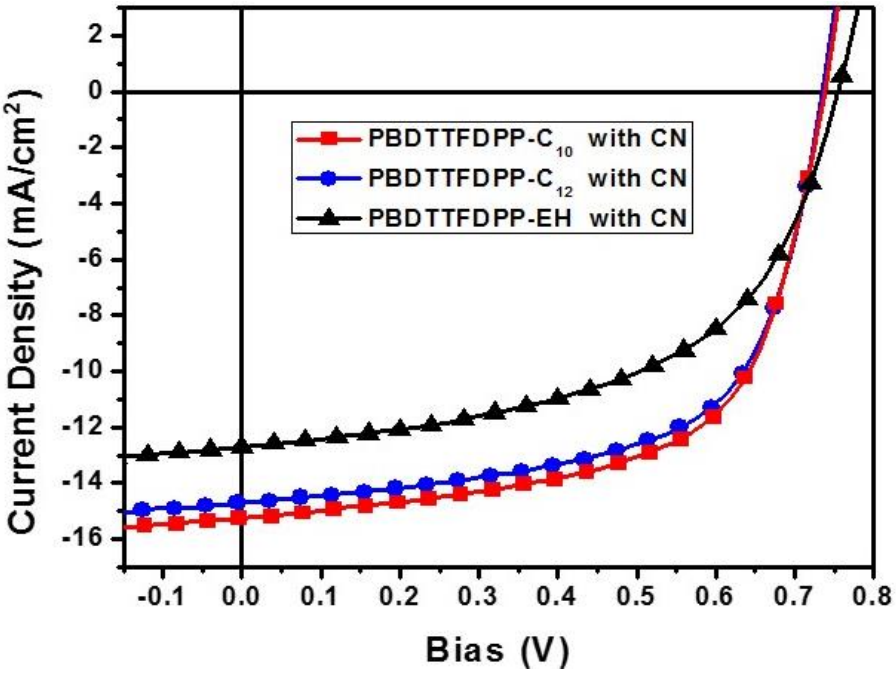

Figure 2.5 Current density-voltage characteristics of polymer: $PC_{71}BM$ single junction solar cells processed with CN under AM1.5G illumination (100 mW/cm^2)

Solar cells fabricated from PBDTTFDPP-C_{10} reached the highest power conversion efficiency (PCE) of 6.9%, with an open circuit voltage (V_{OC}) of 0.73 V, a short circuit current (J_{SC}) of 15.2 mA/cm^2, and a fill factor (FF) of 63% (the average PCE from 20 devices is 6.4%). Slightly lower photovoltaic properties were observed in the best device obtained from PBDTTFDPP-C_{12}, which achieved a peak PCE value of 6.7%, with a V_{OC} of 0.73 V, a J_{SC} of 14.9 mA/cm^2, a FF of 62% (the average PCE from 20 devices is 6.2%). These results are significantly greater than the highest performing PBDTTFDPP-EH based device with a V_{OC} of 0.76 V, a J_{SC} of 12.8 mA/cm^2, a FF of 56%, and a peak PCE of 5.4% (the average PCE from 20 devices is 4.8%). The EQE curves of PBDTTFDPP-C_{10} and PBDTTFDPP-C_{12}-based devices

shown in Figure 2.6 exhibit broad spectra approaching efficiencies of 50%, which is consistent with the high photocurrent.

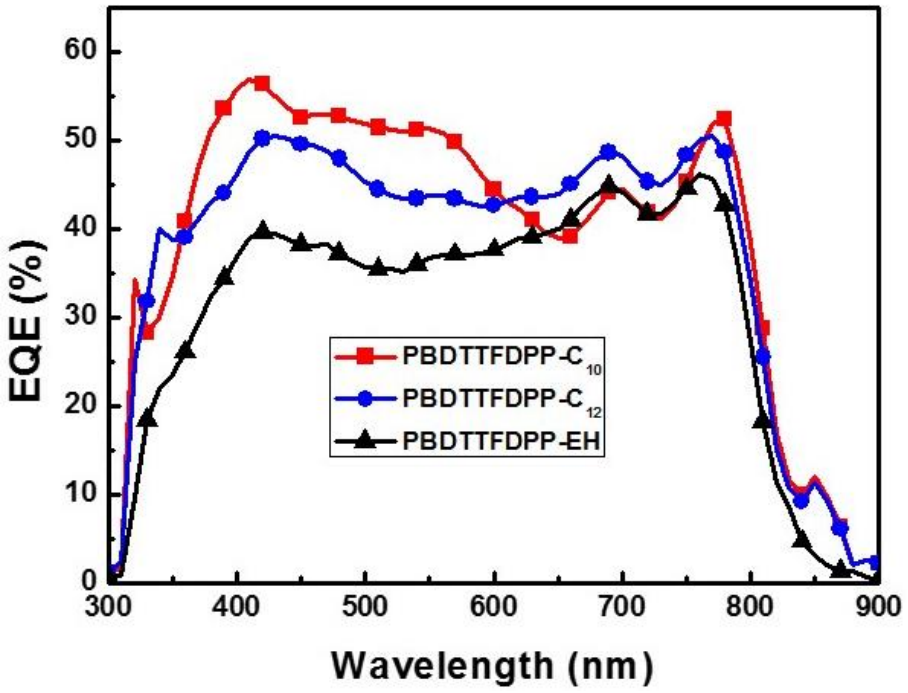

Figure 2.6 EQE curves of polymer: $PC_{71}BM$ single junction solar cells processed with CN under AM1.5G illumination (100 mW/cm^2)

The substantial performance improvements observed in the polymers with linear chains is primarily concentrated in increases in J_{SC} and FF. Both the J_{SC} and FF values are closely related to the film morphology, structural order, and carrier mobility of the polymer. To fully understand the effect of replacing the branched side chains with linear ones, the morphology of pristine polymer and polymer: $PC_{71}BM$ blend thin films were characterized using transmission electron

microscopy (TEM) and grazing incidence wide angle X-Ray Scattering (GIWAXS) spectroscopy [13a-13b]. Carrier mobility was measured using the space charge limited current (SCLC) model.

2.3.3 TEM study on morphology of polymer: C_{71}BM blend thin film

First, we examine the effect of CN as an additive in polymer:PC_{71}BM blends. The TEM images of the PBDTTFDPP-C_{10}:PC_{71}BM, PBDTTFDPP-C_{12}:PC_{71}BM and PBDTTFDPP-EH: PC_{71}BM blend films deposited without CN and with CN are provided in Figures 2.7 (a)-(f).

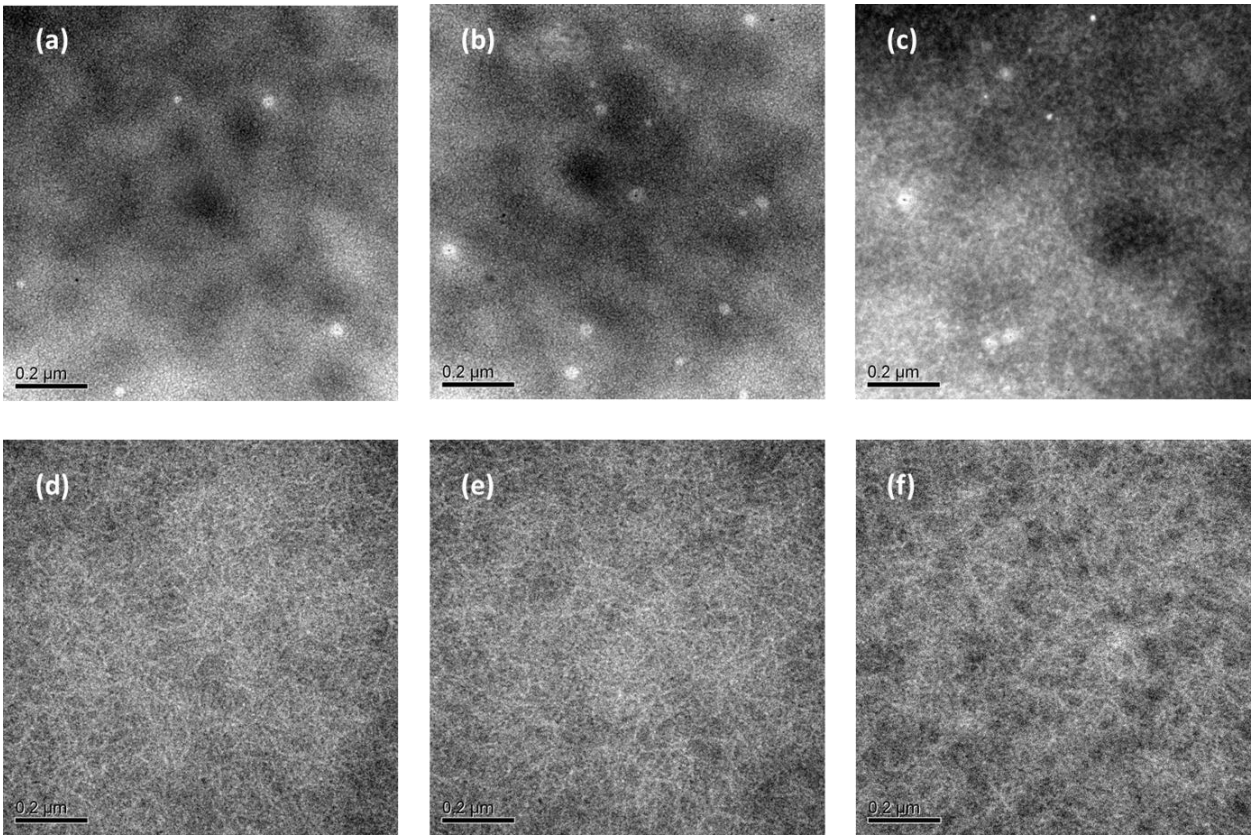

Figure 2.7 TEM images of polymer: PC71BM blend films processed in DCB without CN: (a) PBDTTFDPP-C_{10}:PC_{71}BM, (b) PBDTTFDPP-C_{12}:PC_{71}BM, (c) PBDTTFDPP-EH: PC_{71}BM; and

processed in DCB with 3% CN (volume ratio): (d) PBDTTFDPP-C_{10}:$PC_{71}BM$, (e) PBDTTFDPP-C_{12}:$PC_{71}BM$, (f) PBDTTFDPP-EH:$PC_{71}BM$.

Looking at the non-CN scenario, Figures 2.7 (a), (b) and (c) clearly show non-ideal morphologies composed of large coarse features. For all three polymer: $PC_{71}BM$ blends without the CN additive, the phase separation between polymer-rich and fullerene-rich domains occurs on a scale of ~100-200 nm, which is too large to be considered a favorable morphology. This is further verified by the observation of Resonant Soft X-ray Scattering (RSoXS) (Figure 2.8). [16a]

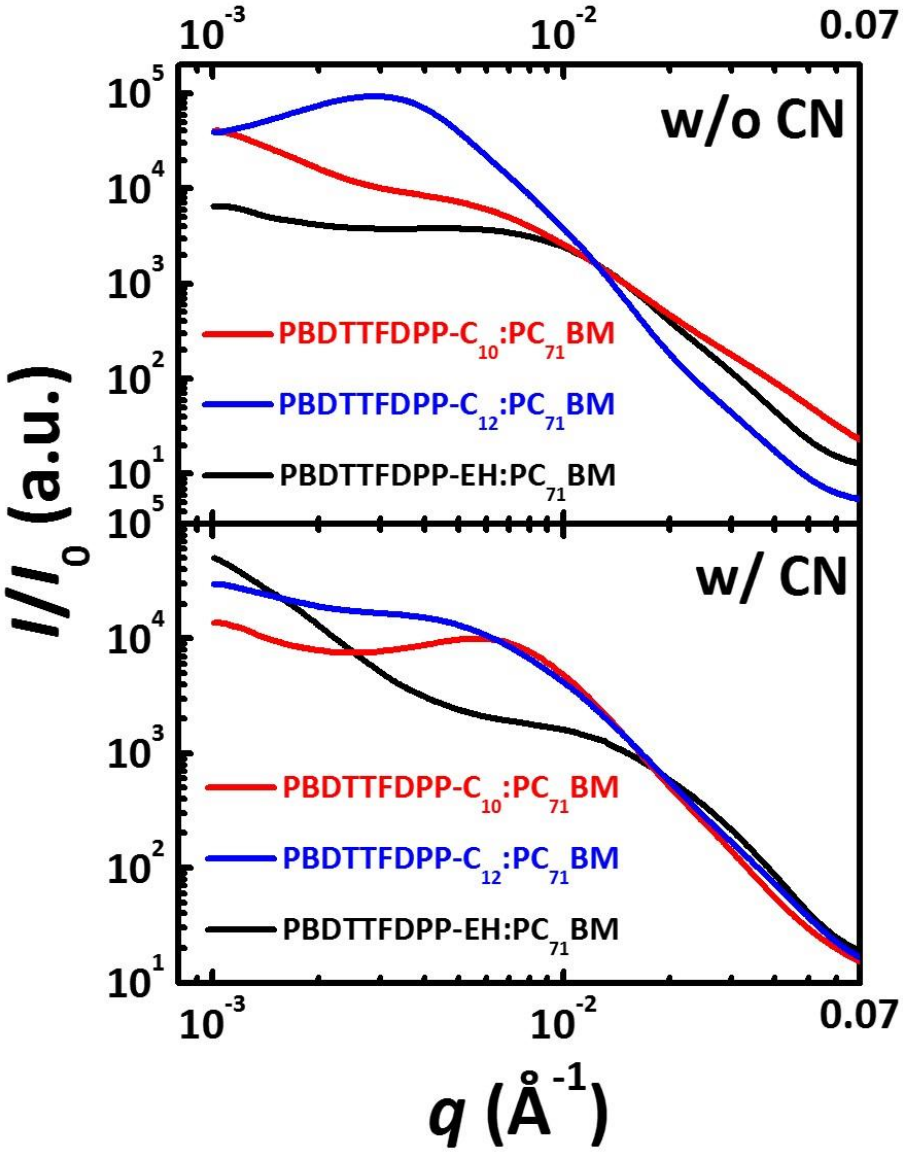

Figure 2.8 RSoXS profiles of thin films of PBDTTFDPP- C_{10}:$PC_{71}BM$, PBDTTFDPP-C_{12}:$PC_{71}BM$ and PBDTTFDPP-EH:$PC_{71}BM$ blends prepared from solutions without CN and with CN under the same conditions as those used for the fabrication of OPV devices.

Due to the large degree of phase separation between polymer and fullerene-rich domains, there is limited interfacial area available for efficient exciton dissociation and carrier generation,

thus resulting in poor device performance. When CN (3% volume) was added to DCB, as shown in Figures 2.7(d), (e), and (f), an interpenetrating nanofibril network is formed as a result of the highly ordered packing of the PBDTTFDPP polymer chains. We also have observed smaller phase-separated domains (Figure 2.8) for all of the thin films deposited with added CN. The presence of the observed nanofibril networks is particularly important to polymer solar cells as it is anticipated to provide percolation pathways for efficient carrier collection and ultimately lead to higher cell efficiency. From these results, we can conclude that CN as an additive can help the penetration of $PC_{71}BM$ into the polymer matrix and result in better intermixing and finer phase-separated domains. Comparing the morphological information obtained from TEM with device performance, we find that the favorable morphology obtained when using PBDTTFDPP polymers with CN as an additive contributes significantly to the device performance. This morphological change upon CN addition also well agrees with the studies of additive effects on several other high performance polymer systems such the PCDTBT and PTB series. [14a-14b]

2.3.4 GIWAXS study on morphology of both pristine polymer and polymer:$PC_{71}BM$ blend films

Additional changes in nanoscale morphology, such as molecular packing and side chain arrangements, were investigated using GIWAXS.[15a-d] The 2-D GIWAXS patterns of three pristine polymers and polymer:$PC_{71}BM$ blend films processed from DCB/CN are shown in Figure 2.9(a)-(f).

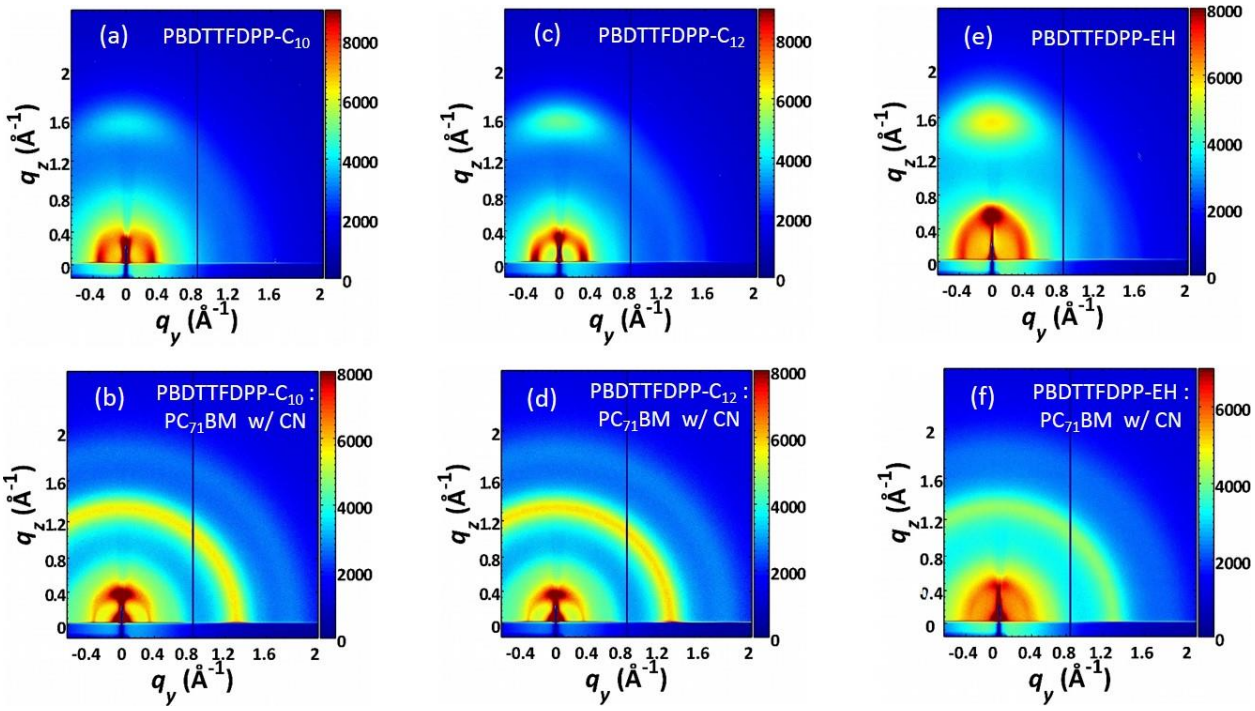

Figure 2.9 Two dimensional GIWAXS patterns of PBDTTFDPP-C_{10}, PBDTTFDPP-C_{12}, and PBDTTFDPP-EH pristine polymer films (a, c, e) and the three polymers: $PC_{71}BM$ blend films processed from DCB/CN (b, d, f)

The corresponding background-subtracted q_y and q_z linecuts of the GIWAXS patterns and fitted parameters are summarized in Figure 2.10, 2.11 and Table 2.1, respectively.

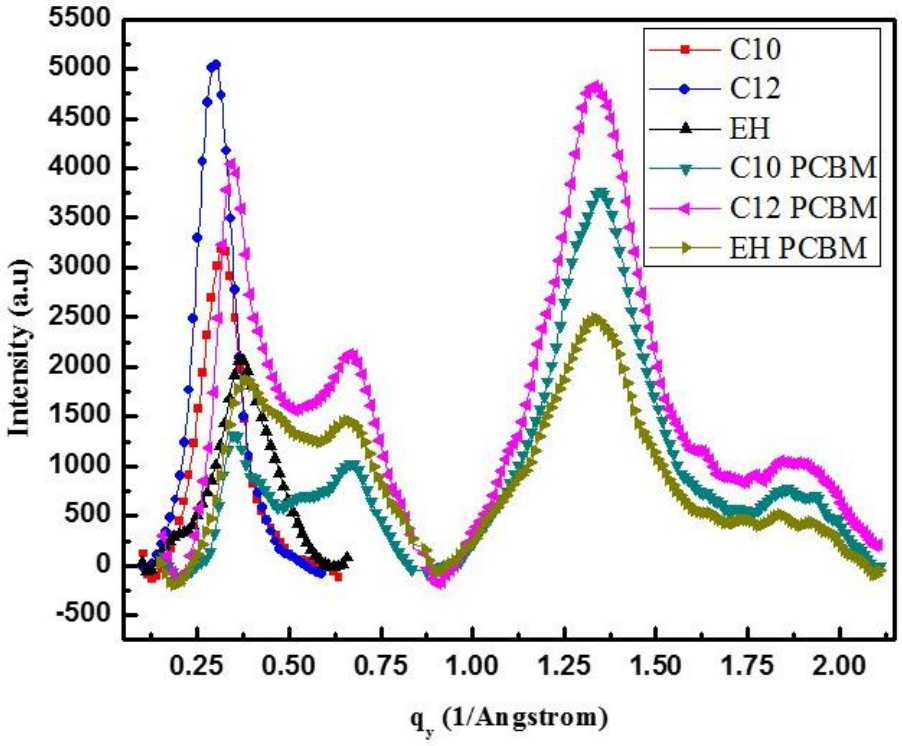

Figure 2.10 Background-subtracted q_y linecuts of GIWAXS patterns of pristine and blend films for PBDTTFDPP-C_{10}, PBDTTFDPP-C_{12} and PBDTTFDPP-EH

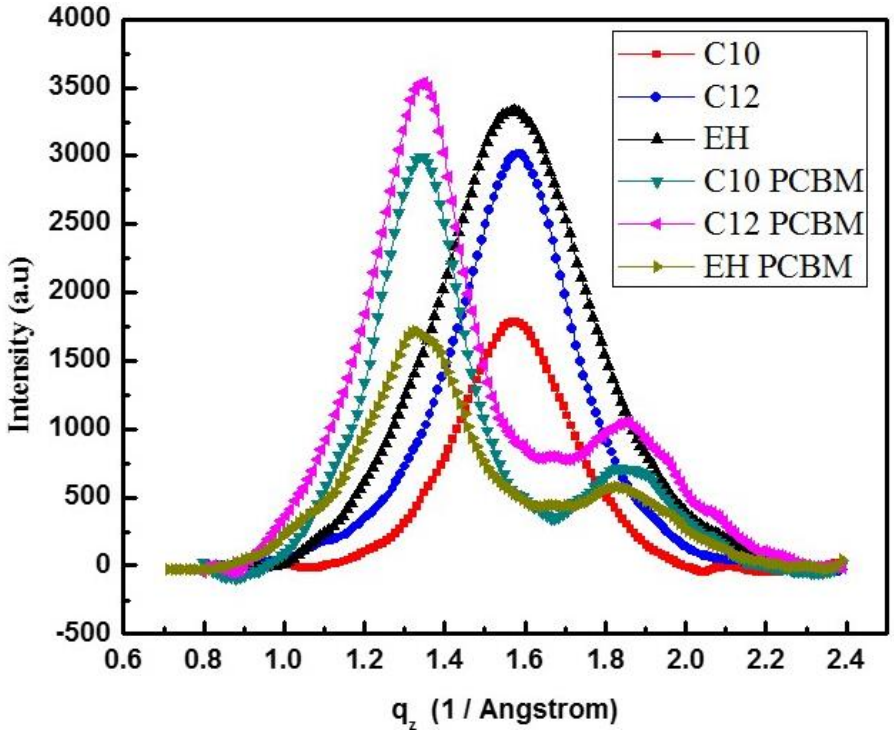

Figure 2.11 Background-subtracted q_z linecuts of GIWAXS patterns of pristine and blend films for PBDTTFDPP-C_{10}, PBDTTFDPP-C_{12} and PBDTTFDPP-EH

Table 2.1 Parameters of GIWAXS fitting results concerning three pristine polymers and the polymer: $PC_{71}BM$ blends processed from DCB/CN.

	Qy [1/Å]	Lamellar spacing [Å]	FWHM [Å]	Polymer lamellar correlation length [Å]	Qz for polymer [1/Å]	π-π spacing [Å]	FWHM [Å]	Polymer π-π correlation length [Å]	Qy for $PC_{71}BM$ [1/Å]	FWHM [Å]	$PC_{71}BM$ correlation length [Å]
PBDTTFDPP-C_{10}	0.317±0.01	19.8	0.12	49	1.55±0.05	4.1±0.2	0.29	21			
PBDTTFDPP-C_{10}:$PC_{71}BM$ w/ CN	0.36±0.01	17.5	0.11	53					1.33	0.30	20
PBDTTFDPP-C_{12}	0.299±0.01	21.0	0.12	49	1.55±0.05	4.1±0.2	0.35	17			
PBDTTFDPP-C_{12}:$PC_{71}BM$ w/ CN	0.34±0.01	18.4	0.11	53					1.33	0.30	20
PBDTTFDPP-EH	0.38±0.01	16.5	0.18	33	1.55±0.05	4.1±0.2	0.45	13			
PBDTTFDPP-EH:$PC_{71}BM$ w/ CN	0.39±0.01	16.1	0.17	35					1.33	0.35	17

As Figures 2.9(a)(c)(e), Figure 2.10, Figure 2.11 and Table 2.1 show, for the pristine polymer thin films, distinct peaks at q_y= 0.317 $Å^{-1}$, 0.299 $Å^{-1}$, and 0.38 $Å^{-1}$ were observed for PBDTTFDPP-C_{10}, PBDTTFDPP-C_{12}, and PBDTTFDPP-EH, corresponding to polymer lamellar spacings of 19.8 Å, 21.0 Å and 16.5 Å. This indicates that when changing from polymers with branched short side chains to those with linear long chains, the distance between single polymer chains increases. The peaks at q_z= 1.55 $Å^{-1}$, corresponding to a π-π stacking spacing of 4.1 Å (shown in Table.2.1), were clearly observed for all three pristine polymers, indicating that the polymer orientation is 'face-on'. This similarity reflects the fact that the side chain modification has a negligible effect on polymer π-π stacking distance. However, the full widths at half maximum (FWHMs) of peaks at q_z= 1.55 $Å^{-1}$ decreased from 0.45 Å for branch side-chained PBDTTFDPP-EH, to 0.29 Å and 0.35 Å for linear side-chained PBDTTFDPP-C_{10} and PBDTTFDPP-C_{12}, respectively. This corresponds to an increase in polymer π-π correlation

length from 13 Å for PBDTTFDPP-EH, to 21 Å and 17 Å for PBDTTFDPP-C_{10} and PBDTTFDPP-C_{12}, as shown in Table 2.1.

The similar situation holds for diffraction peaks in the q_y direction (centered at around 0.3 $Å^{-1}$). The narrowing of the q_y peaks corresponds to an increase in polymer lamellar correlation length from 33 Å for PBDTTFDPP-EH, to 49 Å for both PBDTTFDPP-C_{10} and PBDTTFDPP-C_{12}. Both the increase of the π-π and lamellar correlation lengths indicate that more crystalline polymer domains were formed in films of polymer with linear side chains. In other words, nanoscale structural order is enhanced within polymer domains when branched side chains are replaced with linear ones in pristine polymer films.

When blended with $PC_{71}BM$, we are still able to observe the q_y peaks (centered at around 0.375 $Å^{-1}$) for all three polymers: $PC_{71}BM$ blends, as shown in Figure 2.9(b) (d) (f), consistent with those of the pristine polymer films. However, along the q_z direction, it becomes difficult to differentiate thoroughly the polymer π - π stacking peaks from those of $PC_{71}BM$, as $PC_{71}BM$ has strong scattering signals at the same q. [16c]

However, as shown in Figure 2.11 , all three polymers' π - π stacking peaks around q_z= 1.55-1.60 $Å^{-1}$ ('face-on' stacking) were still discernible even though they were buried in the much stronger $PC_{71}BM$ peaks.[16c] Based on the evidence shown above, we can conclude that the polymer chains are (partially) stacked in a 'face-on' manner in the blend films.[16d] Furthermore, the polymer lamellar correlation lengths for all three polymer:$PC_{71}BM$ blends were found to follow the same trend as that in pristine polymer films: the lamellar correlation length has increased from 35 Å for PBDTTFDPP-EH to 53 Å for both PBDTTFDPP-C_{10} and PBDTTFDPP-$C_{12,}$ as shown in Figure 2.9(b)(d)(f), Figure 2.10, Figure 2.11 and Table 2.1.

Therefore, linear-side-chained polymers can induce more crystalline polymer domains in the polymer: $PC_{71}BM$ blends. This enhanced structure order can act as one of the important factors that contribute to higher carrier mobility and lead to improved device performance.

2.3.5 SCLC study on carrier mobility of polymer: $PC_{71}BM$ blend thin film

The hole mobility of pristine PBDTTFDPP-C_{10}, -$C_{12,}$ and -EH polymers and the polymers in blended films were measured using the space charge limited current (SCLC) method to demonstrate the influence of side chains on carrier mobility.[3c, 4f] The log (J) vs. log (V) curves are shown in Figure 2.12.

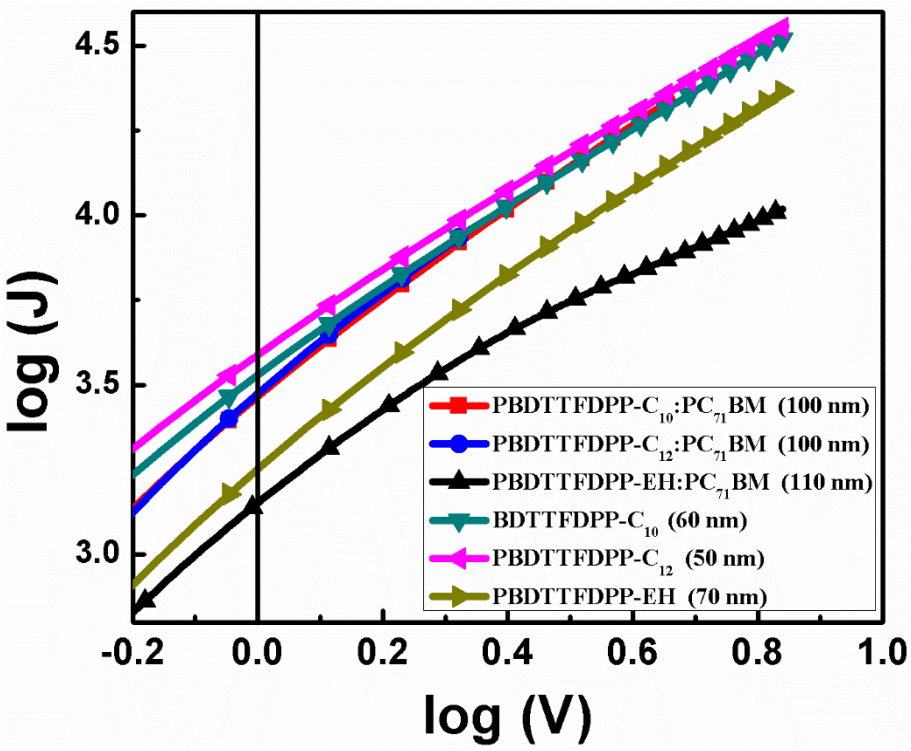

Figure.2.12 Log (J)–Log (V) characteristics of hole-only devices composed of PBDTTFDPP-C_{10}, PBDTTFDPP-C_{12}, and PBDTTFDPP-EH pristine polymer films and polymer: $PC_{71}BM$ blend films, respectively.

Pristine PBDTTFDPP-C_{10}, -C_{12} and PBDTTFDPP-EH films exhibit SCLC hole mobility values as high as 9.3×10^{-4}, 8.1×10^{-4}, and 2.2×10^{-4} cm^2/V s, respectively. The PBDTTFDPP-C_{10}:$PC_{71}BM$, PBDTTFDPP-C_{12}:$PC_{71}BM$ and PBDTTFDPP-EH: $PC_{71}BM$ blend films (processed with CN as an additive) show SCLC hole mobility values as high as 6.7×10^{-4}, 6.3×10^{-4}, and 1.2×10^{-4} cm^2/V s, respectively. All of the mobility data were averaged from three independent measurements. The SCLC results reveal that better charge transport properties have been achieved for the PBDTTFDPP series LBG polymers by changing the branched side chains to linear ones. The small differences between hole mobility extracted from pristine films and from blend films also indicate that fullerenes do not significantly interrupt the formation of crystalline polymer domains, and thus did not compromise the polymer's charge transport properties in the blended film.

2.3.6 Influence of thickness on absorption and current density

Figures 2.13 show the variations of *J*sc with thickness of polymer:PCBM blend based C_{10} and EH and the simulated current. There are two simulated current peaks at ~ 110 nm and ~210 nm, respectively. The simulated curve is similar with optical simulation results for other conjugated polymers; for example, two peaks in the vicinity of ~100 nm and ~200 nm were reported for P3HT/PCBM devices. [19][20] Consistent with the simulated results, the measured

current peaks at device thickness of ~120 nm and ~200 nm with PBDTTFDPP-C_{10}. However, the measured current of EH drops after its peak at ~115 nm without exhibiting a second peak. A plausible explanation for the disappearance of the second current peak in the branch-side-chained polymer is its lower carrier mobility and higher recombination rate relative to the linear-side-chained polymers.

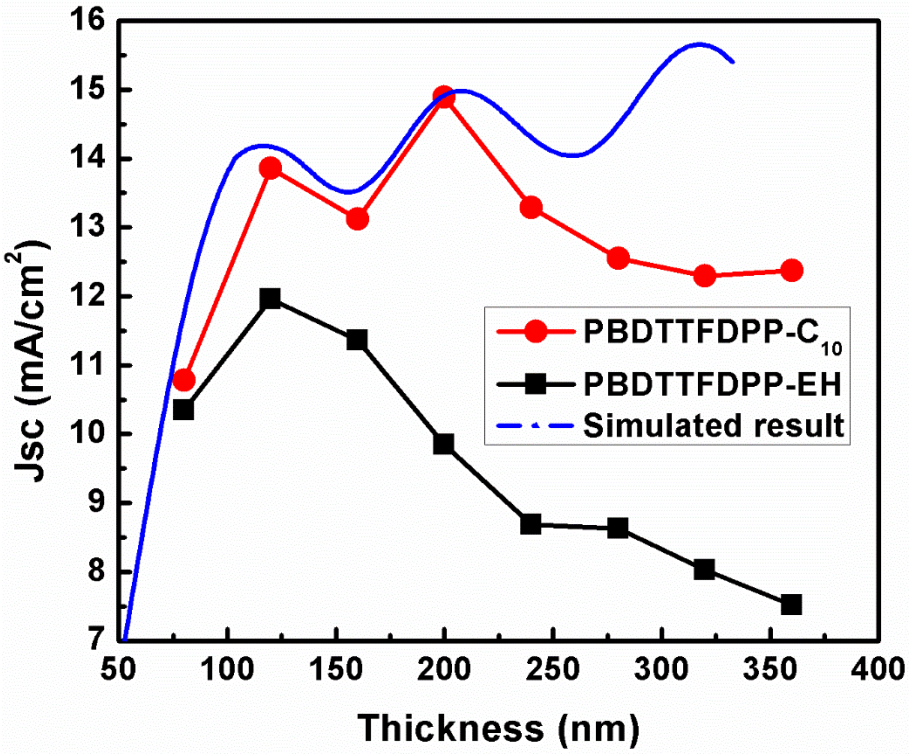

Figure 2.13 Current-thickness dependence curves with optical current simulations for devices made of PBDTTFDPP-C_{10}, PBDTTFDPP-C_{12}, and PBDTTFDPP-EH blended with $PC_{71}BM$.

2.3.7 Efficiency -thickness dependence of polymer: $PC_{71}BM$ blend thin film based device

Finally, we investigated the dependence of device performance on the active layer thickness in devices made using these three polymers. High performance polymer solar cells with thick active layers are very valuable in large-scale manufacturing processes. However, most reported high performance polymers only function well at small active layer thicknesses.[9b,11a, 14a] Figure 2.14 shows that for PBDTTFDPP-EH based devices, the average PCE (4.8%) is observed at 120 nm active layer thickness.

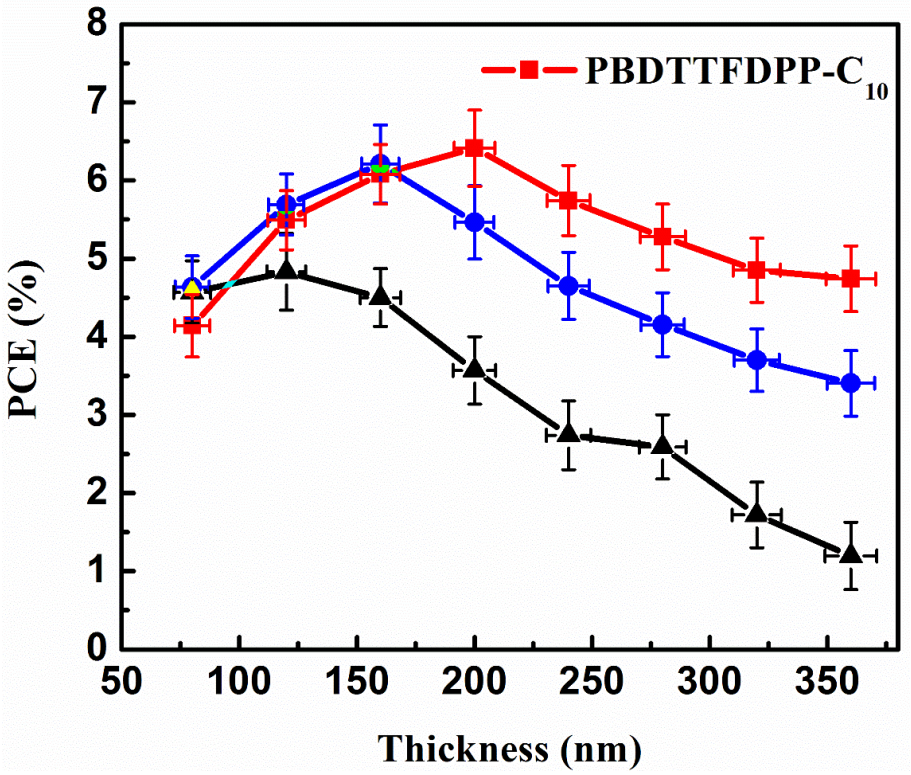

Figure 2.14 Efficiency-thickness dependence curves for devices made of PBDTTFDPP-C_{10}, PBDTTFDPP-C_{12}, and PBDTTFDPP-EH blended with $PC_{71}BM$.

When increasing the thickness of the active layer, the average PCE drops significantly to 3.6% at 200 nm, 2.7% at 240 nm, 1.7% at 320 nm and 1.2% at 360 nm. PBDTTFDPP-C_{12} based devices shows an improved trend of average PCE which peaks at 6.2% at 160 nm and then drops to 5.5% at 200 nm, 3.7% at 320 nm, and 3.4% at 360 nm. PBDTTFDPP-C_{10} based devices with the highest hole mobility show the largest observed optimum thickness of 200 nm, with an average PCE of 6.4%. Beyond 200 nm thickness, PBDTTFDPP-C_{10} based devices still maintain an average efficiency of 4.7 % even at 360 nm active layer thicknesses. In general, the average device performance of PBDTTFDPP-C_{10} remains above 4.7% over the thickness range between 160 nm and 360 nm. As we have shown, all three polymers have almost identical absorption coefficients (within 2% difference), therefore the significant change in optimal device thickness has less to do with optical, [17b] but rather electrical properties of the polymers. The larger optimum active layer thickness of linear side-chained polymer based device can be possibly ascribed to more crystalline polymer domains where carriers exhibit higher carrier mobility, as was discussed in the previous section. [18] High carrier mobility allows charge carriers to travel faster during the charge transport process, and more crystalline domains have fewer traps and defects and thus reduce the chance of recombination. As a result, the benefit of higher absorption at thick active layer film can be realized in the devices containing linear side-chained PBDTTFDPP-based polymers to exhibit higher device performance. However, the poorer transport property in the thick branch side-chained polymer OPV devices may cancel the absorption benefits or even make the device performance worse with a thick blend active layer. This approach of side chain engineering has led to much improved device efficiency in thick polymer solar cells with active layer thickness around 200 nm.

2.4 Conclusion

In conclusion, a series of low bandgap polymers based on thienylbenzodithiophene (BDTT) and furan-substituted diketopyrrolopyrrole (FDPP) units with different side chains have been synthesized. By changing the branched ethylhexyl groups on FDPP unit to linear side chains, the structural order and carrier mobility of the polymers are enhanced accordingly, as determined by the TEM, GIWAXS, and SCLC results on the polymer and the polymer: $PC_{71}BM$ blend films. The power conversion efficiencies of single junction devices are improved from ~5% to ~7%, mainly due to higher short-circuit current and fill factor values. More interestingly, the enhanced structure order and higher carrier mobility found in the more crystalline polymer domains formed by polymers with linear side chains can be among the important factors contributing to improved performance at active layer thicknesses ca 200 nm. The maximum PCE of devices based on PBDTTFDPP-C_{10}:$PC_{71}BM$ blends reaches a peak value of 6.9% at active layer thickness of 200 nm. Most importantly, average PCE values over 4.7% are maintained with active layer thicknesses ranging from 160 nm to 360 nm, showing the advantages of replacing bulky branched side chains with linear side chains. Since relaxing the required level of precision in active layer thickness has important industrial implications for large-area film deposition, our preliminary results can serve as a guideline for the future modification of high performance polymers toward industrial applications. [19][20]]

2.5 References

[1] a) G. Yu, J. Gao, J. C. Hummelen, F. Wudl, A. J. Heeger, *Science* **1995,** *270*, 1789; b) G. Li, V. Shrotriya, J. S. Huang, Y. Yao, T. Moriarty, K. Emery, Y. Yang, *Nat. Mater.* **2005**, *4*, 864; c)

F. C. Krebs, *Sol. Energy Mater. Sol. Cells* **2009**, *93*, 394; d) J. Brabec, N. S. Sariciftci, J. C. Hummelen, *Adv. Funct. Mater.* **2011,** *11*, 15; d) G. Li, R. Zhu, Y. Yang, *Nat. Photon.***2012**, *6*, 153; e) C.-C. Chen, L. T. Dou, R. Zhu, C.-H. Chung, T.-B. Song, Y. B. Zheng, S. Hawks, G. Li, P. S. Weiss, Y. Yang, *ACS Nano* **2012**, *6*, 7185.

[2] a) B. C. Thompson, J. M. J. Frechet, *Angew. Chem. Int. Ed.* **2008**,*47*, 58; b) Y. J. Cheng, S. H. Yang, C. S. Hsu, *Chem. Rev.* **2009**, *109*, 5868; c) P. L. T. Boudreault, A. Najari, M. Leclerc, *Chem. Mater.* **2011**, *23*, 456; d) P. M. Beaujuge, J. M. J. Frechet, *J. Am. Chem. Soc.* **2011**, *133*, 20009; e) Y. F. Li, *Acc. Chem. Res.* **2012**, *45*, 723.

[3] a) H. Y. Chen, J. H. Hou, S. Q. Zhang, Y. Y. Liang, G. W. Yang, Y. Yang, L. P. Yu, Y. Wu, G. Li, *Nat. Photon.* **2009,** *3*, 649; b) Y. Y. Liang, Z. Xu, J. Xia, S. T. Tsai, Y. Wu, G. Li, C. Ray, L. P. Yu, *Adv. Mater.* **2010,** *22*, E135; c) Z. C. He, C. M. Zhong, X. Huang, W. Y. Wong, H. B. Wu, L. W. Chen, S. J. Su, Y. Cao, *Adv. Mater.* **2011,** *23*, 4636; d) C. M. Amb, S. Chen, K. R. Graham, J. Subbiah, C. E. Small, F. So, J. R. Reynolds, *J. Am. Chem. Soc.* **2011**, *133*, 10062; e) T. Y. Chu, J. P. Lu, S. Beaupre, Y. G. Zhang, J. R. Pouliot, S. Wakim, J. Y. Zhou, M. Leclerc, Z. Li, J. F. Ding, Y. Tao, *J. Am. Chem. Soc.* **2011**, *133*, 4250; f) L. J. Huo, S. Q. Zhang, X. Guo, F. Xu, Y. F. Li, J. H. Hou, *Angew. Chem. Int. Ed.* **2011**, *50*, 9697; g) J. B. You, C.-C. Chen, L. T. Dou, S. Murase, H.-S Duan, S. Hawks, T. Xu, H. J. Son, L. P. Yu, G. Li, Y. Yang, *Adv. Mater.* **2012,** *24*, 5267; h) J. Y. Zhou, X. J. Wan, Y. S. Liu, Y. Zuo, Z. Li, He, G. G. G. K. Long, W. Ni, C. X. Li, X. C. Su, Y. S. Chen, *J. Am. Chem. Soc.* **2012**, *134*, 16345; i) Y.-X. Xu, C.-C. Chueh, H.-L. Yip, F.-Z. Ding, Y.-X. Li, C.-Z. Li, X. Li, W.-C. Chen, A. K.-Y. Jen, *Adv. Mater.* **2012**, *24*, *6356;* j) M. A. Green, K. Emery, Y. Hishikawa, W. Warta, E. D. Dunlop, *Prog. Photovolt: Res. Appl.* **2012**, 20, 12.

[4] a) J. Y. Kim, K. Lee, N. E. Coates, D. Moses, T. Q. Nguyen, M. Dante, A. J. Heeger, *Science* **2007**, *317*, 222; b) V. S. Gevaerts, A. Furlan, M. M. Wienk, M. Turbiez, R. A. J. Janssen, *Adv. Mater.* **2012**, *24*, 2130; c) L. T. Dou, J. B. You, J. Yang, C.-C. Chen, Y. J. He, S. Murase, T. Moriarty, K. Emery, G. Li, Y. Yang, *Nat. Photon.* **2012**, *6*, 180; d) L. T. Dou, J. Gao, E. Richard, J. B. You, C.-C. Chen, K. C. Cha, Y. J. He, G. Li, Y. Yang, *J. Am. Chem. Soc.* **2012**, *134*, 10071; e) L. T. Dou, W.-H. Chang, J. Gao, C.-C. Chen, J. B. You, Y. Yang, *Adv. Mater.* **2013**, 25, 825; f) J. B. You, L. T. Dou, K. Yoshimura, T. Kato, K. Ohya, T. Moriarty, K. Emery, C.-C. Chen, J. Gao, G. Li, Y. Yang, *Nat. Commun.* **2013**, 4, 1446. f) H. Zhou, L. Yang, W. You, *Macromolecules.* **2012**, 45, 607.

[5] a) G. Dennler, M. C. Scharber, T. Ameri, P. Denk, K. Forberich, C. Waldauf, C. J. Brabec, *Adv. Mater.* ***2008,*** *20,* 579; b) M. C. Scharber, D. Muhlbacher, M. Koppe, P. Denk, C. Waldauf, A. J. Heeger, C. Brabec, *Adv. Mater.* ***2006,*** *18,* 789; c) L. J. A. Koster, S. E. Shaheen, J. C. Hummelen, *Adv. Energy Mater*. **2012**; d) Z. M. Beiley, M. D. McGehee, *Energy Environ. Sci*. **2012**, 5, 9173.

[6] Y. Kim, S. Cook, S. M. Tuladhar, S. A. Choulis, J. Nelson, J. R. Durrant, D. D. C. Bradley, M. Giles, I. McCulloch, C.-S. Ha, M. Ree, *Nat. Mater.* **2006**, *5*, 197.

[7] a) J. H. Hou, H. Y. Chen, S. Q. Zhang, G. Li, Y. Yang, *J. Am. Chem. Soc.* **2008**, *130*, 16144; b) A. J. Kronemeijier, E. Gili, M. Shahid, J. Pivnay, A. Salleo, M. Heeney, H. Sirringhaus, *Adv. Mater.* **2012,** *24*, 1558; c) J. S. Ha, K. H. Kim, D. H. Choi, *J. Am. Chem. Soc.* **2011**, *133*, 10364.

[8] a) J. C. Bijleveld, A. Zoombelt, S. G. J. Mathijssen, M. M. Wienk, M. Turbiez, D. M. de Leeuw, R. A. J. Janssen, *J. Am. Chem. Soc.* **2009,** *131*, 16616; b) R. C. Coffin, J. Peet, J. Rogers,

G. C. Bazan, *Nat. Chem.* **2009**, *1*, 657; c) M. M. Wienk, M. Turbiez, J. Gilot, R.A. J. Janssen *Adv. Mater*. **2008**, 20, 2556.

[9] a) C. H. Woo, P. M. Beaujuge, T. W. Holcombe, O. P. Lee, J. M. J. Fréchet, *J. Am. Chem. Soc.* **2010,** *132*, 15547; b) A. T. Yiu, P. M. Beaujuge, O. P. Lee, C. H. Woo, M. F. Toney, J. M. J. Frechet, *J. Am. Chem. Soc.* **2012**, *134*, 2180.

[10] a) M. Wang, X. Hu, P. Liu, W.Li, X. Gong, F. Huang, Y. Cao, *J. Am. Chem. Soc*. **2011**, 133, 9638–9641. b) C. Piliego , T. W. Holcombe , J. D. Douglas , C. H. Woo , P. M. Beaujuge , J. M. J. Fréchet, *J. Am. Chem. Soc.,* **2010**, 132,7595-7597 ; b) Y.Zou , A. Najari , P. Berrouard , S. Beaupré, B. R. Aïch , Y.Tao , M. Leclerc, *J. Am. Chem. Soc.* **2010**, 132 , 5330–5331; c) Y. Zhang, S. K. Hau, H.-L. Yip, Y. Sun, O. Acton, A. K.-Y. Jen, *Chem. Mater*. **2010**, 22, 2696–2698; d) M.-S. Su, C.-Y. Kuo, M.-C. Yuan, U.-S. Jeng, C.-J. Su, K.-H. Wei, *Adv. Mater*. **2011**, 23, 3315; e) J. M. Szarko, J. Guo, Y. Liang, B. Lee, B. S. Rolczynski, J Strzalka, T. Xu, S. Loser, T. J. Marks, L.Yu, L. X. Chen, *Adv. Mater*. **2010**, 22, 5468–5472. f) Y. Liang, D. Feng, Y. Wu, S.-T. Tsai, G. Li, C. Ray, L. Yu, *J. Am. Chem. Soc.* **2009**,131,7792-7799. g) Y. Liang, Y. Wu, D. Feng, S.-T. Tsai, H.-J. Son, G. Li, L.Yu *J. Am. Chem. Soc*. **2009**, 131, 56.

[11] a) M. M. Wienk, M. Turbiez, J. Gilot, R.A. J. Janssen, *Adv. Mater*. **2008**, 20, 2556 ;b) J. C. Bijleveld, V.S. Gevaerts, D. Di Nuzzo1, M. Turbiez, S. G. J. Mathijssen, D. M. de Leeuw , M. M. Wienk, René A. J. Janssen, *Adv. Mater*. **2010**, 22, E242–E246.

[12] a) C. V. Hoven, X.-D. Dang, R. C. Coffin, J.Peet, T.-Q. Nguyen, G. C. Bazan, *Adv. Mater.* ***2010***, 22, E63; b) L.M. Chen, Z. Hong, G. Li, Y. Yang, *Adv. Mater*. **2009**, 21, 1434 ; c) Moon, J. S.; Takacs, C. J.; Cho, S.; Coffin, R. C.; Kim, H.; Bazan, G. C.; Heeger, A. J. *Nano Lett*. **2010**, 10, 4005; d) F.-C. Chen, H.-C. T., C.-J. Ko, *Appl. Phys. Lett*. **2008**, 92, 103316.

[13] a) G. Li, Y. Yao, H.Yang, V. Shrotriya, G. Yang, Y. Yang, *Adv. Funct. Mater.* ***2007***, 17, 1636*;* b) C.-W. Chu, H. Yang, W.-J. Hou, J. Huang, G. Li, Y. Yang, *Appl. Phys. Lett*. **2008**, 92, 103306.

[14] a) Y. Liang, Z. Xu, J. Xia, S.-T. Tsai, Y. Wu, Gang Li, .C. Ray, L. Yu, *Adv. Mater*. **2010**, 22, E135–E138;b) J. Peet, J. Y. Kim, N. E. Coates, W. L. Ma, D. Moses, A. J. Heeger,G. C. Bazan, *Nat. Mater*. **2007**, 6, 497.

[15] a) J. Guo, Y. Liang, J. Szarko, B. Lee, H. J. Son, B. S. Rolczynki, L. Yu, L. X. Chen, *J. Phys. Chem. B* **2010**, 114, 742; b) E. Verploegen, R. Mondal, C. J. Bettinger, S. Sok, M. F. Toney, Z. Bao, *Adv. Func. Mater*. **2010**, 20, 3519; c) S. M. Bennington, *J. Phys.: Condens. Matter*. **2000**, 12, L451; d) M.-Y. Chiu, U. S. Jeng, C.-H. Su, K. S. Liang, K.-H. Wei, *Adv. Mater*. **2008**, 20, 2573.

[16] a) W. Chen, T. Xu, F .He, W. Wang, C. Wang, J. Strzalka ,Y. Liu, J. Wen, D. J. Miller, J. Chen, K. Hong, L. Yu, S. B. Darling, *Nano Lett.* **2011**, 11, 3707; b) R.L. Jones, S. K. Kumar, D.L. Ho, R. M. Briber, T.P. Russell, *Nature* ,**1999**,400, 146; c) P. A. Staniec, A. J. Parnell, A. D. F. Dunbar, H. Yi, A. J. Pearson, T. Wang, P .E .Hopkinson, C. Kinane, R. M. Dalgliesh, A. M. Donald, A. J. Ryan, A. Iraqi, R. A. L. Jones, D. G. Lidzey, *Adv. Energy Mater.* **2011,** 1, 499; d) H. J. Son, L. Lu, W. Chen, T. Xu, T. Zheng, B. Carsten, J. Strzalka, S. B. Darling, L. X. Chen, L. Yu, *Adv. Mater*. **2013**, 25, 838.

[17] a) A.J. Mozer, N. S. Sariciftci, L. Lutsen, D. Vanderzande, R. Osterbacka, M. Westerling, G. Juska, *Appl. Phys. Lett*. **2005**, 86, 112104.b) A.J. Moulé, J.B. Bonekamp, K. Meerholz, *Journal of Applied Physics*, **2006**, 100, 094503

[18] S. C. Price, A. C. Stuart, L. Yang, H. Zhou, W. You, J. *Am. Chem. Soc*. **2011**, 133, 4625.

[19] J. Gao, W. Chen, L. Dou, C.-C. Chen, W.-H. Chang, Y. Liu, G.Li, Y. Yang, *Adv. Mater.* **2014**, 26, 3142

[20] J. Gao, L. Dou, W. Chen, C.-C. Chen, X. Guo, J. You, B. Bob, W.-H. Chang, J.Strzalka, C.Wang, G.Li, Y. Yang, *Adv. Energy Mater.* **2014**, 4, 1300739

Chapter 3 Elucidating the Working Mechanisms of Solvent Additives in Morphology Optimization of Diketopyrrolopyrrole-based Narrow Bandgap Polymer Solar Cells

3.1 Introduction

Tremendous efforts have been made in the field of organic photovoltaic cells (OPVs) in the past few years, with the highest reported power conversion efficiency (PCE) reaching over 10%.[1][2][3] The achievements have been realized through chemical structure modification of donors and acceptors[4][5][6], improvement in active-layer processing methods[7][8][9][10], interfacial morphology control[11][12][13] and device structure engineering.[14][15][16]

Narrow band gap polymer materials with a photo-response extended to the infrared region are critical for recent technical breakthroughs. Among narrow band gap polymers with high PCEs, benzodithiophen (BDT)-based and diketopyrrolopyrrole (DPP)-based copolymers are very promising due to their high yield in synthesis, and energy levels that are compatible with commonly used acceptors such as [6,6]-phenyl-C71-butyric acid methyl ester ($PC_{71}BM$). These polymers have enabled high efficiency tandem and visibly transparent OPV devices. [14][15][16] Chemical structure modification of these narrow bandgap polymers has been explored to further improve their efficiency. However, processing difficulties have limited the application of these narrow bandgap polymers to OPV devices. For example, the promising polymer, poly(2,6'-4,8-di(5-ethylhexylthienyl)benzo[1,2-b;3,4-b]dithiophene-alt-5-dibutyloctyl-3,6-bis(5-bromothiophen-2-yl)pyrrolo[3,4-c]pyrrole-1,4-dione] (PBDTP-DPP)[17] was found to be highly

soluble only in chloroform (CF) when its molecular weight exceeded 25 kDa,[18] while limited solubility was observed in organic solvents such as chlorobenzene (CB) and 1,2-dichlorobenzene (DCB). Previous literature demonstrate that, in spite of the processing difficulties, high molecular weight polymers are still preferred for achieving high efficiency.[17][19] In the case of the high-molecular-weight PBDTP-DPP processed with CF, this low-boiling-point solvent prohibits polymer self-organization,[20][21] resulting in a sub-optimal morphology that leads to poor device performance of only 1.5% PCE.[14]

Recent studies have shown that a solvent-mixture approach is an efficient method to induce improved morphology in various narrow-bandgap polymer systems for polymer:fullerene blend films.[7][22][23][24][25] We reported organic solar cells based on a thin film composed of PBDTP-DPP donor and $PC_{71}BM$ acceptor, where 1,8-diiodoctane (DIO) was shown to be an effective additive to CF (CF-DIO), achieving a PCE of 5.8%.[7]

However, DIO itself is not stable for long-term usage. Once exposed to air and in the presence of light, it will react with O_2 and form 8-hydroxyoctanal and I_2; these products are defects or trap sites for carriers, leading to severe deterioration in performance of devices cast under ambient environment. Therefore, fabrication processes involving DIO have to be limited to an air free environment, which is unfavorable for large-area fabrication. As a result, an efficient air-stable solvent additive is strongly desired. [14]

Here, we show that an air-stable solvent additive, DCB, works as an effective additive for processing PBDTP-DPP:$PC_{71}BM$ blends using CF as the main solvent (referred to as CF-DCB). Performance optimization of CF-DCB has led to an enhanced PCE of 6.6%, resulting from an optimized morphology. Also, DCB is found to be superior to DIO for this polymer, with a higher

maximum PCE (6.6% with DCB vs. 5.8% with DIO) and a much wider additive operation window (up to 80% for DCB vs. less than 10% for DIO). More importantly, the morphology formation mechanism in CF-DCB solvent mixture is found to be different from that in the widely-studied DIO solvent additive.

In this chapter, we will first demonstrate the improvements observed in device properties and the corresponding morphology for both solvent mixture systems. Second, we found that DCB outperforms DIO with a higher PCE peak value and a much wider additive operation window. Third, detailed morphology characterization results will be presented to distinguish morphology optimization processes between these two additives. In particular, transmission electronic microscopy (TEM), UV-visible absorption and grazing incidence wide-angle x-ray scattering (GIWAXS) are used to characterize the thin-film morphology, and small angle neutron scattering (SANS) and solution UV-visible absorption spectroscopy are conducted to understand changes in solution-stage polymer conformations.

3.2 Experimental

3.2.1 Device Fabrication

PBDTP-DPP (and the other polymers reported here) and $PC_{71}BM$ were co-dissolved in CF with a weight ratio of 1:2 at a concentration of 8 mg/mL. Mixed solvents with different volume ratios of DIO and DCB were used to further improve the final device performance. ITO-coated glass substrates ($15\Omega/cm^2$) were cleaned stepwise in detergent, water, acetone, and isopropyl alcohol under ultrasonication for 15 minutes each, and subsequently dried in an oven for five hours. A thin layer (~30 nm) of PEDOT:PSS (Baytron P VP A1 4083) was spin-coated onto the

ITO surface, which was pretreated by ultraviolet ozone for 15 minutes. After being baked at 120 ℃ for approximately 20 minutes, the substrates were transferred into a nitrogen-filled glove box (<0.1 ppm O_2 and H_2O). A polymer/$PC_{71}BM$ composite layer (ca. 100 nm thick) was then spin-cast from the blend solutions at 3000 rpm on the ITO/PEDOT: PSS substrate without further special treatments. Then the film was transferred into a thermal evaporator, which was located in the same glove box. A calcium layer (20 nm) and an aluminum layer (100 nm) were deposited in sequence under a vacuum of 2×10^{-6} torr. The active area of the device was measured to be 0.10 cm^2.

3.2.2 Device Characterization

The fabricated devices were encapsulated in a nitrogen-filled glovebox by UV epoxy and a cover glass. The current density-voltage (J-V) curves were measured using a Keithley 2400 source-measure unit. The photocurrent was measured under AM 1.5 G illumination at 100 mW/cm^2 under the Newport Thermal Oriel 91192 1000W solar simulator (4 in. × 4 in. beam size). External quantum efficiencies (EQEs) were measured using a lock-in amplifier (SR830, Stanford Research Systems) with a current preamplifier (SR570, Stanford Research Systems) under short-circuit conditions. The devices were illuminated by monochromatic light from a xenon lamp passing through a monochromator (SpectraPro-2150i, Acton Research Corporation) with a typical intensity of 10 μW. Prior to imposing the incident beam on the device, the monochromic incident beam was chopped with a mechanical chopper that was connected to the lock-in amplifier, and then focused on the testing pixel of the device. The photocurrent signal

was then amplified by the SR570 and detected by the SR830. A calibrated monocrystal silicon diode with a known spectral response was used as a reference.

3.2.3 Morphology Characterization

Grazing Incidence Wide-Angle X-ray Scattering (GIWAXS): GIWAXS measurements were performed at the 8ID-E beam line at the Advanced Photon Source (APS), Argonne National Laboratory (ANL) using x-rays with a wavelength of $\lambda = 1.6868$ Å and a beam size of 200 μm (h) by 20 μm (v). To ensure comparable results to those of OPV devices, the measured samples were prepared on silicon substrates modified by PEDOT:PSS under the same conditions as those used for fabrication of solar cell devices. A 2-D PILATUS 1M-F detector was used to capture the scattering patterns and was situated 204 mm from samples. The background of the line cuts was estimated by fitting two exponential functions, and the parameters of the scattering peaks were obtained through the best fitting line using a Pseudo-Voigt type 1 peak function.

Small Angle Neutron Scattering (SANS): PBDTP-DPP was dissolved in a mixed solution of deuterated chlorobenzene (C_6D_5Cl) and $PC_{71}BM$ (8 mg/ml) to make a 4 mg/ml solution. SANS measurements of these mixed solutions were performed at HFIR GP-SANS (CG2), Oak Ridge National Laboratory (ORNL) and NG7 30m SANS, National Institute of Standards and Technology (NIST). Data was analyzed by the fractal model [46] using the SANS analysis package [47] provided by NCNR, NIST after background subtraction using a mixed solution of deuterated chlorobenzene (C_6D_5Cl) and $PC_{71}BM$ (8 mg/ml).

Absorption Spectrum: Absorption measurements were performed on a Hitachi U-4100 Spectrumphotometer on films with an ITO/PEDOT/Active layer configuration in the wavelength range of 300 nm-900 nm. Solution absorption spectra were measured with the polymers dissolved in CF solution with different additives and under different concentration conditions.

TEM measurement: TEM (Transmission Electron Microscopy) was conducted on the Model JEM 1200-EX instrument with C_s=1.9 at an accelerating voltage of 80 kV on thin films of polymer:fullerene blends processed with or without CN. The film thickness was the same as that of the devices. The sample holder was a TEM GRID 400 MESH from Tedpella. Inc, with grid hole size of 42 μm and Carbon Type-B as the supporting film. The bright-field images were taken with a magnification of 150K.

Mobility measurement: Hole and electron mobilities was measured using the space charge limited current model (SCLC) ,with diode configuration of ITO/PEDOT:PSS/polymer:$PC_{71}BM$/ Au or ITO/Al/polymer:$PC_{71}BM$/Ca/Al by taking current-voltage curves in the range of 0-6 V and fitting the results to a space charge limited form, described by $J= (8/9)\ \varepsilon_r\ \varepsilon_0\ \mu_e\ (V^2/L^3)$,where ε_0 is the permittivity of free space, ε_r is the dielectric constant of the polymer, μ_e is the hole mobility, V is the voltage drop across the device and L is the polymer thickness. The dielectric constant ε_r was assumed to be 3, which is a typical value for conjugated polymers or fullerenes. The thickness of the films was measured with a Dektek profilometer.

3.3 Results and Discussion

3.3.1 Device performance

Both the synthesis and characterization of PBDTP-DPP have been described elsewhere.[14] The chemical structure of PBDTP-DPP is shown in Figure 3.1.

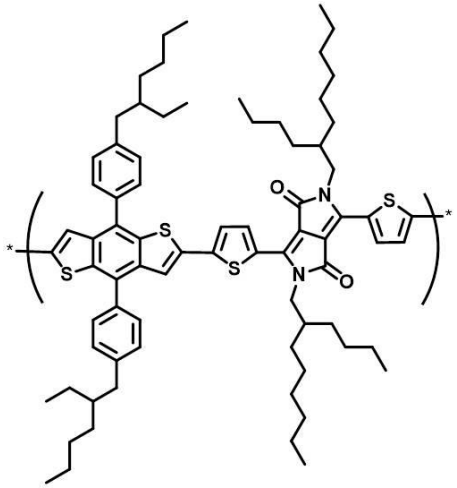

Figure 3.1 Chemical structure of PBDTP-DPP

The solar cells fabricated from different solvent mixture conditions are characterized by current-voltage (*J*-*V*) measurements. Figures 3.2 and 3.3 present the variations of the short-circuit current (J_{sc}) and the device efficiency with different volume percentages of solvent additives in CF solvent. The data points and error bars are derived from at least eight devices fabricated under each condition.

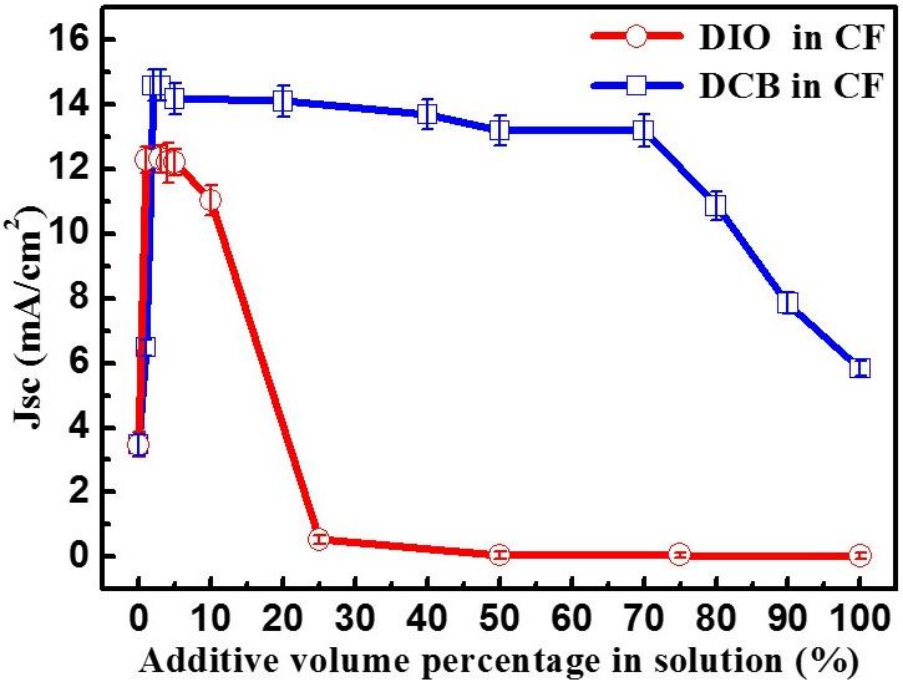

Figure 3.2 Variations of short-circuit current density (Jsc) of PBDTP-DPP: $PC_{71}BM$ blend thin-film cells with different amounts of DIO and DCB additives in CF solution.

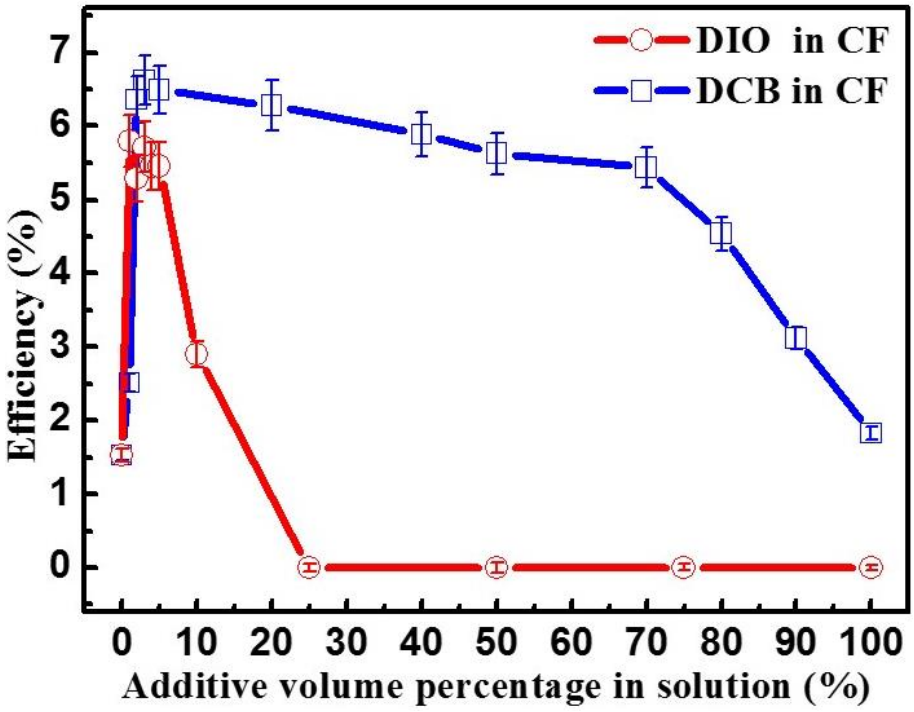

Figure 3.3 Variation of efficiency of PBDTP-DPP:$PC_{71}BM$ blend thin-film cells with different amounts of DIO and DCB additives in CF solution.

As shown in Figure 3.2 and 3.3, the best device efficiencies were achieved under CF-1% DIO (PCE 5.8%) and CF-3% DCB (PCE 6.6%), while the devices fabricated from pure CF exhibited only 1.5% PCE. The corresponding J-V curves are shown in Figure 3.4 and the related performance parameters are summarized in Table 3.1.

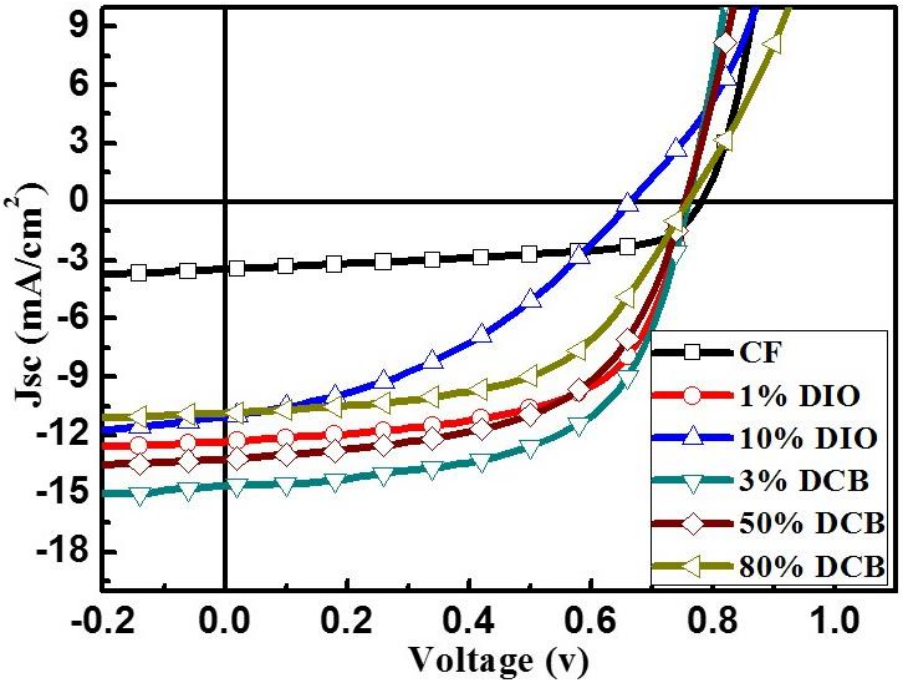

Figure 3.4 Variation of current-voltage curve of PBDTP-DPP:$PC_{71}BM$ blend thin-film cells with different amount of DIO and DCB additives in CF solution

Table 3.1 Parameters related to PBDTP-DPP: PC71BM BHJ device at optimum condition

Solvent Composition	PCE [%]	Voc[V]	Jsc [mA/cm^2]	FF [%]	Hole Mobility [cm^2/(V*S)]
CF	1.5	0.78	3.47	57	$9.04*10^{-5}$
CF-DIO (1%)	5.84	0.75	12.3	62	$2.87*10^{-4}$
CF-DCB (3%)	6.62	0.76	14.60	60	$9.79*10^{-4}$

The active layer thickness was ~120 nm in all fabricated devices. Figure 3.5 shows the external quantum efficiency (EQE) curves of the three devices made from CF only, CF-1% DIO, and CF-3% DCB mixture.

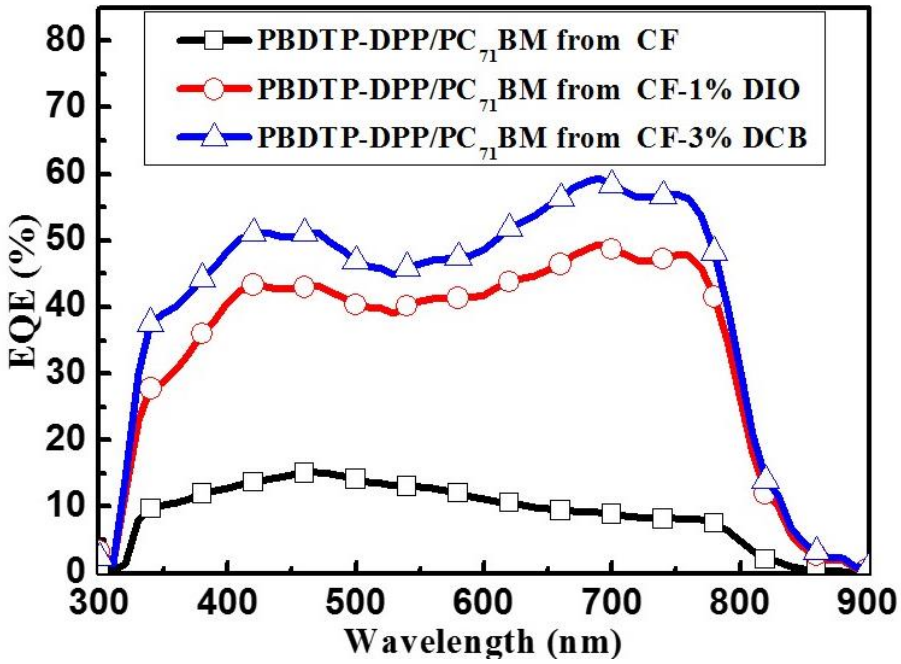

Figure 3.5 Variations of EQE curve of PBDTP-DPP: $PC_{71}BM$ blend thin-film cells with different amount of DIO and DCB additives in CF solution

The carrier mobility was measured by SCLC, with the log J vs. Log V curves shown in Figure. 3.6.

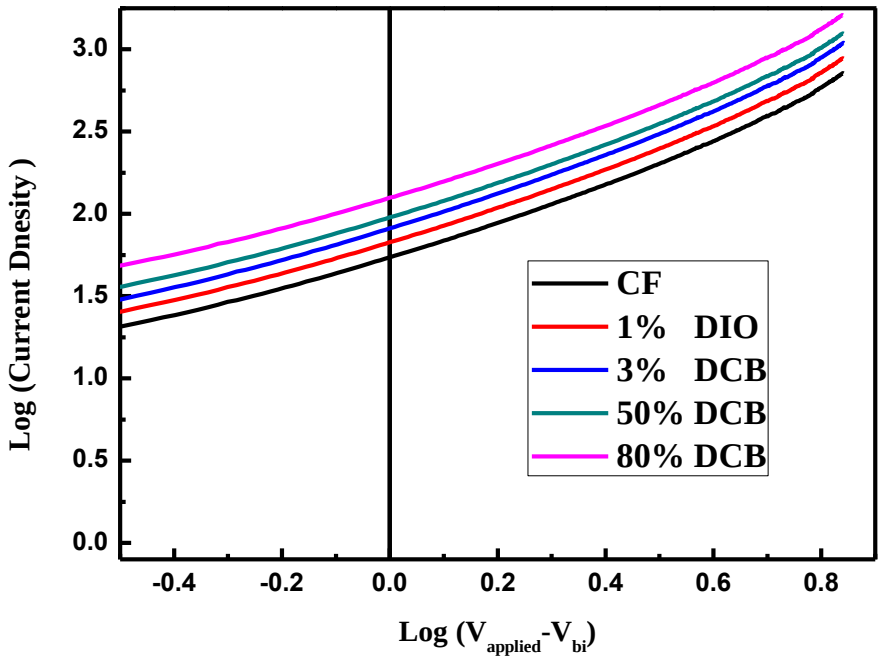

Figure 3.6 J-V curves of PBDTP-DPP:PCBM blend films in hole-only device from the SCLC model.

The peak EQE value increases from 15% in the CF device to 47% in the CF-1% DIO device, and the maximum EQE further increases to 57% in the CF-3% DCB device. Furthermore, the EQE shape changes as the peak position shifts from 460 nm to ~700 nm, thus the biggest improvements are in the long wavelength region. The significantly enhanced long wavelength response, particularly the clear shoulders at ~770 nm, along with the GIWAXS data shown later, indicate enhanced polymer crystallinity in the active layer. The CF-DCB devices outperformed the CF-DIO samples in both PCE and effective solvent additive working window (the range of DIO or DCB additive amount allowed in CF while maintaining high efficiency) as shown in Figure 3.2 and 3.3. The much wider working window of CF-DCB (over 4.5% PCE with 1-80% volume percentage of DCB) compared to that of CF-DIO (less than 3% PCE when approaching and beyond 10% DIO) suggests there might be a different working mechanism for morphology

evolution. The significantly wider solvent mixture operation window of CF-DCB could be beneficial in industrial settings, as less restriction and care are needed during solution preparation.

3.3.2 Thin-film morphology study by TEM

The morphology of active layer was first studied using TEM. [31][32] An image of a polymer:fullerene film from the CF-only solution is shown in Figure 3.7(a) with relatively coarse domains of size ~200 nm.

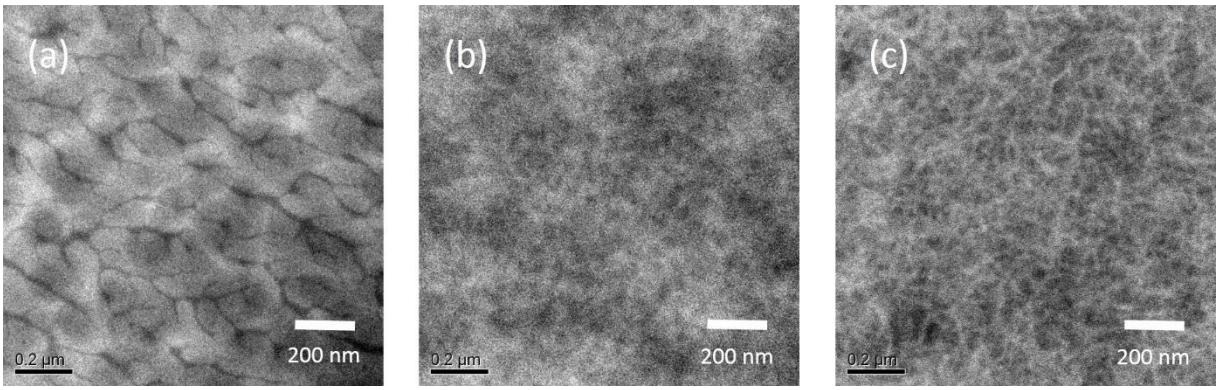

Figure 3.7 TEM images of thin-film PBDTP-DPP: $PC_{71}BM$ blend cast from solutions of (a) CF only (b) 1% DIO in CF and (c) 3% DCB in CF.

When 1% DIO (CF-1% DIO, Figure 3.7 (b)) and 3% DCB was added into CF (CF-3% DCB, Figure 3.7(c)), fibrillar-structured polymer domains were observed in both cases,

indicating the formation of ordered polymer domains, which facilitate carrier transport. [31][33] This result is consistent with the corresponding device performance mentioned previously.

3.3.3 Thin-film morphology study by photoluminescence (PL)

PL results from films made with different solvent mixtures are shown in Figure 3.8. The degree of PL quenching is significantly increased by adding 1% DIO and 3% DCB, indicating enhanced exciton dissociation efficiencies with additives. This is consistent with improved device performances obtained under these two conditions. However, further increasing the DCB content (80% DCB) leads to increased PL intensity, suggesting that the polymer domain size exceeds the exciton diffusion length, making excitons recombine before reaching polymer & fullerene interface. [39] In the 100% DCB case, the polymer correlation length (190 Å in Table 3.2) becomes too large for efficient exciton dissociation and gives rise to much stronger PL signals than all the other situations in Figure 3.8. This explains why CF, instead of DCB, is used as the main solvent for this polymer system in the first place.

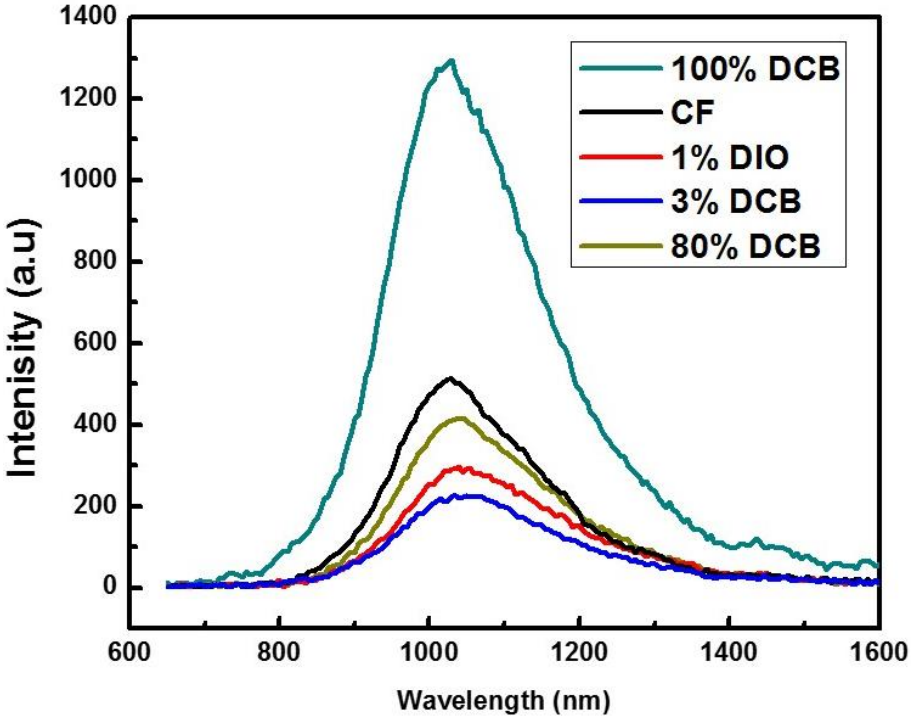

Figure 3.8 Variation of PL of PBDTP-DPP:$PC_{71}BM$ blend thin-film cells with different amount of DIO and DCB additives in CF solution

3.3.4 Thin-film morphology study by GIWAXS

In order to investigate the morphology at the molecular level, GIWAXS measurements (Figure 3.9 and Table 3.1) were conducted to obtain information on polymer chain packing, crystallite size and orientation distribution in the films. [34-37]

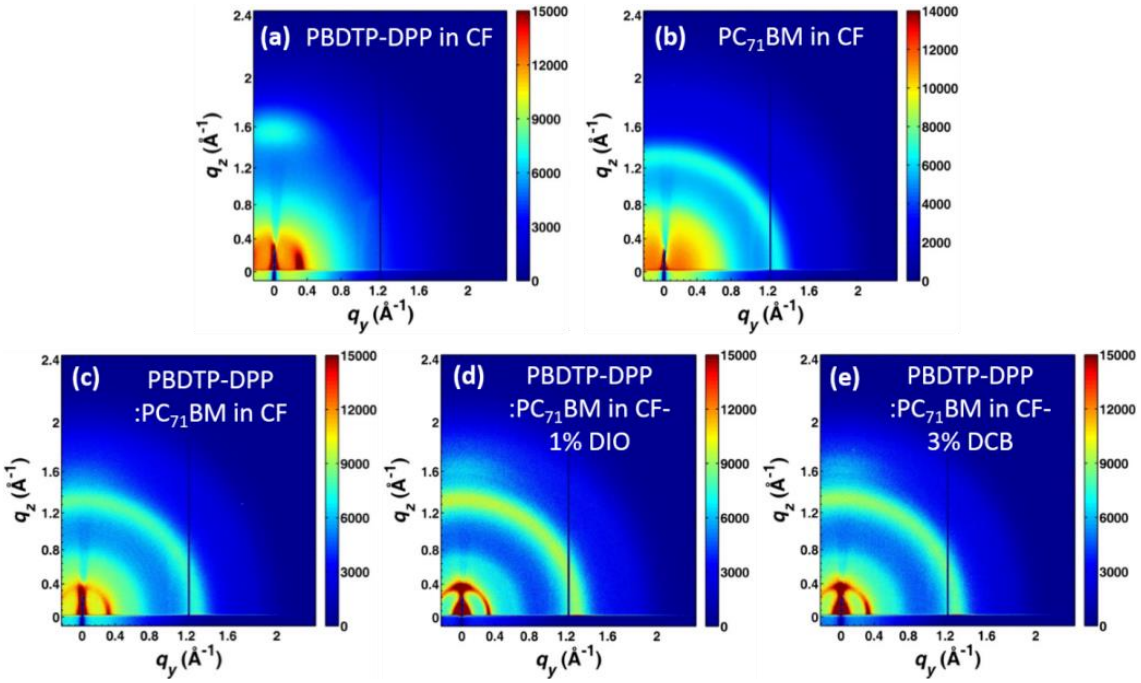

Figure 3.9 2-D GIWAXS patterns for (a) PBDTP-DPP only thin film cast from CF (b) $PC_{71}BM$ only thin film cast from CF (c) PBDTP-DPP: $PC_{71}BM$ blend thin film cast from CF (d) PBDTP-DPP: $PC_{71}BM$ blend thin film cast from 1% DIO in CF (e) PBDTP-DPP: $PC_{71}BM$ thin film cast from 3% DCB in CF

Figure 3.9(a) and (b) show the 2-D GIWAXS patterns of the polymer-only and $PC_{71}BM$-only films. For PBDTP-DPP-only film, a pronounced peak centering at 1.55±0.05 $Å^{-1}$ in the q_z direction was observed, indicating that π-π stacking of polymer chains along the out-of-plane (OOP) direction follows a 'face-on' manner. Figure 3.9(b) shows the 2-D GIWAXS pattern of $PC_{71}BM$-only film cast from CF. Here, three characteristic peaks centering at 0.72±0.02 $Å^{-1}$, 1.29±0.04 $Å^{-1}$ and 1.86±0.06 $Å^{-1}$ were observed, representing $PC_{71}BM$.[38]

Table 3.2 summarizes the parameters extracted from intensity linecuts along both the in-plane (IP) direction (q_y) and out-of-plane (OOP) direction (q_z).

Table 3.2 Parameters extracted from 2-D GIWAXS profiles PBDTP-DPP:$PC_{71}BM$ thin film case from different solution compositions

Solvent Composition	Qy (1/Å)	Lamellar Spacing (Å)	Qy FWHM	PBDTP-DPP Lamellar Correlation Length (Å)	Qz (1/Å)	π-π Spacing (Å)	Qz FWHM	$PC_{71}BM$ Correlation Length (Å)
PBDTP-DPP in CF	0.315±0.009	19.9±0.6	0.065	91	1.55±0.05	4.1±0.2		
$PC_{71}BM$ in CF					1.29±0.04		0.26	23
PBDDTP-DPP:PCBM in CF	0.324±0.009	19.4±0.6	0.066	89	1.55±0.05	4.1±0.2	0.31	19
PBDTP-DPP:PCBM in CF 1%DIO	0.329±0.009	19.1±0.6	0.049	121	1.59±0.05	4.0±0.2	0.31	19
PBDTP-DPP:PCBM in CF 3%DCB	0.332±0.009	18.9±0.6	0.052	114	1.60±0.05	3.9±0.2	0.29	20
PBDTP-DPP :PCBM in DCB	0.311±0.009	20.2±0.6	0.032	190	1.55±0.05	4.1±0.2	0.36	16

The polymer packing information in the blend films cast from various solvent systems were also studied. Figure 3.9(c), (d) and (e) show the 2-D GIWAXS patterns of polymer: $PC_{71}BM$-blend films cast from solutions of CF-only, CF-1% DIO and CF-3% DCB, respectively. For all cases listed in Table 3.2, the variations in the π-π spacing are within the experimental resolution limit, suggesting no significant change in π-π stacking of polymer chains in the films cast from different solvent mixtures. However, the lamellar correlation length (defining the crystalline region area) of PBDTP-DPP in the blend film [34] increases from 89 Å in CF-only case, to 121 Å in CF-1% DIO, and to 114 Å in CF-3% DCB. This demonstrates that PBDTP-DPP polymer chains are more ordered in the blend films cast from the mixed solvent systems. The largest correlation length of PBDTP-DPP is 190 Å from the pure DCB solvent cast film. Ultimately, the GIWAXS results reveal that the PBDTP-DPP polymers form a proper domain

size with the correlation length of 110 - 120 Å in blend film cast from both CF-1% DIO and CF-3% DCB solvent mixtures.[37]

3.3.5 Solution morphology study by SANS

To better understand the differences in the two solvent mixture systems, small angle neutron scattering (SANS) was performed to investigate polymer conformation in the solution state.[37-38] Figure 3.10 shows the Kratky curves of PBDTP-DPP polymers in the mixed solvent systems, based on Porod-Debye approximations.[40] Kratky curves [41] were plotted for qualitatively assessing polymer chain conformations in solution, based on the fact that neutrons are scattered distinctly by polymers assuming different shapes. In CF and CF-10% DIO solutions, parabolic decay relationships were acquired, indicting tightly folded, round polymer conformations. In contrast, a hyperbolic decay is observed for the CF-80% DCB case, indicating an unfolded structure.[41] Kratky curves demonstrated that polymers chains are relatively coiled and folded in CF and CF-DIO solution, while in CF-DCB solution, they are well stretched and extending along the main chain direction.

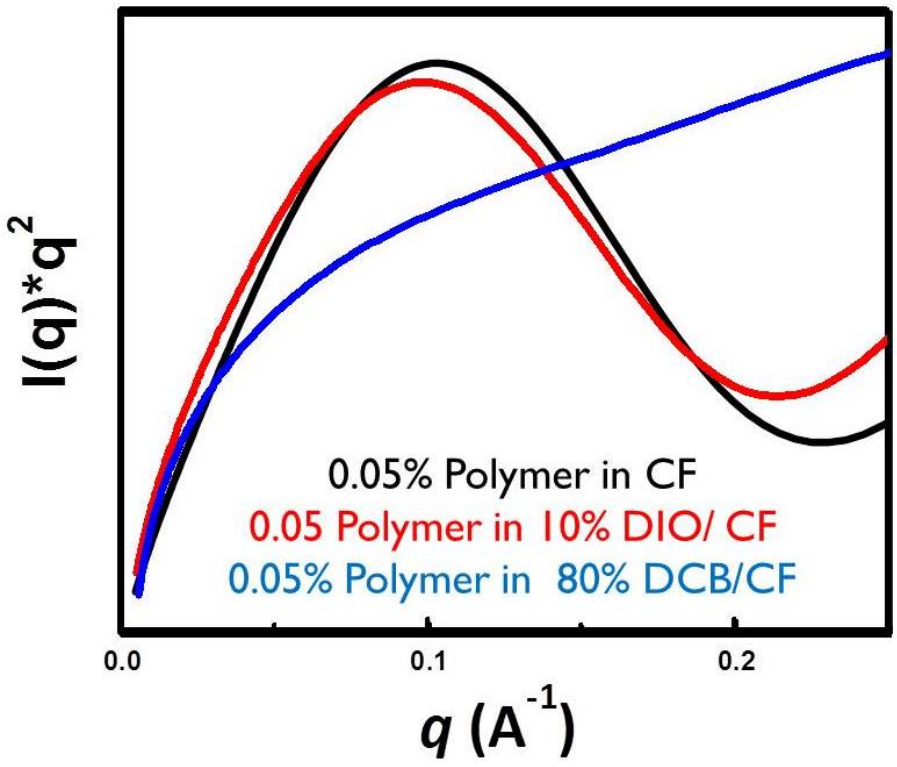

Figure 3.10 Kratky plots of PBDTP-DPP in solutions of (a) CF only (b) 10% DIO in CF and (c) 80% DCB in CF.

3.3.6 Solution morphology study by absorption spectroscopy

Variations in the position, intensity, and shape of the absorption spectra can also be a useful measure of polymer conformations in different solvents. UV-vis spectra of the dilute solutions (0.05 wt.%) and films cast from various CF-DIO/CF-DCB compositions are shown in Figure 3.11.

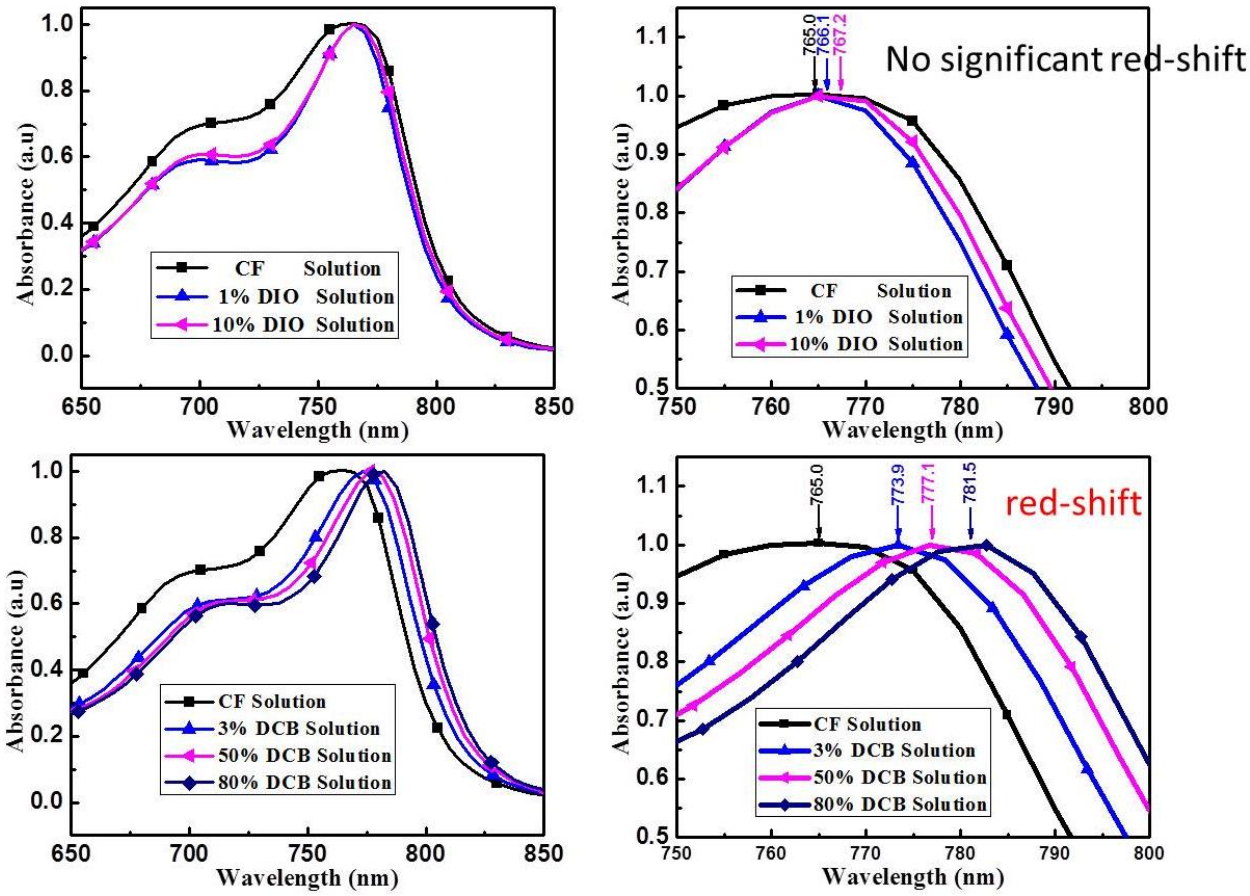

Figure 3.11 Absorbance of PBDTP-DPP in dilute solution (0.05 wt.%) under different solvent mixtures.

In CF-DIO solutions, as shown in Figure 3.11(a) and (b), the absorption peaks show no significant shifts in the spectrum when DIO is gradually added to the CF solution, i.e., 765.0 nm in CF-only, 766.1 nm in CF-1% DIO, and 767.2 nm in CF-10% DIO. In contrast, The CF-DCB solution absorption results shown in Figure 3.11(c) and (d) exhibit noticeable redshifts in comparison to CF (peak position at 765.0 nm): +8.9 nm (3% DCB in CF), +12.1 nm (50 % DCB in CF), and +16.5 nm (80% DIO in CF). These red shifts of the absorption peak positions are different from those in the CF-DIO solutions.

In dilute solutions, polymer chains are separate from each other. As demonstrated earlier by SANS, with increased DCB content in solution, the tight-folded backbone of a single polymer chain in CF would gradually adjust its conformation to a well-extended structure, leading to an increased conjugation length. This serves as a plausible explanation for the observed redshifts of absorption peak position. [42]

Another possible explanation for the observed red-shift is solvatochromism.[43] Solvatochromic shifts result from the fact that both polymers' absorption and emission spectra are strongly dependent on solvent polarity. Since the polarities of the ground and excited states of a polymer chain are different, variations in solvent polarity will lead to different degrees of stabilization of the ground and excited states, giving rise to a change in the energy gap between these electronic states.[43] The Lippert-Mataga equation has been widely used to assess quantitatively the difference between the ground- and excited state dipole moments ($\Delta\mu_e$) from the shift in spectra. The equation gives a relationship based on the static dielectric constant (ε_s) and refractive index (n) of the solvents as follows: [44]

$$\bar{\nu} = -\frac{2(\Delta\mu_e)^2}{hcs^3}\left[\frac{\epsilon_s - 1}{2\epsilon_s + 1} - \frac{n^2 - 1}{4n^2 + 2}\right]$$

Where h, c, s and $\bar{\nu}$ are Planck's constant, the speed of light, and the semi-major axis of an ellipsoidal cavity containing the polymer chain, the spectral shift of the emission band maximum, respectively.[44]

If we assume $\left[\frac{\epsilon_s - 1}{2\epsilon_s + 1} - \frac{n^2 - 1}{4n^2 + 2}\right]$ is signifiable by X and $-\frac{2(\Delta\mu_e)^2}{hcs^3}$ is a constant, then its value equals to the slope of the plot of $\bar{\nu}$ vs. X. Through calculations based on this equation, we obtained data points representing CF, CF-3% DCB, CF-50% DCB and CF-80% DCB, as shown in Figure 3.12, where line fitting results show that $-\frac{2(\Delta\mu_e)^2}{hcs^3}$ is -4.09E10^{-4}. [45]

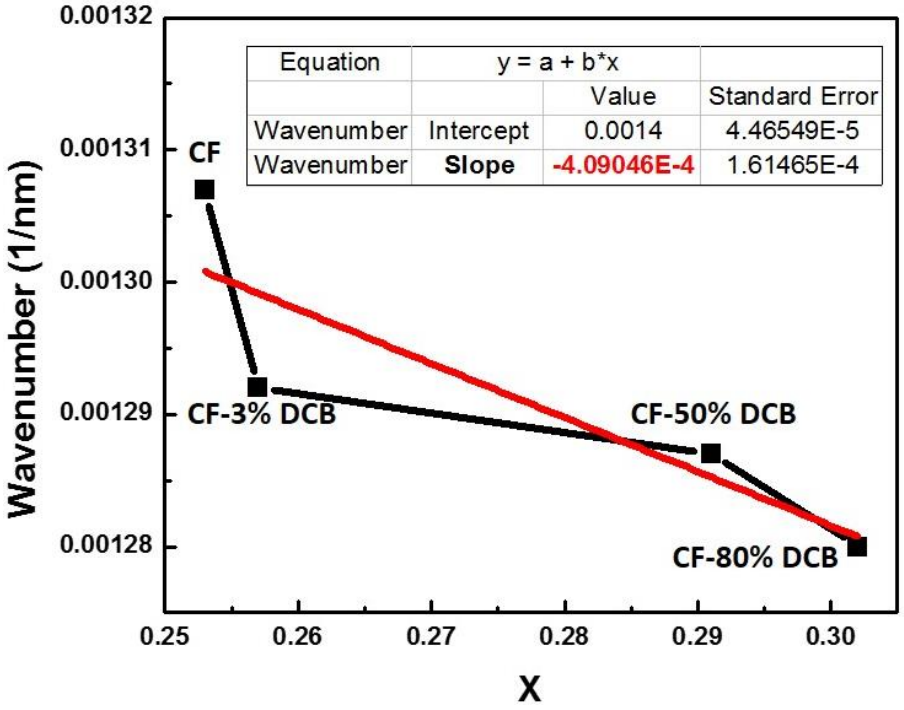

Figure 3.12 Wavenumber vs. X plots for PBDTP-DPP in CF-DCB solutions

Through plugging the value of $-\frac{2(\Delta\mu_e)^2}{hcs^3}$ into the Lippert-Mataga equation, we found that the calculated positions (in wavelengths) of peaks shifted due to solvatochromism itself are 766.0 nm for CF-3% DCB ,774.2 nm for CF-50% DCB and 776.9 nm for CF-80% DCB, respectively.

Therefore, the calculated red-shifts (in wavelengths) by solvatochromic effects alone are +1.0 nm for CF-3% DCB, +9.2 nm for CF-50% DCB and +11.9 nm for CF-80% DCB.[44] By comparing the calculated results with the measured ones (+8.9 nm for CF-3% DCB, +12.1 nm for CF-50% DCB, and +16.5 nm for CF-80% DCB), it appears that, in addition to the contributions from solvents' polarity, changes of polymer conformations are also responsible for causing the red-shifts, even though this effect is less pronounced than that of solvatochromism.

Furthermore, a dramatic red-shift in Figure 3.12 is observed with the addition of 3% DCB into CF, whose slope is significantly larger than those of changes caused by continuing adding DCB (e.g. from CF-3% DCB to CF-50% DCB, CF-50% DCB to CF-80% DCB, etc.). This indicates that the addition of 3% DCB might have already caused substantial conformation changes of polymer chains, as their absorption spectra exhibit a much larger degree of red-shifts than predicted by solvatochromic effects at this composition ratio. As changes from CF-3% DCB to CF-50% DCB and from CF-50% DCB to CF-80% DCB are less drastic, it is reasonable to assume that most coiled polymer chains in CF have already experienced chain-stretching with 3% DCB added, and further increasing DCB concentration will only lead to minor conformation changes. This is also consistent with the wide additive operation window discussed earlier in this chapter, within which the device performance is not significantly sensitive to DCB concentration. As a result, red-shifts observed beyond 3% DCB are mostly likely caused by solvatochromism, with their values closely following the trends described by Lippert-Mataga equation.

Given the discussions above, the solution absorption data are consistent with the SANS data, as they both indicate the existence of polymer chain conformation changes from coiled to unfolded structures with addition of DCB into CF. [44]

3.3.7 Morphology formation mechanism

Even though the working mechanism of DIO for morphology optimization has been extensively studied since its discovery, there is still no definite answer to why DIO helps morphology. Peet et al. proposed that through adding DIO, a pronounced difference in the distribution of the three phases: polymer-rich domains, PCBM-rich domains and polymer:PCBM domains (Figure 3.13) could explain the improved device performance.[24] As the low boiling point solvent (here CF) evaporates fast and leaves the system first during the film formation process, the remaining solution is dominated by the slow-drying DIO ,which modifies the degree of phase separation and local structural order in the resultant film, as shown in Figure 3.13.[7][24][26] This explanation is consistent with the improved polymer structural order in CF-DIO cases discussed earlier in this work. [24]

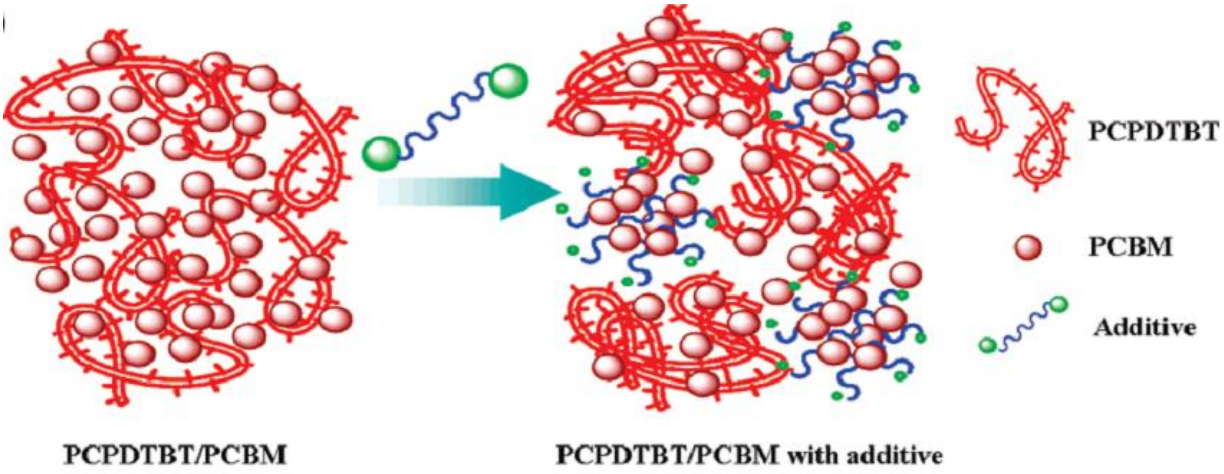

Figure 3.13 Proposed mechanisms for DIO in polymer/PCBM morphology control [24]

Given the differences in polymer chain conformations between CF-DIO and CF-DCB solutions demonstrated by SANS and absorption spectroscopy, here we are going to explain this interesting phenomenon in terms of interactions between solute functional groups and solvent molecules.

CF belongs to the category of non-aromatic solvents. According to the principle of ‘‘like dissolves like’’, [38] it will solvate the unconjugated segments of polymers such as solubilizing side chains. In contrast, CF would tend to avoid contact with the aromatic main chains, whose chemical structure is significantly different. As a result, when dissolved in CF, the polymer main chains are expected to coil to maximize the interaction between non-conjugated side chains and non-conjugated solvents, while minimizing the contact between aromatic segments and nonaromatic CF molecules.[44][45] This scenario is shown schematically in Figure. 3.14.

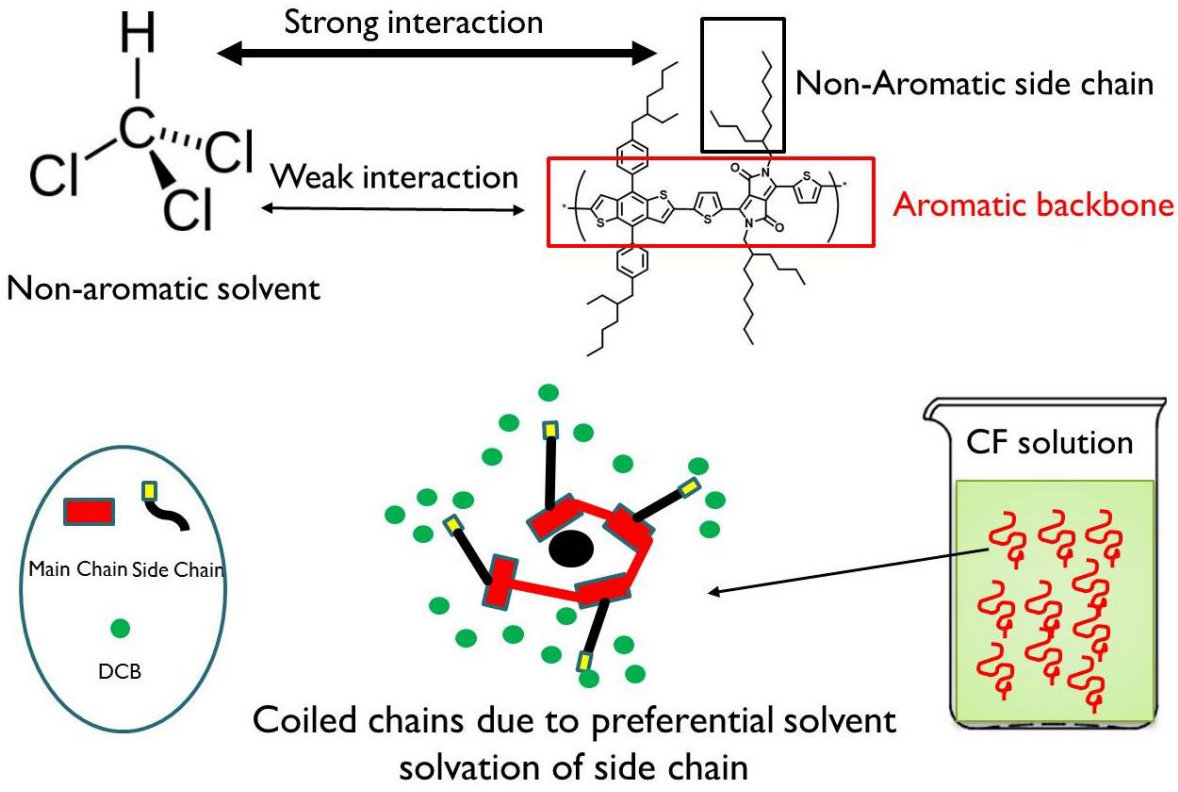

Figure 3.14 Schematic presentations of polymer/CF interactions and the resultant polymer chain conformations

In contrast, DCB is an aromatic solvent, thus exhibits a stronger tendency to interact with the aromatic segments (backbones of polymer chains) than side chains.[44][45] Therefore, adding DCB into CF will induce the polymer chain conformation changes, from tightly folded coils in CF to unfolded and stretched structure in CF-DCB solutions, as interpreted in Figure 3.15.

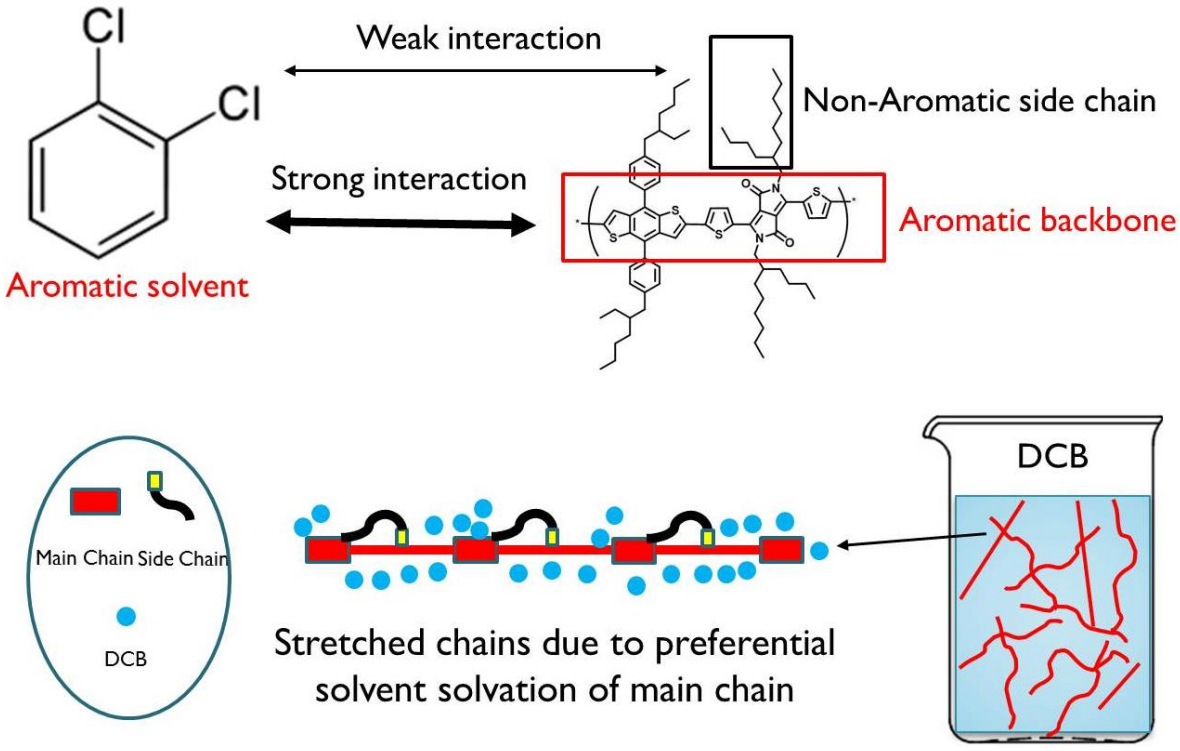

Figure 3.15 Schematic presentations of polymer/DCB interactions and the resultant polymer chain conformations

The assumption that solution-stage polymer conformations have a profound influence on the properties of as-cast thin film is proposed by Schwartz et al; [44] they suggest that open and well-extended conformations of polymer chains in solution have a high tendency to survive into the as-cast thin-films; polymer chains keep a memory of their spatial arrangements though the film casting process. [44--47]

During the solvent removal stage, CF leaves the system first due to its relatively low boiling point. The slower evaporation of high-boiling point solvent DCB allows more time for polymers to organize themselves, thus these well-extended chains exhibit a high tendency to

preserve their solution-stage configurations into the as-cast thin-films, where they form crystalline regions. [44] Schematic illustration of this process is shown below in Figure 3.16.

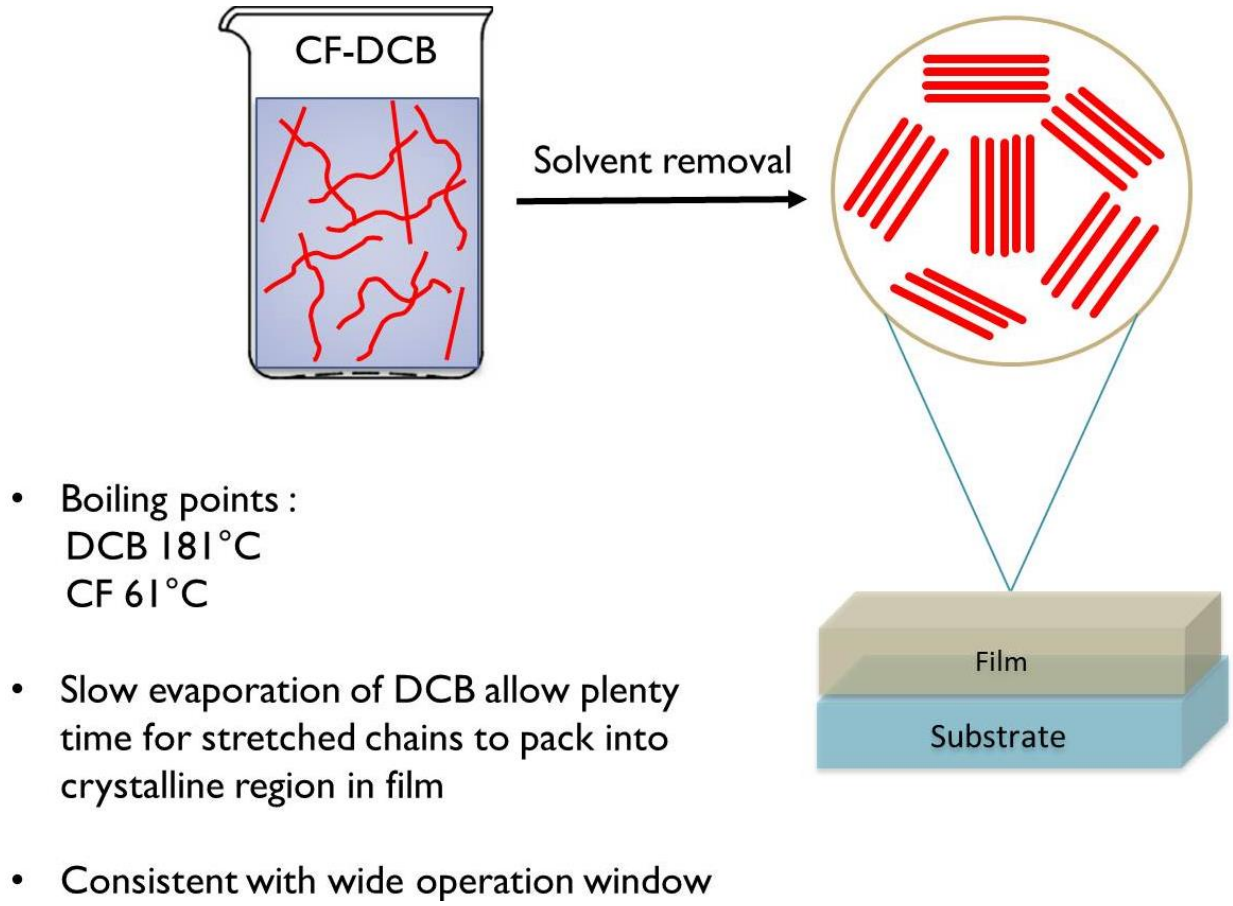

Figure 3.16 Schematic presentations of solution to film transition process

Since most CF evaporates out of the system first, DCB controls the properties of remaining solution, regardless of the amount initially added in solution. This agrees well with its wide additive operation window (up to 80% in volume ratio) in the solvent system. However, using DCB alone as the main solvent, as discussed earlier, will induce those larger-than-proper

crystallites (190 Å in terms of correlation length), where the exciton dissociation (at the donor acceptor interface, prefer a smaller domain size) and charge carrier transport (prefers a large crystallite size) are not balanced. [48] [49] The corresponding DCB-only device exhibits J_{sc} of only 6 mA/cm^2 and a PCE less than 2%. As a result, in this work, DCB is more suitable to be used as a solvent additive than the main processing solvent.

3.4 Conclusion

In summary, both CF-DIO and CF-DCB systems are effective in improving the nanoscale morphology, particularly in enhancing polymer packing order in PBDTP-DPP: $PC_{71}BM$ OPV devices. Our results provide clear evidences of two distinct morphology optimization mechanisms in these solvent mixture systems. SANS and UV-vis absorption spectra indicate the existence of folded, coiled polymer chains in CF-DIO solution, while polymer chains are well-extended in CF-DCB solution. [48]

Differences in polymer conformations could be explained by solute-solvent interactions, which are strongly chemical-structure dependent. Polymer chains are folded in CF in order to avoid unfavorable contact between aromatic backbones and non-aromatic CF molecules. Based on the chemical structure of DIO, it is reasonable to argue that DIO probably did substantially modify polymer conformation when added into CF solution. In contrast, addition of DCB would cause polymer chains to stretch in order to maximize the preferred interactions between backbones and aromatic DCB molecules. [48]

During solvent removal stage, the long drying period and preferential solubility of PCBM of DIO modifies the degree of phase-separation, which further facilitates polymer crystallization.

On the other hand, the slow evaporation of high-boiling DCB allows more time for polymer organization and facilitates the preservation of these stretched-chains formed in CF-DCB solutions into the as-cast thin-films, where they form crystalline regions. [48]

As a result, the mechanism of morphology control by DCB is well-connected to the much wider solvent additive operation window (up to 80%) in CF-DCB system, which is expected to be a valuable piece of processing information for OPV fabrication.

3.5 References

[1] Z. He, C. Zhong, X. Huang , W. Wong , H. Wu , L. Chen , S. Su , Y. Cao, *Adv. Mater.* **2011**, 23, 4636.

[2] L. Dou, J. You, J. Y, C. C. Chen, Y. He, S. M, T. M, K. E, G. Li, Y. Yang, *Nat. Photonics.* **2012**, *6*, 180.

[3] a) G. Li, R. Zhu, Y. Yang, *Nat. Photonics.* **2012**, 6, 153.

[4] a) Y. Liang, Z. Xu, J. Xia, S-T. Tsai, Y. Wu, G. Li, C. Ray, L. Yu, *Adv. Mater.* **2010**, 22, E135; b) J. Gao, L. Dou, W.Chen, C.-C. Chen, X. Guo, J. You, B. Bob, W.-H. Chang, J. Strzalka, C. Wang, G. Li, Y. Yang, *Adv. Energy Mater*. **2014**, 4, 1300739; c) W.-H. Chang, J. Gao, L. Dou, C.-C. Chen, Y. Liu, Y. Yang, Adv. *Energy Mater*. **2013**, 4, 1300864.

[5] H-Y. C., J.Hou, S. Zhang, Y. Liang, G. Yang, Y. Yang, L. Yu, Y. Wu, G. Li, *Nat. Photonics.* **2009**, 3, 649.

[6] a) Y. Li, *Acc.Chem.Res.* 2012, 45,723; b) Y. He, H.-Y.Chen, J.Hou, Y.Li, *J.Am.Chem.Soc.* **2010**, 132, 1377.

[7] J. Peet, J. Y. Kim, N. E. Coates, W. L. Ma, D. Moses, A.J. Heeger, G. C. Bazan, *Nat. Mater.* **2007**, 6, 497.

[8] W. Ma, C. Yang, X. Gong, K. Lee, A. J. Heeger, *Adv. Funct. Mater.* **2005**, 15, 1617.

[9] G. Li, V. Shrotriya, Y. Yao, Y. Yang, *J. Appl. Phys.* **2005** ,98, 043704 .

[10] F. Padinger, R.S. Rittberger, N.S. Sariciftci, *Adv. Funct. Mater.* ***2003***, 13, 85.

[11] V. Shrotriya, G. Li, Y. Yao, C.-W. Chu, Y. Yang, *Appl. Phys. Lett.* **2006**, 88, 073508.

[12] G. Li, C.-W. Chu, V. Shrotriya, J. Huang, and Y. Yang, *Appl. Phys. Lett*. **2006**, 88, 253503.

[13] M. S. White, D. C. Olson, S. E. Shaheen, N. Kopidakis, D. S. Ginley, *Appl. Phys. Lett.* **2006**, 89, 143517.

[14] L. Dou, J. Gao, E. Richard, J. You, C.-C. Chen, K. C. Cha, Y. He, G. Li, Y. Yang, *J. Am. Chem. Soc***. 2012,** 134, 10071.

[15] a) C.-C. Chen, L. Dou, R. Zhu, C.-H. Chung, T.-B. Song, Y. B. Zheng, S. Hawks, G. Li, P. S. Weiss, Y. Yang, *ACS Nano.* ***2012***, 6, 7185; b) C.-C. Chen, L. Dou, J. Gao, W.-H. Chang, G. Li, Y. Yang, *Energy Environ. Sci.*, **2013**, 6, 2714.

[16] L. Dou, W.-H. Chang, J. Gao, C.-C. Chen, J. You, Y. Yang, *Adv. Mater*.**2012**, 25,825

[17]J. C Bijleveld, A. P. Zoombelt, S .G .J .Mathijssen, M .M. Wienk, M. Turbiez, D.M. de leeuw, R. A. J. Janssen, *J. Am. Chem. Soc***. 2009,** 131, 16616**.**

[18] H. Bronstein, Z.Chen, R.S. Ashraf, W. Zhang, J. Du, J .R. Durrant, P .S . Tuladhar, K. Song, S. E. Watkins, Y. Geerts, M. M. Wienk, R. A. J. Janssen, T. Anthopoulos, H. Sirringhaus, M. Heeney, I. McCulloch, *J. Am. Chem. Soc*. **2011,** 133, 3272**.**

[19] R.C. Coffin, J. Peet, J. Rogers, G. C. Bazan, *Nature Chemistry*. **2009**, 1, 657.

[20] G. Li, Y.Yao, H. Yang, V. Shrotriya, G. Yang, Y. Yang, *Adv. Funct. Mater*. **2007**, 17, 1636.

[21]C.-W. Chu, H. Yang, W.-J. Hou, J. Huang, G. Li, Y. Yang, *Appl. Phys. Lett*., **2008**, 92, 103306.

[22] F. Zhang, K. G. Jespersen, C. Björström, M. Svensson, M. R. Andersson,V. Sundström, K. Magnusson, E. Moons, A. Yartsev, and O. Inganäs, *Adv.Funct.Mater*. **2006**, 16, 5, 667.

[23] M. M. Wienk, M. Turbiez, J. Gilot, R. A. J. Janssen, *Adv. Mater*. **2008**, 20, 2556.

[24] J.K. Lee, W.L. Ma, C. J. Brabec, J. Yuen, J. S. Moon, Jin Y. Kim, K. Lee, G. C. Bazan, A. J. Heeger , *J. Am. Chem. Soc*. **2008** , 130 , 3619.

[25] R. Qin, W. Li, C. Li, C. Du, C. Veit, H. Schleiermacher, M. Andersson, Z. Bo, Z. Liu, O. Inganas, U. Wuerfel, F. Zhang , *J. Am. Chem. Soc*. **2009** , 131 , 14612.

[26] Y. Yao, J. Hou, Z. Xu, G. Li, Y. Yang, *Adv. Funct. Mater*. **2008**, 18, 1783.

[27] A. J. Moulé, K. Meerholz, *Adv. Mater*. **2008**, 20, 240

[28] S. Berson, R. De Bettignies, S. Bailly, S. Guillerez, *Adv. Funct. Mater*. **2007**, 17, 1377.

[29] P. J. Brown, D. S. Thomas, A. Kohler, J. S. Wilson, J. S. Kim, C. M. Ramsdale, H. Sirringhaus, R. H. Friend, *Phys. Rev. B*. **2003**, 67, 064203.

[30] M. M. Bouman, E. E. Havinga, R. A. J. Janssen, E. W. Meijer, Mol. *Cryst. Liq. Cryst. Sci. Technol., Sect. A.* **1994**, 256,439.

[31] J. C. Bijleveld , V. S. Gevaerts , D. D. Nuzzo , M.Turbiez , S. G. J. Mathijssen , D. M. de Leeuw , M. M. Wienk, R. A. J. Janssen, *Adv. Mater*. **2010**, 22, E242–E246.

[32] K. Maturova, S. S. van Bavel, M. M. Wienk, R. A. J. Janssen, M. Kemerink, *Nano. Lett*. **2009**, 98, 3033.

[33] S. H. Park , A. Roy , S. Beaupre, S. Cho, N. Coates , J. S. Moon , D. Moses , M. Leclerc, K.Lee and A. J. Heeger, *Nat. Photonics.* **2009**, *3*, 297.

[34] Chen, W.; Nikiforov, M. P.; Darling, S. B. *Energy Environ. Sci.* **2012.**

[35] M. R. Hammond, R. J. Kline, A. A. Herzing, L. J. Richter, D. S. Germack,H.-W. Ro,C. L. Soles, D.A. Fischer, T. Xu, L. Yu, M. F. Toney, D. M. DeLongchamp, *ACS nano.* **2011**.5, 8248.

[36] M.-Y. Chiu, U-S. Jeng, C.-H. Su, K.S. Liang, K.-H. Wei, *Adv. Mater*. **2008**, 20, 2573

[37] W.Chen, T. Xu, F. He, W.Wang, C. Wang, J. Strzalka, Y. Liu, J. Wen, D. J. Miller, J. Chen, K. Hong, L.Yu, S. B. Darling, *Nano Lett*. **2011**, 11, 3707

[38] T. Erb, U. Zhokhavets, G. Gobsch, S. Raleva, B. Stühn, P. Schilinsky, C. Waldauf, C. J. Brabec. *Adv. Funct. Mater. **2005**,15,1193.*

[39] S. J. Lou, J. M. Szarko, T. Xu, L. Yu , T. J. Marks, L.X. Chen, *J. Am. Chem.Soc*. **2011**, 133, 20661.

[40] D. Chen, A. Nakahara, D.Wei, D. Nordlund, T.P.Russell, *Nano Lett.*, **2011**, 11, 561.

[41] Sinha, S. K.; Freltoft, T.; Kjems, J.; *In Kinetics of Aggregation and Gelation*, edited by F. Family and D. P. Landau, pp. 87-90. Amsterdam: North Holland.

[42] a) Chen, S.-H., Teixeira, J. *Phys. Rev. Lett.*, **1986**, 57, 2583-2586; b) Teixeira, J. *J. Appl. Cryst.* 1988, **21**, 781-785.

[43] a) S. A. Jenekhe, L. Lu, M. M. Alam, *Macromolecules.* **2001**, 34, 7315; b) B.Boldrini, E. Cavalli, A. Painelli, F. Terenziani, *J. Phys. Chem. A* .**2002**, 106, 6286; c) R. V. Pereira, A.P. G.Ferreira, M. H. Gehlen, J. Phys. Chem. A. **2005**, 109, 5978; d) W. Liptay, *Angew. Chem. internat. Edit*. **1969**, 8, 177.

[44] a) T.-Q.Nguyen, V. Doan, B. J. Schwartz, *J. Chem. Phys*. **1999,** 110, 4068; b) R.D. Schaller, L.F. Lee, J.C. Johnson, L.H. Haber, R. J. Saykally, J. Vieceli and I. Benjamin, T.-Q. Nguyen, B.J. Schwartz, *J. Phys. Chem. B,* 2002, 106, 9496.

[45] J. Liu, Y.Shi, Y. Yang, *Adv. Funct. Mater. **2001***, 11, 1.

[46] Teixeira, J. *J. Appl. Cryst.* **1988**, 21, 781-785.

[47] Kline, S. R. *J. Appl. Cryst.* **2006**, 39, 895-900.

[48] J. Gao, W. Chen, L. Dou, C.-C. Chen, W.-H. Chang, Y. Liu, G.Li, Y. Yang, *Adv. Mater.* **2014**, 26, 3142

[49] J. Gao, L. Dou, W. Chen, C.-C. Chen, X. Guo, J. You, B. Bob, W.-H. Chang, J.Strzalka, C.Wang, G.Li, Y. Yang, *Adv. Energy Mater.* **2014**, 4, 1300739

Chapter 4 Future work and perspectives

One point worth considering in the future is to fully explore the applicability of other advanced characterization tools, such as in-situ and cryogenic techniques to fully monitor the complete dynamic film-formation process for deeper understanding.

Another important aspect of future work is to see how well apply these principles applies to other systems. Given the convincing evidence obtained on these representative low-band-gap polymers, which share the common features, we believe the morphology optimization process described in this work will be of great potential for future applications.

With the urgent need to integrate current research-stage OPVs into industrial scale mass production, the result in this work could serve as a guiding for materials synthesis and solvent selection to satisfy the high-standards of industry for the ultimate goal of achieving a highly cost-productive, environmental-friendly OPV fabrication process.